GARCIA
CENTER FOR POLYMERS AT ENGINEERED INTERFACES

Summer Research Scholars
2024

GARCIA

CENTER FOR POLYMERS AT ENGINEERED INTERFACES

2024 Research Scholar Program

"This year's Garcia logo encapsulates the three tenets of scientific research: curiosity, collaboration, and precision, which are fundamental to Garcia's mission. Garcia has taught us to see the world through the lens of science, ask questions to test our hypotheses and persevere even through unsuccessful experiments. Each step of our projects required us to pay careful attention to detail, ensuring the reliability and reproducibility of our results. Just as DNA is passed down from our parents, our research this summer was founded on the work of the scientific community and past Garcia students and will be continued by future Garcia students. Thank you, Garcia 2024, for an incredibly enjoyable and meaningful summer!" **Maya Puterman '24**

This year the Garcia Program would like to highlight the amazing activities of our high school students to advance the forefronts of science in dentistry, medicine, energy, robotics, and materials. Their success was based on adherence to the underlying fundamental principals of the Garcia program; inclusion, collaboration, and mutual respect. In this manner, strong connections are forged between students involved in experimental research with those working on theory and simulation—where the idea of building a true digital twin, using AI, machine learning, and large data becomes reality. The digital twin concept opens up immense promise for rapid progress in multiple areas, ranging from drug design, tissue engineering, and robust microgrid design with clean renewable energy sources. Therefore this year the Garcia Program would like to honor, **Professor Yuefan Deng**, a leader in multi-scale modeling, and mentor to many of our students, to be our **keynote speaker**.

The Garcia Center for Polymers at Engineered Interfaces was founded in 1996 and is named after the late Queens College professor, Narciso Garcia, who was a pioneer in the integration of education and research. The Center focuses on the broad application of materials research to engineering, medicine, and energy, and recently, AI, machine learning, and computational modeling. The Center also supports innovation through entrepreneurship and has multiple collaborations with industry and national laboratories. In the research program, high school students work together with undergraduates, PhD , post PhD and faculty who collaborate in addressing challenges at the cutting edge of modern science. The students are encouraged to publish in refereed scientific journals, present their results at national conferences, and develop patents to protect their intellectual property. Our goal is to convey to the students the excitement we enjoy daily in research and provide for them a supportive network within the scientific community. Research is a lifelong experience and we hope to remain as a resource to our students long after "graduation".

Sincerely,

Miriam Rafailovich

Jonathan Sokolov

Cover Background: Fluorescent microscope image of human fibroblast cells with immunohistochemical stain for actin and the nucleus.
(Credit: Daniel You)

High School Students

Leah Abrahams

Aryan Agahtehrani

Ananya Anand

Yuchen Bai

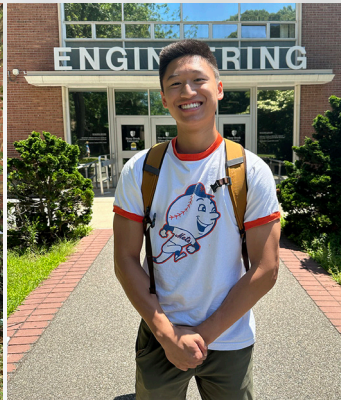Ishita Banerjee

Anastasiia (Nastia) Bezugla

Dhruva Bhat

Dvita Bhattacharya

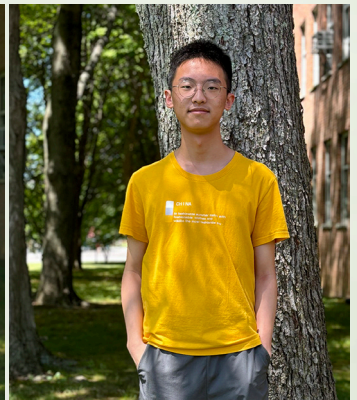
Indus Boddu

Aadi Bordia

Christian Chan

Isabelle Chan

Megan Chan

Damien Crowley

Dylan Steng

Hongfan (James) Deng

High School Students

Shuyi (Candy) Deng

Silas Dorsky

Shira Fisher

Payton Fromm

Rong (Jennifer) Gao

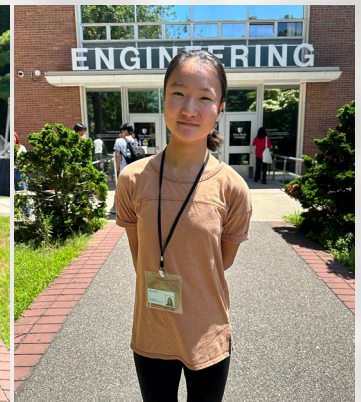Jerry Gu

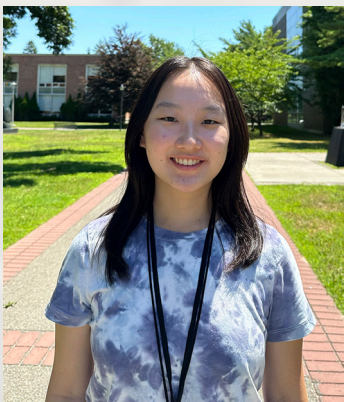Michelle Guo

Runjing Guo

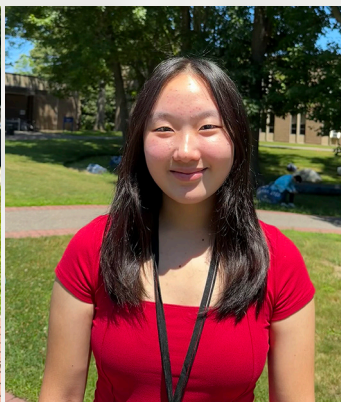Rohan Hablani

Alice He

Ashley Jisue Hong

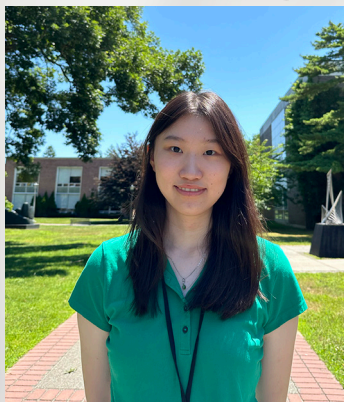Alice Hu

Audrey Huang

Marissa Huang

Eva Jain

Evan Ji

High School Students

Zihan (Jenny) Jia

Qingyi (Emily) Jiang

Ariel (Ari) Khavulya

Matthias Kim

Tei Kim

Aditi Kiran

Eli Krasnoff

Kevin Lee

Jhen-Bahn (Benjamin) Li
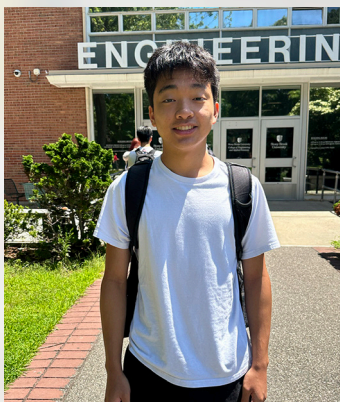
Daniel Liang

Jingwen (Linda) Liang
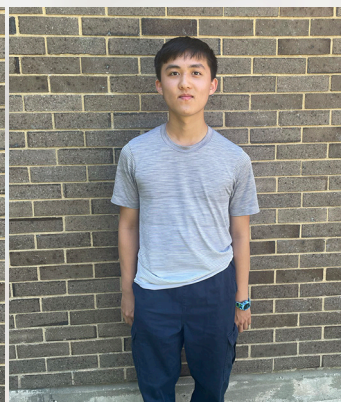
Daniel Lim

Richard Lin
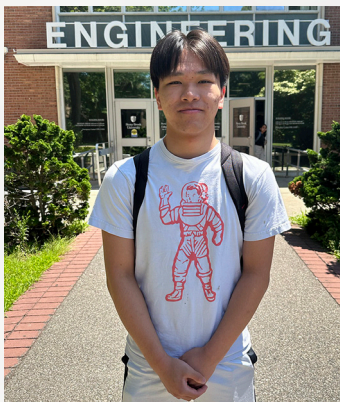
Thomas Lin
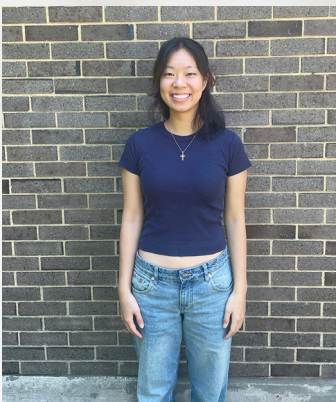
Amanda Liu

Ruoheng (Sylvie) Liu

High School Students

Sichen (Theresa) Liu
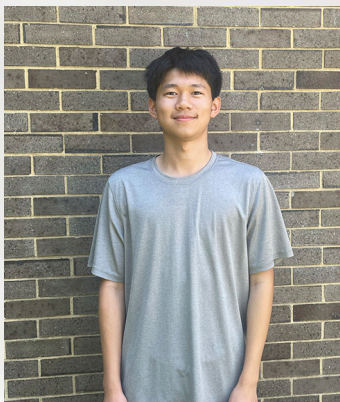
Vincent Lo

Reilin Lyu

Xingchuan (Ryan) Ma

Hunter Maguire

Arohi Mahajan

Elena Mingorance

Joshua Mu

Viraj Pahuja
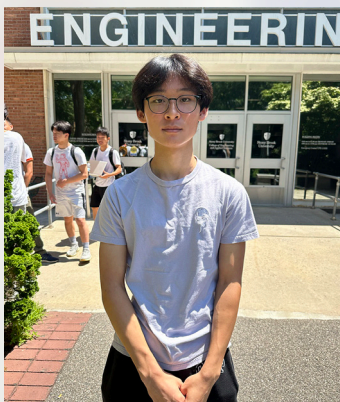
Leo Pan-Wang

Seohee (Ella) Park

Maya Puterman

Brandon Qi
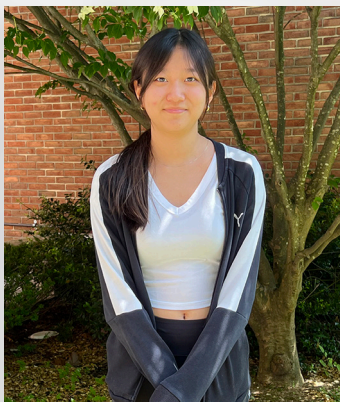
Cynthia Qian

Nathan Qiu

Brenna Ren

High School Students

Risa Rogers
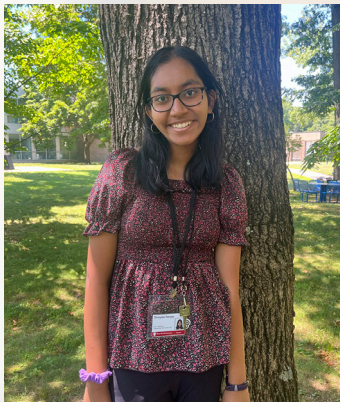
Shreyaa Sanjay

Niranjana Sankar
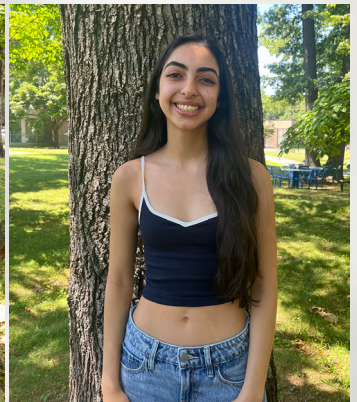
Mira Setia

Sadie Seulal
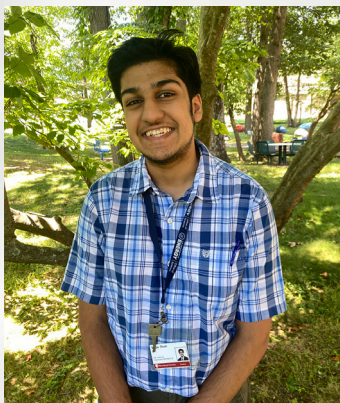
Vinav Shah
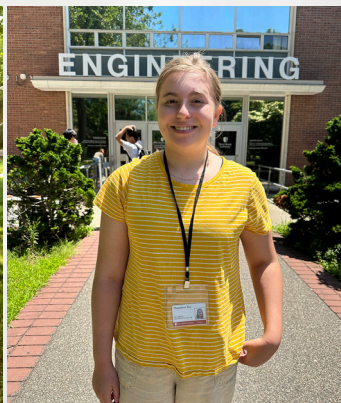
Theodora (Thea) Siu

Jingyu (Stella) Song

Yoonsoo (Leah) Song

David Sun

Ruoshui (Rochelle) Sun

Catherine Suo

Emily Tarrab
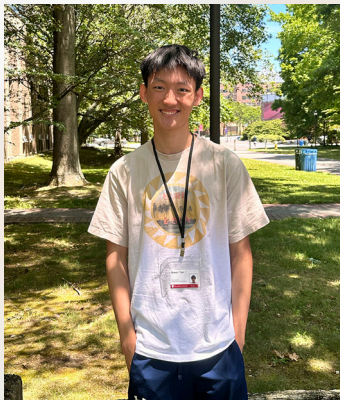
Bowen Tian
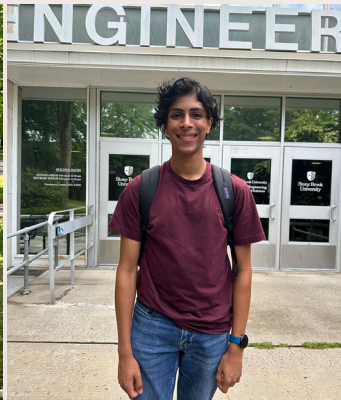
Aaryan Vira

Dylan Wang

High School Students

Keyu (Corin) Wang

Kimberly Wang

Erin Wong

Ella Wunderlich

Evan Xie

Zheming (Dennis) Xu

Sarah Yagudayev

Zeyu (Peter) Yao
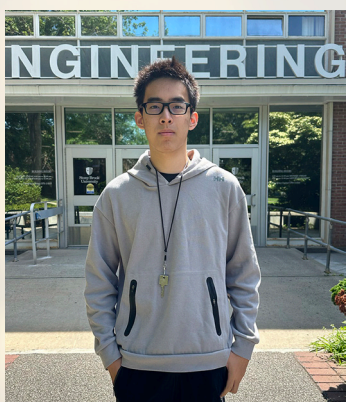
Xinyu (Daniel) You
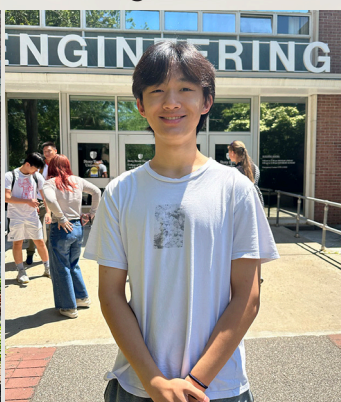
Calvin Yu

Hau Hong Joseph Yung

Corey Zhang

Dorothy Zhang

Emily Zhang

Jenny Dinh Nhu Zhang

Kevin Zhang

High School Students

Laura Zhang

Brianna Zheng

Xinyan (Ava) Zhou

Research Experience for Undergraduates (REU)

Tavan Bhatia

Philip Colman

Navya Gautam

Eugene Jiang

Nikita Karnik

Zoe Katevatis

Patrick Lewis

Danielle Liu

Research Experience for Undergraduates (REU)

Michael Lotwin

Katherine Martinez Diaz

Cosmo Perfetti

Brooklyn Ratel

Catherine Reyes

Divleen Singh

Leora Stochel

Oluomachi Uwakwe

Grace Wong

Kevin Wu

Jonathan Xavier

Graduate Students

Allen Bethancourt

Haoyan Fang

Yiwei Feng

Shi Fu

Adam Hansen

Jessica Hofflich

Huiting Luo

Abdelhameed Mahmoud

Md Farabi Rahman
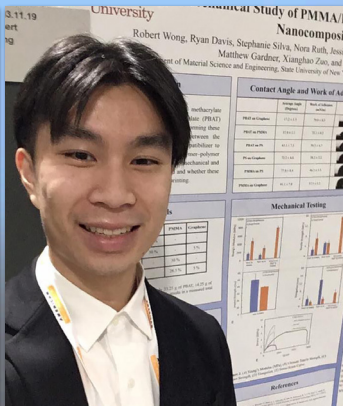
Robert Wong

Chaofan Lin

Fumi Honda

Karin Hasegawa

Leela Sotsky

Georgios Kementzidis

Ziyuan Niu
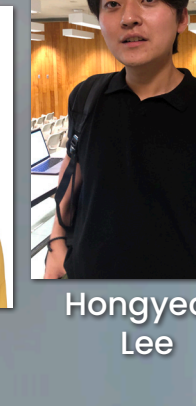
Hongyeon Lee

Yongseok Kim

Faculty and Staff

Jonathan Sokolov

Jawaad Sheriff

Nilanjan Chakraborty

Michael Cuiffo

Chandramouli Sadasivan

Stephen Walker

Marcia Simon

Rachel Brownlee

John Jerome
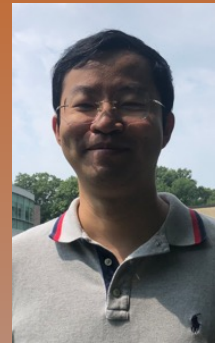
Kao Li
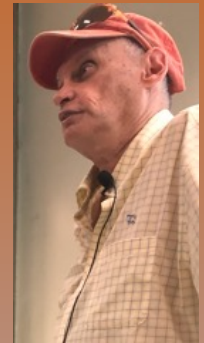
Vitaly Citovsky

David Sprouster

Gurtej Singh

Rebecca Isseroff

Aaron Sloutsky

Peng Zhang

Herb Weiss

Dilip Gersappe

Yuefan Deng
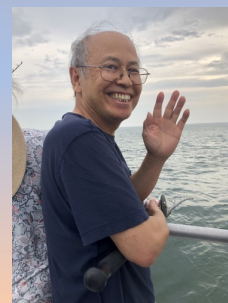
Jay Gao
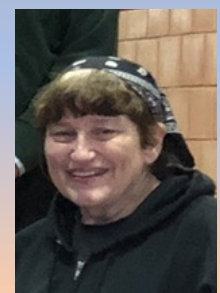
Miriam Rafailovich
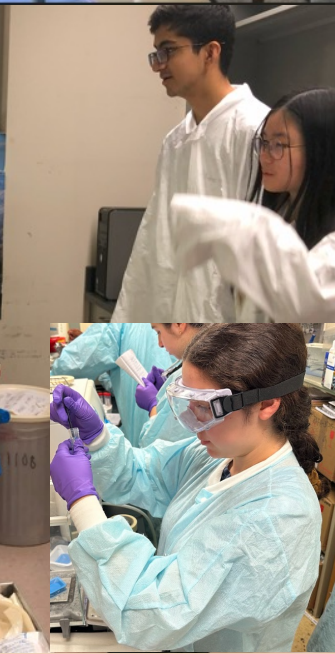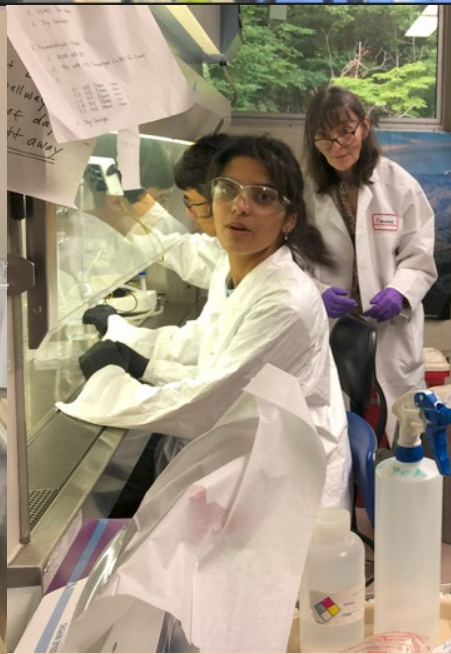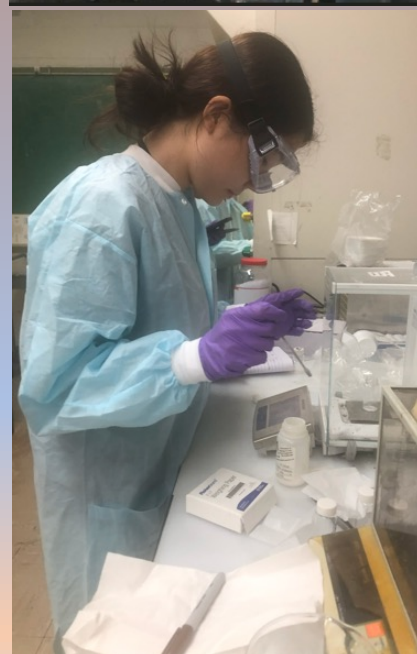
In the Lab
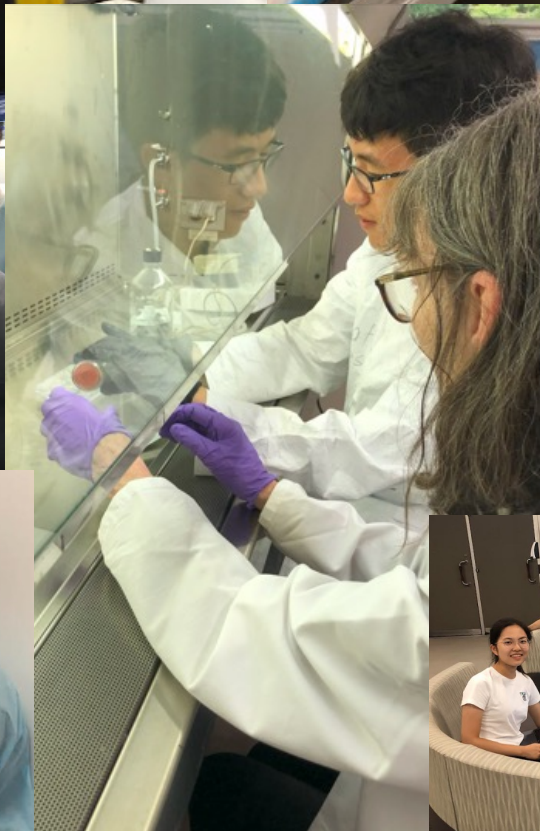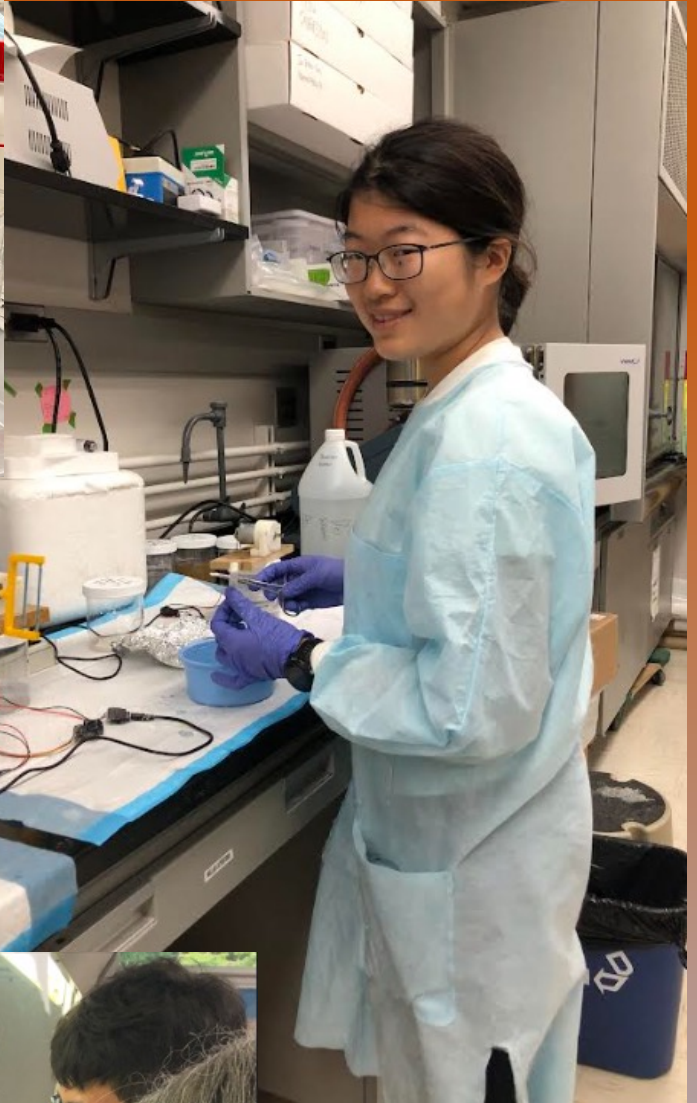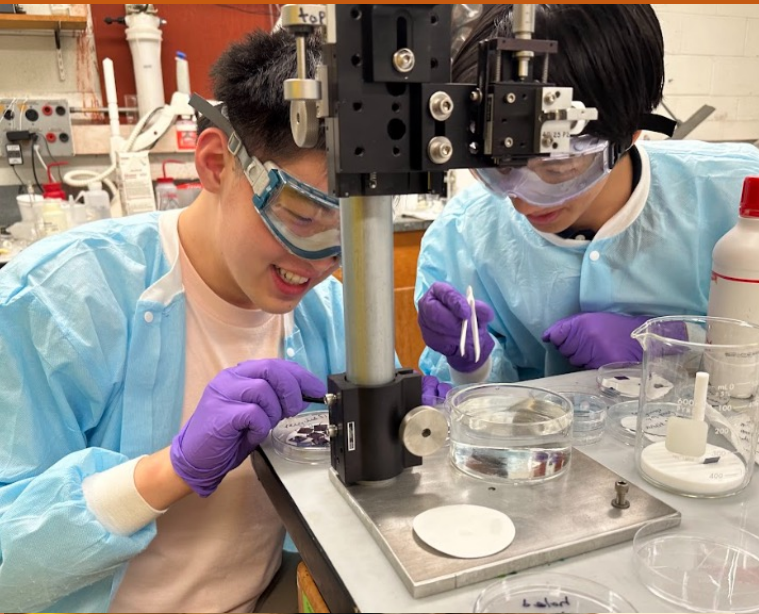
Presentations!
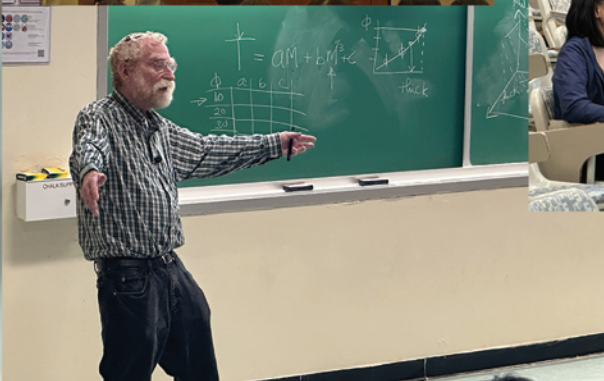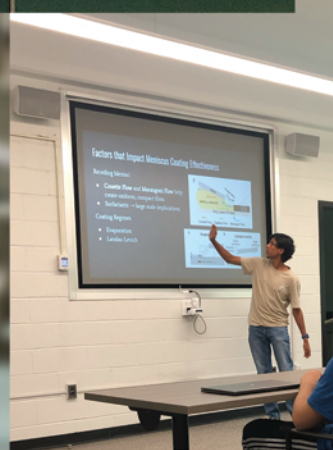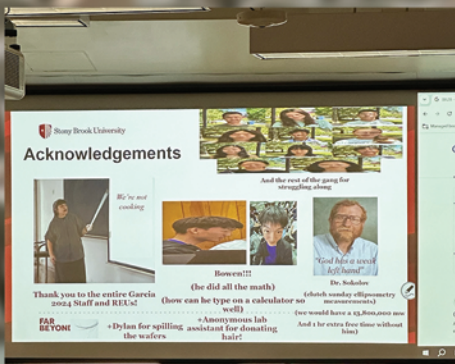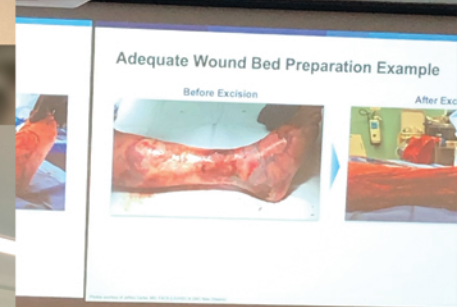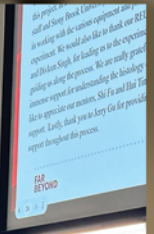
Fishing!
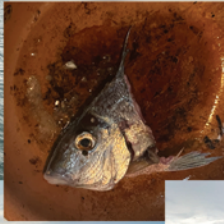
Canoeing!

Getting Active!
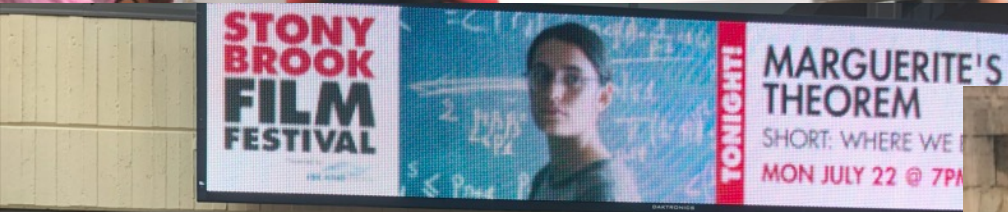
Off The Clock

Summer Scholar Schedule of Weekly Activities

2024 Research Scholar Program

Each day starts with a mandatory group meeting at 10:15 AM!

Daily Schedule: Week of 6/26

		Wednesday – 6/26	Thursday – 6/27	Friday – 6/28
		10:15 – 10:30: Dr. Anne-Marie Scheidt: Welcome	**10:15 – 10:30:** Greetings by: SBU Provost Dr. Carl Lejuez & Morin Charitable Trust Officer Steve Vaccarelli	**10:15 – 10:30:** Organizational Meeting
		10:30 – 11:00: Introduction	**10:30 – 11:15:** Dr. Steve Walker: Working with Bacteria & Microbial Resistance	**10:30 – 11:45:** Dr. Ying Liu, EH&S: Chemical Safety Training
		11:00 – 12:00: Dr. Vitaly Citovsky: *Agrobacterium tumefaciens – Pathogen and useful tool*	**11:15 – 12:00:** Dr. Tai-De Li: XPS, TOF-SIMS, & AFM Imaging	**11:45 – 12:45:** Walter Julias, EH&S: Waste Management Safety Training
		12:00 – 12:45: Dr. Mimi Borelli: RECell Spray-On Skin Cells	**12:00 – 12:45:** Dr. Dennis T. Lee: Exploring Porous Materials	**12:30 – 1:00:** Pizza Working Lunch
		12:45 – 3:00: Lunch, & Greenhouse & Dental School Tour	**12:30 – 1:00:** Pizza Working Lunch	**1:00 – 1:40:** Dr. Frank Han: Exopolysaccharides in Plants and Soils
		3:00 – 4:00: Dr. Yuefan Deng Algorithms for Modeling Blood Clots	**1:00 – 4:15:** Facilities Tour	**1:40 – 2:15:** Justin Burzachiello: Root Volume Quantification with a CT Scanner
		4:00 – 4:30: Dr. Yu-Chung Lin Micro-CT: Nanocomposites and Roots		Karin Hasegawa: AI-Enabled & CNN Biologic Studies

Summer Scholar Schedule of Weekly Activities

Each day starts with a mandatory group meeting at 10:15 AM!

Daily Schedule: Week of 7/1

Monday – 7/1	Tuesday – 7/2	Wednesday – 7/3	Thursday – 7/4	Friday – 7/5
10:15 – 10:20: Organizational Meeting **10:20 – 11:05:** Clara Tran: SBU's Library Databases **11:05 – 12:00:** Rebecca Isseroff: Graphene Materials, Lab Notebooks, and the MRS **12:00 – 1:00:** Lunch **1:00 – 2:00:** Janet Oseni, EH&S: Radiation Proximity Awareness Training **2:00 – 3:15:** Chris Kuhlow, EH&S: Hazardous Biologic Materials **3:15 – 4:00:** Dr. Gurtej Singh: Scar and Wound Healing **4:00 – 4:15** Polystyrene Fundamentals	**10:15 – 10:30:** Organizational Meeting **10:30 – 3:30:** Spin Casting Experiment Part I **3:30 – 4:30:** Dr. Jonathan Sokolov: Understanding Ellipsometry	**10:15 – 10:30:** Organizational Meeting **10:30 – 4:00:** Spincasting Experiment Part II **4:00 – 4:30:** Evan Xie: Machine Learning Program for Polystyrene Spin Casting	**Happy Fourth of July!**	**10:15 – 10:30:** Organizational Meeting & Statistics Lecture **10:45 – 1:00:** Journal Club **12:45 – 1:00:** Working Pizza Lunch **1:00 – 1:40:** Dr. Nilanjan Chakraborty: Robotics **1:00 – 1:40:** Dr. Aaron Sloutski: Introduction to Polymer Science

![GARCIA — Center for Polymers at Engineered Interfaces — 2024 Research Scholar Program]

Summer Scholar Schedule of Weekly Activities

Each day starts with a mandatory group meeting at 10:15 AM!

Daily Schedule: Week of 7/8

Sunday – 7/7	Monday – 7/8	Tuesday – 7/9	Wednesday – 7/10	Thursday – 7/11	Friday – 7/12
Trip to Nassau Symphony Pops Orchestra in Concert at Hecksher Museum Park Featuring Prof. John Jerome & Bagels & Ice Cream on the Lawn	**10:15 – 10:20:** Organizational Meeting **10:20 – 11:30:** Spin Casting Clinic: Grad Students & Alex Wang **11:30 – 12:15:** Giorgos Kementzdis: Fibrinogenesis Modeling **12:15 – 1:15:** Lunch **1:15 – 2:00:** Dr. David Sprouster: X-ray Characterization of Transmutant Products in Irradiated Tungsten **2:00 – 3:00:** Dr. Chander Sadasivan: Minimally Invasive Treatment of Brain Aneurysms **3:00 – 4:00:** Prof. Jonathan Sokolov: DNA **4:00 – 4:15** Dr. Jaesung Koo: Supercritical CO_2	**10:15 – 10:20:** Organizational Meeting **10:20 – 10:45:** Scott Gershonowitz: Fire Safety Training **10:45 – 11:30:** Dr. Jawaad Sheriff: Biofluid Cardiovascular Mechanics – Thrombosis **11:30 – 12:10:** Dr. Marcia Simon: Engineering Skin **12:10 – 1:10:** Lunch **1:10 – 3:20:** Spin Casting Presentations: Battle of the Groups **3:20 – 4:45:** Project Fair Part I: Presentations by Graduate Staff	**10:15 – 10:20:** Organizational Meeting **10:20 – 11:05:** Dr. Ying Liu, EH&S: SOP Training **11:05 – 12:45:** Project Fair Part II: Presentations by Graduate Staff **12:45 – 1:45:** Lunch **1:45 – 2:30:** Dr. Samantha Lucker: Biopolymer Performance Evaluation for Levee Embankments **2:30 – 4:05:** Project Fair Part III: Presentations by Graduate Staff **4:05:** Selection of Projects	**10:15 – 10:30:** Organizational Meeting **10:30 – 4:15:** Write SOPs & **Lab Work!** (According to your group's schedule)	**10:15 – 10:20:** Organizational Meeting **10:20 – 10:30:** Dvita Bhattacharya: Introduction to Journal of Ethics in Scientific and Technological Innovations (JESTI) **10:30 – 2:15:** **Lab Work!** (According to your group's schedule) **11:45 – 1:00:** BBQ Under The Trees

GARCIA
CENTER FOR POLYMERS AT ENGINEERED INTERFACES
2024 Research Scholar Program
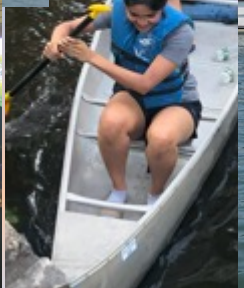
Summer Scholar Schedule of Weekly Activities

Each day starts with a mandatory group meeting at 10:15 AM!

Daily Schedule: Week of 7/15

Monday – 7/15	Tuesday – 7/16	Wednesday – 7/17	Thursday – 7/18	Friday – 7/19
10:15 – 10:20: Organizational Meeting	**10:15 – 10:20:** Organizational Meeting	**10:15 – 10:20:** Organizational Meeting	**10:15 – 10:20:** Organizational Meeting	**10:15 – 10:20:** Organizational Meeting
10:20 – 10:25: Shreyaa Sanjay: ReGroup Magazine Introduction	**10:20 – 10:50:** Dr. Gang Liu: Review of Polymer Rheology	**10:20 – 10:50:** Dr. Michelle Hutchins VIPER Program at University of Pennsylvania	**10:20 – 10:50:** Prof. Michael Rubenstein Polymer Panel	**10:20 – 10:50:** Madeline Augustine: Materials Science at Boeing
10:25 – 10:45: Eliana Matsil: Energy Microgrids for the Shinnecock Nation	**10:50 – 4:15:** **Lab Work!** (According to your group's schedule)	**10:50 – 4:15:** **Lab Work!** (According to your group's schedule)	**10:50 – 4:15:** **Lab Work!** (According to your group's schedule)	**10:50 – 2:15:** **Lab Work!** (According to your group's schedule)
10:45 – 4:15: **Lab Work!** (According to your group's schedule)		**3:30 – 4:30:** Beat the Heat: Ice Cream Social Feat. Mr Softee!	**5:30:** Annual Garcia Softball Game Feat. Dunkin' and Baskin Robbins	**12:00:** Working Pizza Lunch

GARCIA
CENTER FOR POLYMERS AT ENGINEERED INTERFACES
2024 Research Scholar Program

Summer Scholar Schedule of Weekly Activities

Each day starts with a mandatory group meeting at 10:15 AM!

Daily Schedule: Week of 7/22

Sunday – 7/21	Monday – 7/22	Tuesday – 7/23	Wednesday – 7/24	Thursday – 7/25	Friday – 7/26
Tour of Brookhaven National Laboratory NSLS-II & Trip to Long Island Game Farm	**10:15 – 10:20:** Organizational Meeting **10:20 – 11:00:** Dr. Jack Fuhrer: Applying for a Career in Medicine – Renaissance School of Medicine at Stony Brook University **11:00 – 4:15:** **Lab Work!** (According to your group's schedule)	**10:15 – 10:20:** Organizational Meeting **10:20 – 11:00:** Noe Escobar: Considering a Career in Dentistry – Stony Brook University School of Dental Medicine **11:00 – 4:15:** **Lab Work!** (According to your group's schedule)	**10:15 – 10:20:** Organizational Meeting **10:20 – 11:00:** Nanoparticles: Good or Bad? **11:00 – 4:15:** **Lab Work!** (According to your group's schedule) **11:00 – 4:15:** Research Reports and Ice Cream: Deng Group Projects	**Trip to the Long Island Aquarium**	**10:15 – 10:20:** Organizational Meeting **10:20 – 11:00:** Dr. Julie True: Patents and Intellectual Property **10:30:** Bagel Brunch **11:00 – 12:00:** Research Reports **10:30 – 2:15:** **Lab Work!** (According to your group's schedule)

![GARCIA — CENTER FOR POLYMERS AT ENGINEERED INTERFACES — 2024 Research Scholar Program]

Summer Scholar Schedule of Weekly Activities

Each day starts with a mandatory group meeting at 10:15 AM!

Daily Schedule: Week of 7/29

Monday – 7/29	Tuesday – 7/30	Wednesday – 7/31	Thursday – 8/1	Friday – 8/2
10:15 – 10:20: Organizational Meeting	**10:15 – 10:20:** Organizational Meeting	**10:15 – 10:20:** Organizational Meeting	**9:00 – 2:30:** Annual Garcia Canoe Trip — On the Nissequogue River	**10:15 – 10:20:** Organizational Meeting
10:20 – 4:15: Lab Work! (According to your group's schedule)	**10:20 – 11:00:** Prof. Jonathan Sokolov: ImageJ Tutorial	**10:20 – 10:50:** Prof. Dilip Gersappe Polymer Theory		**10:20 – 10:50:** Lauren Lowen: Materials Research Society (MRS) Meeting Preparation and Information
	11:00 – 4:15: Lab Work! (According to your group's schedule)	**10:50 – 4:15:** Lab Work! (According to your group's schedule)		**10:50 – 12:50:** Bagel Brunch & Research Updates
	4:00 – 5:00: Ice Cream & Research Updates	**4:00 – 5:00:** Research Updates & Mochi Ice Cream	**2:30 – 4:15:** Lab Work! (According to your group's schedule)	**10:50 – 2:15:** Lab Work! (According to your group's schedule)

Summer Scholar Schedule of Weekly Activities

GARCIA — CENTER FOR POLYMERS AT ENGINEERED INTERFACES — 2024 Research Scholar Program

Each day starts with a mandatory group meeting at 10:15 AM!

Daily Schedule: Week of 8/5

Monday – 8/5	Tuesday – 8/6	Wednesday – 8/7	Thursday – 8/8	Friday – 8/9
10:15 – 10:20: Organizational Meeting	**10:15 – 10:20:** Organizational Meeting	**10:15 – 10:50:** Organizational Meeting	**10:15 – 10:20:** Organizational Meeting	
10:20 – 11:00: Prof. Fred Grinnell: Ethical Considerations	**10:20 – 10:45:** Discussing the Symposium	**10:50 – 4:15:** **Lab Work!** (According to your group's schedule)	**2:30 – 4:15:** **Lab Work!** (According to your group's schedule)	
10:20 – 4:15: **Lab Work!** (According to your group's schedule)	**11:00 – 4:15:** **Lab Work!** (According to your group's schedule)	**6:30 – 8:00:** Basketball Tournament – Grad Students VS High Schoolers & REUs @ Campus Recreation Center	**4:00 – 5:00:** Research Updates & Liquid Nitrogen Ice Cream	**Garcia End-of-Summer Research Symposium!**
4:00 – 5:00: Research Updates & Mochi Ice Cream	**5:00:** Abstract Deadline		**7:00 – 8:30:** Ping Pong Tournament Feat. Dr. Yu-Chung Lin @ Campus Recreation Center	
	7:00 – 8:30: Indoor Soccer Match @ Campus Recreation Center			

Please join us for the

Garcia End of Summer Symposium

When: Friday, August 9, 2024
10:15 AM-1:30 PM

Where: Bauman Center for Leadership and Service
Program: Welcome –Steven Vaccarelli, BBH
representing the Louis Morin Charitable Trust
Musical arrangement –Garcia Ensemble
led by Prof. John Jerome
Research Presentations: Garcia Program Students
Formal Luncheon
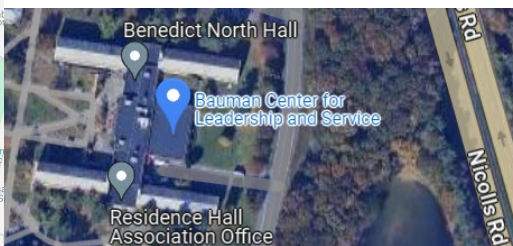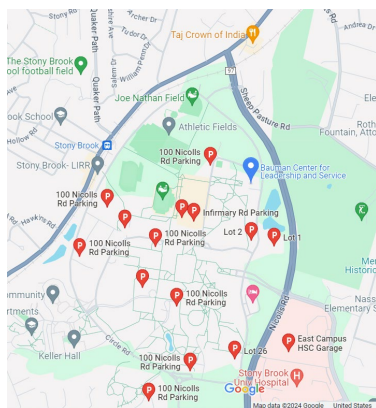
Find Bauman on Waze and Google maps

GARCIA
CENTER FOR POLYMERS AT ENGINEERED INTERFACES
2024 Research Scholar Program

End-of-Summer Research Symposium **Friday, August 9** – Bauman Center for Leadership and Service	

10:00 AM	***Musical Arrangement: Conducted by Prof. John Jerome*** *Performers: Erin Wong, Jonathan Xavier, David Sun, Ishita Banerjee, Dhruva Bhat, Joshua Mu*
Coffee & Muffins	**Welcome** Mr. Steven Vaccarelli, Vice President, Senior Trust Officer Brown Bros Harriman and the Morin Charitable Trust
	Keynote Speaker Professor Yuefan Deng, Applied Math & Statistics, Stony Brook University
10:30 AM	**Session 1: DNA Segmentation** **Chairs: Danielle Liu & Patrick Lewis**
	A Novel Approach for Ordered Fragmentation of Mouse DNA Using Tn5 Transposase **Alice Hu**, King High School, Tampa, FL **Aditi Kiran**, BASIS Independent Fremont, Fremont, CA **Kevin Lee**, The Albany Academies, Albany, NY **Elena Mingorance**, South Side High School, Rockville Centre, NY **Jingyu (Stella) Song**, Phillips Exeter Academy, Exeter, NH **Kevin Zhang**, North Hunterdon High School, Annandale, NJ
	A Novel Method for UV Thin-Film Backside Development for Ordered DNA Fragmentation **Kevin Zhang**, North Hunterdon High School, Annandale, NJ **Jingyu (Stella) Song**, Phillips Exeter Academy, Exeter, NH **Elena Mingorance**, South Side High School, Rockville Centre, NY **Kevin Lee**, The Albany Academies, Albany, NY **Aditi Kiran**, BASIS Independent Fremont, Fremont, CA **Alice Hu**, King High School, Tampa, FL
10:35 AM	**Session 2: 3D Printing of Vascular Devices** **Chairs: Leora Stochel, Kevin Wu, & Grace Wong**
	Characterizing Mechanical Properties of Poly(vinyl alcohol) and Resorcinol Diphenyl Phosphate Blend Vascular Grafts **Risa Rogers**, Schechter School of Long Island, Williston Park, NY **Hau Hong Joseph Yung**, Georgetown Preparatory School, North Bethesda, MD
	Developing a Novel Method for the Production of Poly(vinyl alcohol) Vascular Grafts **Hau Hong Joseph Yung**, Georgetown Preparatory School, North Bethesda, MD

	Bioprinting Human Vasculature within a Collagen Gel
	Ananya Anand, Johns Creek High School, Johns Creek, GA **Jerry Gu**, Princeton International School of Mathematics and Science, Princeton, NJ **Zihan (Jenny) Jia**, The Experimental High School Attached to Beijing Normal University, Beijing, China **Viraj Pahuja**, The Wheatley School, Old Westbury, NY **Shreyaa Sanjay**, West Windsor-Plainsboro High School North, Plainsboro, NJ **Theodora (Thea) Siu**, Ward Melville High School, East Setauket, NY **Jenny Dinh Nhu Zhang**, Renaissance International School Saigon, Ho Chi Minh City, Vietnam
	Engineering a Reverse Thermo-Responsive Injectable Liquid Embolic Agent for Brain Aneurysm Treatment
	Leah Abrahams, The Frisch School, Paramus, NJ **Dhruva Bhat**, Foothill High School, Pleasanton, CA **Shira Fisher**, Yeshiva University High School For Girls (Central), Holliswood, NY **Joshua Mu**, Illinois Mathematics and Science Academy, Aurora, IL **Catherine Suo**, Hong Kong International School, Hong Kong, Hong Kong SAR **Kimberly Wang**, Jericho Senior High School, Jericho, NY **Sarah Yagudayev**, Yeshiva University High School for Girls (Central), Queens, NY
10:45 AM	## Session 3: Theory, Simulation, & CT Segmentation **Chairs: Navya Gautam & Tavan Bhatia**
	Session 3a: Theory & Simulation
	An integrated in silico approach for AI-enhanced discovery of novel eIF4E inhibitors targeting drug-resistant ER+ breast cancer
	Audrey Huang, Woodbridge High School, Irvine, CA **Xingchuan (Ryan) Ma**, Portsmouth Abbey School, Portsmouth, RI **Zeyu (Peter) Yao**, Stamford American International School, Singapore, Singapore
	Molecular Dynamics and Conditional Generative Adversarial Network Prediction of the Spike Protein in SARS-CoV-2 at Various Temperatures and pH Levels
	Ashley Jisue Hong, Punahou School, Honolulu, HI
	Molecular Dynamics and Conditional Variational Autoencoder Prediction of the Spike Protein in SARS-CoV-2 at Various Temperatures and pH Levels
	Marissa Huang, Woodbridge High School, Irvine, CA
	Molecular Dynamics of Fibrinogen Binding with PLA
	Calvin Yu, Weston High School, Weston, MA **Leo Pan-Wang**, The Peddie School, Highstown, NJ **Brandon Qi**, Davis Senior High School, Davis, CA
	Reinforcement Learning Based Simulated Annealing
	Daniel Liang, Ward Melville High School, East Setauket, NY **Nathan Qiu**, Canyon Crest Academy, San Diego, CA **Qingyi (Emily) Jiang**, Shenzhen College of International Education, Shenzhen, China

	Sequential backmapping: Stepwise reconstruction of all-atomic configurations from coarse-grained structures **Erin Wong**, Great Neck South High School, Great Neck, NY
	Binding Dynamics of SARS-CoV-2 Spike Glycoprotein to Polylactic Acid **Reilin Lyu**, Williamsville East High School, East Amherst, NY **Ruoshui (Rochelle) Sun**, Beijing National Day School, Beijing, China
	ProLiDE: A comprehensive AI-driven approach with multi-source biological data integration for enhanced drug discovery and optimization **Zeyu (Peter) Yao**, Stamford American International School, Singapore
	Session 3b: CT Segmentation
	Using Landmark Detection to Identify Maturation Stage of Cervical Vertebrae in Cone Beam Computed Tomography Scans **Aaryan Vira**, North Shore High School, Glen Head, NY
	Plant Root Morphology Analysis and 3D Printed Dental Models Dimensional Accuracy Evaluation for Clear Aligners via Computed Tomography and Image Processing Tools **Xinyan (Ava) Zhou**, Bellport High School, Bellport, NY **Sichen (Theresa) Liu**, Shanghai Foreign Language School Affiliated to SISU, Shanghai, China
	Deep Learning-Based CT Volumetry for Maxillary Sinus Segmentation in Patients with Mucus Infections and Mucosal Retention Cysts **Niranjana Sankar**, Monta Vista High School, Cupertino, CA **Thomas Lin**, The Stony Brook School, Stony Brook, NY
11:10 AM	**Session 4: Robotics** **Chair: Eugene Jiang**
	Face Digital Image Speckle Correlation (DISC) Application as a Non-Invasive, Accessible Tool to Detect Acoustic Neuroma **Corey Zhang**, Eastlake High School, Sammamish, WA **Yoonsoo (Leah) Song**, Maclay School, Tallahassee, FL **Jerry Gu**, Princeton International School of Mathematics and Science, Princeton, NJ **Shreyaa Sanjay**, West Windsor-Plainsboro High School North, Plainsboro, NJ **Zihan (Jenny) Jia**, The Experimental High School Attached to Beijing Normal University, Beijing, China
	Demonstration Acquisition System for Complex Manipulation Tasks **Ishita Banerjee**, The Academy For Math, Science & Engineering, Rockaway, NJ **Sadie Seulal**, South Side High School, Rockville Centre, NY
	Utilizing Machine Learning to Inform Tomato Harvesting in Containerized Vertical Farming **Megan Chan**, Great Neck South High School, Great Neck, NY

11:20 AM	Video Presentation
11:23 AM	**Session 5: Materials Under Extreme Conditions** **Chairs: Michael Lotwin & Philip Colman**
	Silica Aerogels: A Review of Synthesis and Application in Hydrogen Storage **Brianna Zheng**, BASIS Independent Silicon Valley, San Jose, CA **Seohee (Ella) Park**, Dwight School Seoul, Seoul, South Korea **Leo Pan-Wang**, The Peddie School, Highstown, NJ
	Assessing the Impact of Polydispersity on the Thickness of Polystyrene Thin Films to Adapt a Monodisperse Polystyrene Machine Learning Model **Dhruva Bhat**, Foothill High School, Pleasanton, CA **Dvita Bhattacharya**, Kent Place School, Summit, NJ **Isabelle Chan**, DeBakey High School for Health Professions, Houston, TX **Aditi Kiran**, BASIS Independent Fremont, Fremont, CA **Eli Krasnoff**, The Loomis Chaffee School, Windsor, CT **Brenna Ren**, The Harker School, San Jose, CA
	Microstructural Analysis of Mechanically-Alloyed Tungsten-Titanium-Chromium Microstructural Analysis of Ultra-High Temperature Ceramics: Tungsten Carbide and Vanadium Carbide **Silas Dorsky**, High School for Math Science & Engineering at the City College of New York, New York, NY **Jhen-Bahn (Benjamin) Li**, Northern Valley Regional High School at Demarest, Demarest, NJ **Daniel Lim**, Staten Island Technical High School, Staten Island, NY **Ruoheng (Sylvie) Liu**, Hefei Thomas School, Hefei, Anhui, China **Brandon Qi**, Davis Senior High School, Davis, CA **Bowen Tian**, College Station High School, College Station, TX
11:33 AM	**Session 6: Clean Energy Generation** **Chairs: Oluomachi Uwakwe & Leela Sotsky**
	Optimization of Aquivion Proton Exchange Membrane Fuel Cells with Synthesized Graphene Oxide **Indus Boddu**, High Technology High School, Lincroft, NJ **Dylan Deng**, Westview High School, San Diego, CA **Maya Puterman**, Ramaz Upper School, New York, NY
	Enhancing AEM Fuel Cell Performance Using Partially Reduced Graphene Oxide **Eva Jain**, Tesla STEM High School, Redmond, WA **Amanda Liu**, Redlands High School, Redlands, CA **Ella Wunderlich**, The Pingry School, Basking Ridge, NJ **Evan Xie**, Deerfield Academy, Deerfield, MA

	Improving Proton Exchange Membrane Fuel Cells by Thiol-Capped Silver Nanoparticles **Yuchen Bai**, Experimental High School Attached to Beijing Normal University, Beijing, China **Hongfan (James) Deng**, Hefei Thomas School, Hefei, China **Evan Ji**, Del Norte High School, San Diego, CA **Cynthia Qian**, Jericho High School, Jericho, NY
	Microgrid Design for Energy-Independence in the Shinnecock Nation **Vinav Shah**, The Pingry School, Basking Ridge, NJ **Nathan Qiu**, Canyon Crest Academy, San Diego, CA **Qingyi (Emily) Jiang**, Shenzhen College of International Education, Shenzhen, China **Zihan (Jenny) Jia**, The Experimental High School Attached to Beijing Normal University, Beijing, China
11:45 AM	## Session 7: Nanocomposites **Chairs: Katherine Martinez & Cathy Reyes**
	Compatibilizing Recycled Polymer Blends **Damien Crowley**, Wantagh High School, Wantagh, NY **Brianna Zheng**, BASIS Independent Silicon Valley, San Jose, CA
	Sustainable Fabrication of Silver Nanoparticles on Functionalized Cotton Fibers **Runjing Guo**, The Experimental High School Attached to Beijing Normal University, Beijing, China
11:50 AM	## Session 8: Antibacterial Devices **Chair: Zoe Katevatis**
	An Innovative Injectable, Retrievable, and Sustainable Drug Delivery System for Endodontic Therapy **Aadi Bordia**, Archimedean Upper Conservatory, Miami, FL **Shuyi (Candy) Deng**, YK Pao School, Shanghai, China **Eli Krasnoff**, The Loomis Chaffee School, Windsor, CT **Jingwen (Linda) Liang**, Experimental High School Attached to Beijing Normal University, Beijing, China **Brenna Ren**, The Harker School, San Jose, CA **Mira Setia**, New Providence High School, New Providence, NJ
	Effects of graphene oxide and partially reduced graphene oxide on Escherichia Coli and Staphylococcus aureus **Sichen (Theresa) Liu**, Shanghai Foreign Language School Affiliated to SISU, Shanghai, China **Ariel (Ari) Khavulya**, Rambam Mesivta, Lawrence, NY **Anastasiia (Nastia) Bezugla**, American International School Salzburg, Salzburg, Austria
11:56 AM	## Session 9: Molecular Models for Thrombosis **Chairs: Nikita Karnik & Jonathan Xavier**

	Utilizing Machine Learning to Analyze the Effects of PI3K Inhibitor TGX-221 on Shear-Mediated Platelet Kinematics and Adhesion **Aryan Agahtehrani**, duPont Manual High School, Louisville, KY **Isabelle Chan**, DeBakey High School for Health Professions, Houston, TX **Vincent Lo**, Evergreen Valley High School, San Jose, CA
	Partially Reduced Graphene Oxide as a Promoter of Thrombin Activity and Fibrinogen Clot Formation **Rong (Jennifer) Gao**, Shanghai Pinghe School, Shanghai, China **Emily Zhang**, Roy C. Ketcham Senior High School, Wappingers Falls, NY
	Differential Impacts of Hyperglycemia and P12 Inhibition on Fibrin Formation and Thrombosis -- Impact of Surface Hydrophobicity on Fibrinogen Adsorption and Thrombosis Development -- The Role of Viral Infections in Modulating Cell Surface Thrombosis **Aryan Agahtehrani**, duPont Manual High School, Louisville, KY **Isabelle Chan**, DeBakey High School for Health Professions, Houston, TX **Payton Fromm**, Smithtown High School West, Smithtown, NY **Vincent Lo**, Evergreen Valley High School, San Jose, CA **Hunter Maguire**, Garden City High School, Garden City, NY **David Sun**, Joseph A. Gregori High School, Modesto, CA **Dylan Wang**, Trinity Preparatory School, Winter Park, FL **Xinyu (Daniel) You**, Western Reserve Academy, Hudson, OH **Calvin Yu**, Weston High School, Weston, MA
12:10 PM	## Session 10: Tissue Engineering **Chairs: Brooklyn Ratel & Divleen Singh**
	Determining the Correlation between Aging and Cellular Mechanics **Ananya Anand**, Johns Creek High School, Johns Creek, GA **Jerry Gu**, Princeton International School of Mathematics and Science, Princeton, NJ **Zihan (Jenny) Jia**, The Experimental High School Attached to Beijing Normal University, Beijing, China **Viraj Pahuja**, The Wheatley School, Old Westbury, NY **Shreyaa Sanjay**, West Windsor-Plainsboro High School North, Plainsboro, NJ **Theodora (Thea) Siu**, Ward Melville High School, East Setauket, NY **Jenny Dinh Nhu Zhang**, Renaissance International School Saigon, Ho Chi Minh City, Vietnam
	Effects of Titanium Dioxide Nanoparticles on UV-Exposed Human Dermal Fibroblasts **Aryan Agahtehrani**, duPont Manual High School, Louisville, KY **Isabelle Chan**, DeBakey High School for Health Professions, Houston, TX **Payton Fromm**, Smithtown High School West, Smithtown, NY **Vincent Lo**, Evergreen Valley High School, San Jose, CA **Hunter Maguire**, Garden City High School, Garden City, NY **David Sun**, Joseph A. Gregori High School, Modesto, CA **Dylan Wang**, Trinity Preparatory School, Winter Park, FL **Xinyu (Daniel) You**, Western Reserve Academy, Hudson, OH **Calvin Yu**, Weston High School, Weston, MA

	Evaluating the Effect of TiO2 on Angiogenesis and Anastomosis During Wound Healing on Mice Models **Yoonsoo (Leah) Song**, Maclay School, Tallahassee, FL **Corey Zhang**, Eastlake High School, Sammamish, WA **Ananya Anand**, Johns Creek High School, Johns Creek, GA **Jerry Gu**, Princeton International School of Mathematics and Science, Princeton, NJ **Zihan (Jenny) Jia**, The Experimental High School Attached to Beijing Normal University, Beijing, China **Viraj Pahuja**, The Wheatley School, Old Westbury, NY **Shreyaa Sanjay**, West Windsor-Plainsboro High School North, Plainsboro, NJ **Theodora (Thea) Siu**, Ward Melville High School, East Setauket, NY **Jenny Dinh Nhu Zhang**, Renaissance International School Saigon, Ho Chi Minh City, Vietnam
	Enhancing Osteogenic Differentiation of Dental Pulp Stem Cells via Iron Oxide Nanoparticles in Static Magnetic Field **Dvita Bhattacharya**, Kent Place School, Summit, NJ **Rohan Hablani**, Arnold O. Beckman High School, Irvine, CA **Alice He**, Phillips Academy, Andover, MA **Matthias Kim**, Interlake High School, Bellevue, WA
12:20 PM	# Session 11: Biopolymers ## Chairs: Cosmo Perfetti & Craig Chen
	Chemical Characterization of Rhizobium Tropici Ethanol Precipitated Materials (Rt EPM) and Modeling the Rt EPM-clay interactions **Zheming (Dennis) Xu**, High School Affiliated to Renmin University of China, Beijing, China **Shede (Dorothy) Zhang**, Beijing National Day School, Beijing, China
	Assessing the Effect of Nanofillers on Polyelectrolyte Hydrogels **Keyu (Corin) Wang**, Beijing National Day School, Beijing, China **Vinav Shah**, The Pingry School, Basking Ridge, NJ **Laura Zhang**, Great Neck South High School, Great Neck, NY
	Rhizobium Tropici-Produced EPS Biopolymer: Analyzing Its Influence on Gene Expression in Arabidopsis Thaliana **Christian Chan**, South Side High School, Rockville Centre, NY **Michelle Guo**, Tesoro High School, Las Flores, CA **Tei Kim**, Stanford Online High School, Redwood City, CA **Arohi Mahajan**, Cambridge International Foundation School, Jalandhar, Punjab, India **Seohee (Ella) Park**, Dwight School Seoul, Seoul, South Korea **Emily Tarrab**, Yeshivah of Flatbush Joel Braverman High School, Brooklyn, NY
	Analyzing the Rheology of a Rhizobium tropici-produced entangled exopolysaccharide and Its Effect on Soil Stability **Damien Crowley**, Wantagh High School, Wantagh, NY
12:35 PM	*Gala Luncheon provided by Wing Wan of West Hempstead*

Session I:
DNA Segmentation

Daniel Liu and Patrick Lewis
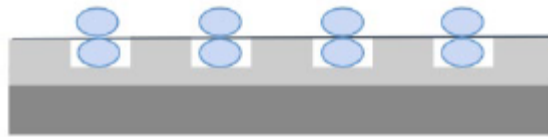
Fig.1 Tn5-bound DNA stretched over pre-developed PMMA grid.

A Novel Approach for Ordered Fragmentation of Mouse DNA Using Tn5 Transposase

Alice Hu[1†], Aditi Kiran[2†], Kevin Lee[3†], Elena Mingorance[4†], Stella Song[5†], Kevin Zhang[6†], Navya Gautam[7†], Patrick Lewis[8†], Danielle Liu[9†], Jonathan Sokolov[8], Miriam Rafailovich[8]

[1] King High School, FL, 33610, [2] BASIS Independent Fremont, CA, 94539, [3] The Albany Academies, NY, 12208, [4] South Side High School, NY, 11570, [5] Phillips Exeter Academy, NH, 03833, [6] North Hunterdon High School, NJ, 08801, [7] Duke University, NC, 27708, [8] Stony Brook University, NY, 11794, [9] University of Pennsylvania, PA, 19104

Genome reassembly has posed an enormous computational challenge to Next-Generation Sequencing (NGS) and Whole-Genome Sequencing (WGS) due to the formation of chimeric sequences and fragmented contigs without a complete reference genome. To address this, the project utilizes the *E. coli* transposase Tn5, which has an artificially modified 19-base pair recognition site for DNA binding and
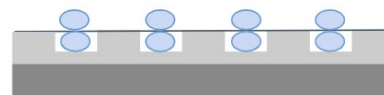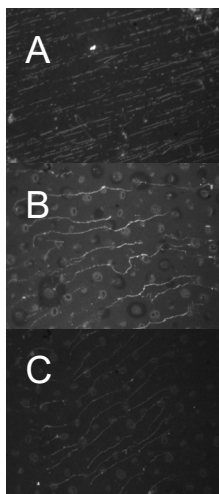

Fig.1 Tn5-bound DNA stretched over pre-developed PMMA grid.

cleaving [1]. This allows for the attachment of unique barcodes and labels, such as PCR handles, to DNA, indicating each fragment's spatial origin and order, which is essential for accurate post-sequencing genome assembly. Thus, we hypothesize that ordered fragmentation can be achieved by stretching Tn5-bound DNA over UV-patterned polymethylmethacrylate (PMMA) surfaces (**Fig. 1**), activating Tn5 for cleavage, and then using proteinase K to digest the Tn5 with minimal disturbance.

Molecular combing was used to stretch DNA across a hydrophobic PMMA surface with developed UV patterns that provide steric clearance for Tn5 binding and cleaving while limiting loss of genetic

Fig. 2 A) Control 0.5% DNA post-digestion B) 8uL Tn5-bound DNA pre-digestion C) B post-digestion

information. Such surfaces were created by spin casting 996K PMMA dissolved in 25 to 100 mg/mL of toluene on clean silicon wafer squares at 2500 rpm. PMMA was chosen for its compatibility with DNA and ability to serve as a positive photoresist under UV exposure of wavelength 254 nm. UV patterns were created using 1000 or 2000 mesh copper grids of various shapes and then developed in solutions of 7:3 isopropyl alcohol:water. During development, the shorter-chained, exposed PMMA was washed away, leaving "wells" over which Tn5-bound DNA can stretch. To find the optimal conditions for DNA cleaving, the Tn5-DNA solutions were prepared using various concentrations of mouse DNA (2, 4, and 8uL) mixed with 10uL of Tn5. Solutions were then heated to 55°C for 7 minutes to activate the Tn5 cleaving of target DNA sequences. Using a stepper motor with a linear stage, we dipped the predeveloped patterned PMMA-coated silicon wafer into the activated Tn5-DNA solutions to stretch the DNA across the grid. After cutting, a 1.41% V/V proteinase K solution in DNase I buffer was used to digest the Tn5 from the stretched DNA [2].

Fluorescence microscopy, with SyBr Gold dye staining of DNA, was performed to test the efficacy of Tn5-DNA solutions and proteinase K for ordered fragmentation. A control sample with stretched DNA without Tn5 was run, which confirmed that the presence of proteinase K does not disturb the DNA (**Fig. 2A**). Then, a comparison of a marked location on the patterned PMMA pre- and post-proteinase K deposition was imaged using samples with either 2, 4, or 8uL Tn5-bound DNA. Post-proteinase K deposition, the 8uL sample showed notably successful Tn5 cleaving of DNA. However, a dimming of DNA strands was observed, which was likely due to the weakening of dye or the lifting off of dye molecules (see **Fig. 2B** vs. **Fig. 2C**). Image analysis shows several cleave sites along singular DNA strands, suggesting that future studies may investigate the optimal proteinase K concentration for Tn5 digestion and the optimal fragmentation density.

[1] Li, N., Jin, K., Bai, Y., Fu, H., Liu, L., & Liu, B. (2020). Tn5 Transposase Applied in Genomics Research. *International journal of molecular sciences*, *21*(21), 8329. https://doi.org/10.3390/ijms21218329

[2] Righini, M., Costa, J., & Zhou, W. (2021). DNA bridges: A novel platform for single-molecule sequencing and other DNA-protein interaction applications. *PloS one*, *16*(11), e0260428. https://doi.org/10.1371/journal.pone.0260428

A Novel Method for UV Thin-Film Backside Development for Ordered DNA Fragmentation

Kevin Zhang[1,2 †], Stella Song[1,3 †], Elena Mingorance[1,4], Kevin Lee[1,5], Aditi Kiran[1,6], Alice Hu[1,7], Danielle Liu[8], Patrick Lewis[1], Navya Gautam[9], Jonathan Sokolov[1], Miriam Rafailovich[1]
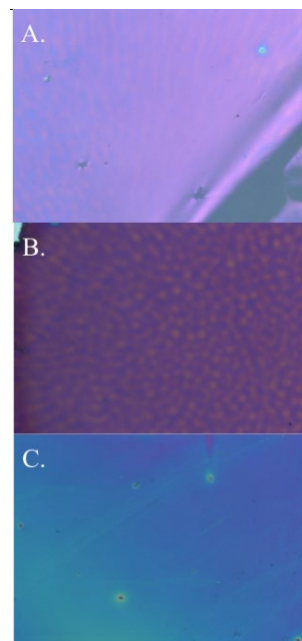
[1] Stony Brook University, NY, 11794, [2] North Hunterdon High School, NJ, 08801, [3] Phillips Exeter Academy, NH, 03833, [4] South Side High School, NY, 11570, [5] The Albany Academies, NY, 12208, [6] BASIS Independent Fremont, CA, 94539, [7] King High School, FL, 33610, [8] University of Pennsylvania, PA, 19104, [9] Duke University, NC, 27708

Alternative DNA sequencing methods are necessary to overcome shortcomings specific to conventional sequencing methodologies—most critically, these methods are unable to sequence long sections of DNA due to the loss of order of DNA fragments during PCR. The *E. coli* compound transposon Tn5 was chosen to investigate cutting of mouse DNA because of its ability to add unique barcodes to target sequences, which facilitates ordered DNA fragmentation and accurate genome assembly. However, the transposase is unable to dimerize when DNA is fixed to the polymer surface [1]. Thus, DNA bridging, which is the process of suspending singular strands of DNA across wells on a patterned polymer surface, was used to create steric clearance for Tn5 adsorption [2]. UV radiation was used to create wells on thin poly(methyl methacrylate) (PMMA) films spun on silicon wafers. Samples were dipped in mouse DNA for molecular combing, then developed in a 7:3 isopropyl alcohol(IPA):water solution, followed by a water bath, to wash away exposed PMMA regions. However, fluorescence microscopy pre- and post-development showed that IPA significantly disturbs DNA deposition, likely due to DNA precipitation. Therefore, we aim to optimize a novel "backside" development method to minimize such disturbance, as the developer would ideally never come into prolonged contact with DNA.

To prepare for backside development, a 0.5" x 0.5" silicon wafer square was coated with a bottom layer of 4% polyvinyl alcohol (PVA) and a top layer of 996K PMMA. The wafer was submerged in distilled water to dissolve the PVA layer, allowing for the remnant PMMA to "float" off onto the water's surface. Then, the floating PMMA layer was deposited onto a separate silicon wafer with a 3mm hole in the center, which allows IPA to develop exposed PMMA from below. Varying concentrations of PMMA (20, 50, and 100 mg/mL) were used to determine the optimal conditions for floating. Afterward, a copper mesh grid was placed onto the PMMA thin film and developed under a UV light source of 100mA for a varying number of hours (3 hr, 4 hr, 4.5 hr, 5 hr, 6 hr). The samples were then dipped and developed.

Fig. 1. A) Floated 996K PMMA 3 hour exposure 1000 hex mesh. B) Floated 996K PMMA 4 hour exposure 2000 square mesh. C) Floated 996K PMMA 5 hour exposure 2000 square mesh

Initial trials used PMMA at a concentration of 20 mg/mL. However, the films proved to be too thin and teared under all UV light exposure times due to the copper grids sticking to the film. Thus, higher concentrations of PMMA with 50 mg/mL solutions were used. Imaging demonstrated that visible grid patterns were achievable with all UV light exposure times, except for 6 hours, where the PMMA thin film teared (**Fig. 1**). However, the majority of the 50 mg/mL PMMA thin films advanced to the dipping but collapsed or tore at the developing stage. Current trials of 100 mg/mL concentration PMMA thin films have been exposed for 4.5 hours and have remained viable up to the dipping stage.

[1] Li, N., Jin, K., Bai, Y., Fu, H., Liu, L., & Liu, B. (2020). Tn5 Transposase Applied in Genomics Research. International journal of molecular sciences, 21(21), 8329. https://doi.org/10.3390/ijms21218329

[2] Cho, N., Goodwin, S., Budassi, J., Zhu, K., McCombie, W. R., & Sokolov, J. (2017). Fragmentation of Surface Adsorbed and Aligned DNA Molecules Using Soft Lithography for Next-generation Sequencing. *Journal of Biosensors & Bioelectronics*, *08*(03). https://doi.org/10.4172/2155-6210.1000247

[3] Li, N., Jin, K., Bai, Y., Fu, H., Liu, L., & Liu, B. (2020). Tn5 Transposase Applied in Genomics Research. International journal of molecular sciences, 21(21), 8329. https://doi.org/10.3390/ijms21218329
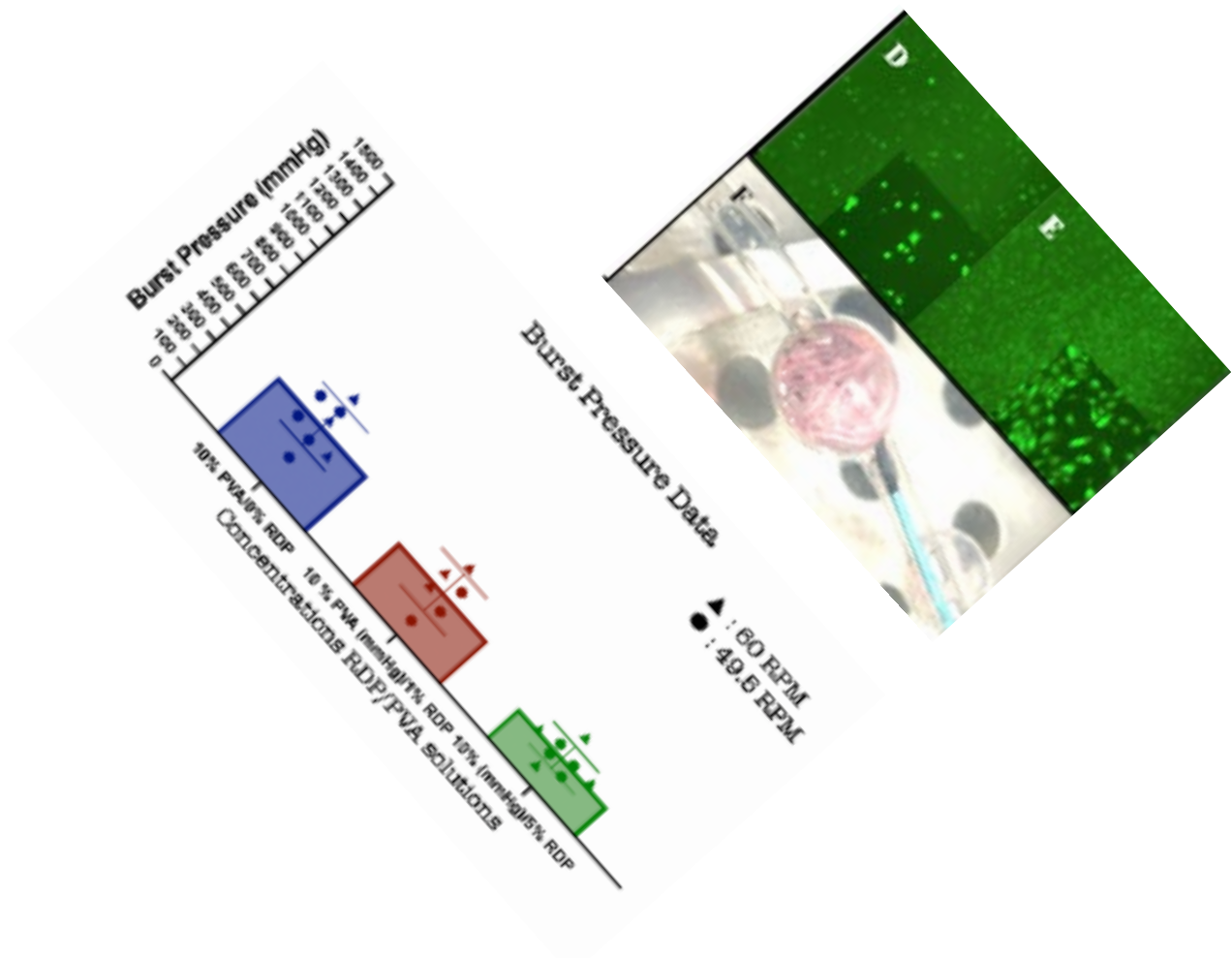
Session II:
3D Printing of Vascular Devices

Robert Wong and Aaron Sloutski

Characterizing Mechanical Properties of Poly(vinyl alcohol) and Resorcinol Diphenyl Phosphate Blend Vascular Grafts

Risa Rogers[1], Joseph Yung[2], Dhruva Bhat[3], Leora Stochel[4], Grace Kyoko Wong[5], Kevin Wu[6], Robert Wong[7], Aaron Sloutski[7], Chander Sadasivan[8], Miriam Rafailovich[7]

[1] Schechter School of Long Island, Williston Park, NY, 11596, [2] Georgetown Preparatory School, 10900 Rockville Pike, MD 20852, [3] Foothill High School, 4375 Foothill Rd, CA 94588, [4] University of Massachusetts Amherst, Amherst, MA 01003, [5] University of Oxford, Oxford, UK, [6] SUNY Geneseo, Geneseo, NY, [7] Department of Materials Science and Chemical Engineering, Stony Brook University, Stony Brook, NY 11794, [8] Department of Neurological Surgery, Stony Brook University Medical Center, Stony Brook, NY 11794

Poly(vinyl alcohol) (PVA), due to its biocompatibility and mechanical properties, has been found to be a potential candidate material for constructing vascular grafts used *in vivo* and for modelling brain aneurysms [1, 2]. However, limited by their lack of cell adhesion, PVA grafts currently remain inapplicable to humans, but could be improved by the addition of Resorcinol Diphenyl Phosphate (RDP) clay [3]. RDP has previously been successful in enhancing the mechanical and cell adhesion properties of other polymers [3]. This research aims to characterize the effect of different concentrations of RDP on the properties of PVA vascular grafts and optimize its synthesization methodology.

Previous researchers devised a three-step process to form the vascular grafts [2]. First, 10% (w/w) PVA solutions with 0%, 1% and 5% (w/w) RDP intermediate solutions were crosslinked by adding 15% (w/w) sodium trimetaphosphate (STMP) and 30% (w/w) sodium hydroxide (NaOH) aqueous solutions drop-wise. After magnetically stirring the PVA/RDP solutions overnight, a single-axis spinner was set up, and wax rods of 2 mm diameter were dip-coated into the solutions and spun for 15 minutes, a process which was repeated ten times, and then left overnight to dry. The grafts were cut into 2.5 cm pieces to test burst pressure with a PG-5 Digital Pressure Gauge, and the thickness and diameter of the grafts were measured using a Keyence VHX-7000 microscope.
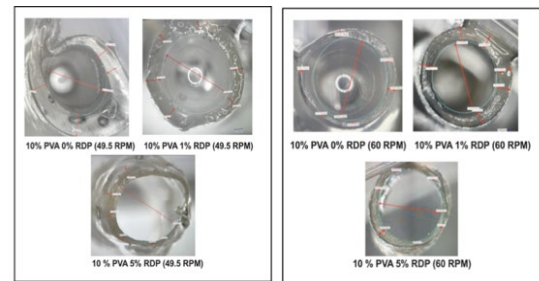
Figure 1: Keyence microscope imaging of 49.5 RPM and 60 RPM of all RDP/PVA concentrations
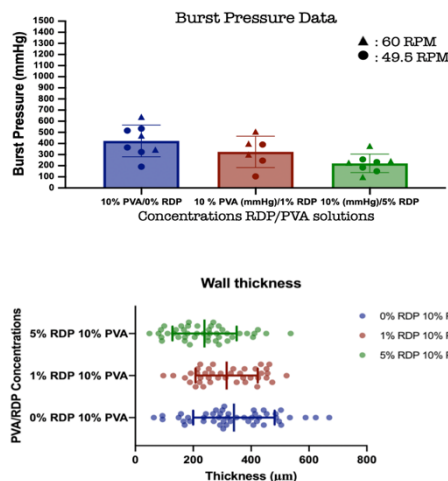
Figure 2: Top graph plots the indivudal values, mean and standard deviation of each RDP concentration in respective to the different RPMs. Bottom graph plots the indivudal wall thickness values, its mean and standard deviation of the varying RDP concentrations.

During vessel production, it was observed that spinning the wax rods at 49.5 rotations per minute (rpm)—the previous methodology developed—produced non-uniform vessels that lacked consistency in wall thickness [2]. Attributing this phenomenon to an insufficiently high spin rate, the motor was set to spin at 60 rpm and compared to 49.5 rpm. The diameter distributions of 60 rpm grafts (0% RDP: 1820.8 ± 207.8 μm, 1% RDP: 1974.495 ± 134.8 μm, 5% RDP: 2078.03 ± 109.7 μm) had a smaller standard deviation and were mostly closer to the desired 2000 μm as opposed to 49.5 rpm (0% RDP: 1845.7 ± 412.4 μm, 1% RDP: 1425.6 ± 274.5 μm, 5% RDP: 1497.1 ± 504.3 μm). For in vivo applications, burst pressure values must be well above physiological blood pressures. Higher burst pressure values were also generally observed with the increase in rpm (Mean of 49.5 rpm: 0% RDP: 382.4 mmHg, 1% RDP: 247 mmHg, 5% RDP: 206.3 mmHg. 60 rpm: 0% RDP: 492.3 mmHg, 1% RDP: 402.7 mmHg, 5% RDP: 237.5 mmHg); When 49.5 rpm and 60 rpm vascular grafts were imaged under the Keyence microscope, a notable difference in increased uniformity was detected. The grafts, both qualitatively and quantitatively, showed increased uniformity and enhanced properties that better resembled human vasculature. The underlying mechanism for this effect is likely caused by the heightened drying speed of the PVA solution surrounding the wax rod, which decreases fluid motion across the rod and increased uniformity. In addition, the diameter, wall thickness, and burst pressure of the vessels decreased as the RDP concentration increased, although 0% and 1% RDP exhibited greater similarity in properties (Figure 2). The decreased burst pressure can be attributed to the increased pinhole leaks as RDP concentration increases, and the variance in diameter and wall thickness can potentially be explained by the difference in swelling factors.

Assessing the current data, it can be concluded that 60 rpm is the optimal spin rate for dip-coating vascular grafts. With the relative similarity of the mechanical properties of 1% RDP and 0% RDP grafts, as opposed to the 5% RDP grafts, cell proliferation results and suture retention analysis—currently being obtained—will further validate our hypothesis that 1% RDP may be the optimal concentration.

[1] Conconi, M. T., et al. (2014). Evaluation of Vascular Grafts Based on Polyvinyl Alcohol Cryogels. Molecular Medicine Reports.

[2] Oh et al. (2023). Mechanical Characterization of Poly(vinyl alcohol) and Resorcinol Diphenyl Phosphate Clay Blend Vascular Grafts. Materials Research Society Fall Meeting.

[3] Feng K-C, et al. (2018). Investigating the Effects of Different Spun-Cast and Molded Polylactic Acid (PLA) and Polystyrene (PS) Composites on the Proliferation Differentiation and Biomineralization of Dental Pulp Stem Cells. Materials Research Society Fall Meeting.

Developing a Novel Method for the Production of Poly(vinyl alcohol) Vascular Grafts

Joseph Yung[1], Grace Kyoko Wong[2], Robert Wong[3], Aaron Sloutski[3], Chander Sadasivan[4], Miriam Rafailovich[3]

[1]Georgetown Preparatory School, 10900 Rockville Pike, MD 20852, [2]University of Oxford, Oxford, UK, [3]Department of Materials Science and Chemical Engineering, Stony Brook University, Stony Brook, NY 11794, [4]Department of Neurological Surgery, Stony Brook University Medical Center, Stony Brook, NY 11794

Poly(vinyl alcohol) (PVA) is a promising candidate material for use in *in vivo* vascular grafts for brain aneurysm treatment due to its non-toxicity, biocompatibility and tuneable mechanical properties [1]. To produce the vascular grafts, we utilize a three-step process. However, multiple limitations are associated with this existing methodology due to its time-consuming nature and failure to deliver optimal consistency and uniformity in wall thickness, diameter, and burst pressure values, which inhibits quality mass-production of vascular grafts for *in vivo* applications. This study aims to adapt a more consistent and efficient approach of using radical crosslinkers to increase PVA vascular graft quality and production efficiency.

PVA-MA, which is synthesized along with isocyanatoethyl methacrylate (IEMA), contains carbon-carbon double bonds in the methacrylate groups that could be radically crosslinked with Ammonium Persulfate (APS) and methylethylenediamine (TEMED), of which the crosslinking duration could be manipulated by APS and TEMED concentrations [2,3,4]. To examine the viability of using such a method, the optimal APS concentration was determined using a Kinexus Pro + rheometer (Netzsch), and an enlarged version of a blood vessel was produced by crosslinking 20% PVA-MA, 50mg/ml APS, and 4% TEMED in a temporary vessel mold. Imaged and measured under a Keyence VHX-7000 microscope, the wall thickness (674.5 ± 44.82 μm) is observed to be more uniform (Figure 1) compared to the traditional 0% RDP 10% PVA dip-coating method (346.81 ± 88.488 μm).
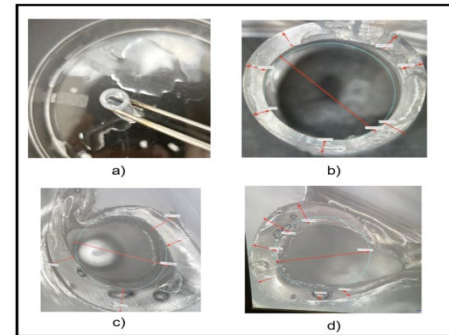
Figure 1: a) and b): Vascular graft synthesized with 20% PVA-MA crosslinked with 50mg/ml APS + 4% TEMED with enlarged vessel mold. c) and d): Vascular grafts synthesized using tradional dip coating method
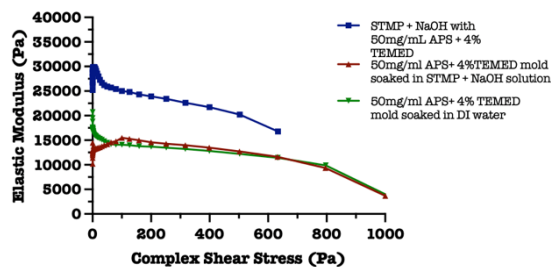
Figure 2: Elastic Modlulus (Pa) plotted agaisnt complex shear stress (Pa) for different crosslinking processes

However, the APS + TEMED crosslinked PVA exhibited gel-like properties, lacking the desired elasticity and strength achieved by the dip coated vascular grafts with an average elastic modulus of 35 kPa [3]. The existing crosslinking process for the three step process utilizes Sodium trimetaphosphate (STMP) and Sodium hydroxide NaOH to undergo phosphoesterification with the PVA hydroxyl groups. Therefore, to enhance the mechanical properties of the APS + TEMED crosslinked vascular grafts, dual crosslinking was attempted (Figure 2). Oscillatory amplitude sweeps (0.1 to 1000 Pa stress range at 37°C) were conducted with Kinexus Pro + Rheometer (Netzsch) to test their properties. The gel crosslinked with STMP + NaOH (50 mg/ml APS) exhibited the greatest similarity in properties to the original method, but failed to gel within the desired timeframe. APS concentrations of 100mg/ml, 333.3mg/ml, 400mg/ml and 500mg/ml were then tested with STMP +NaOH and 4% TEMED. Gelation was induced within 10 min for 333.3mg/ml of APS, and both 400mg/ml APS and 500mg/ml APS gelled within 1 min. The mechanical properties of each are currently being assessed.

The radical crosslinking process was then refined as follows: the designated amount of 20% PVA-MA was first added into a glass vial, and for every gram of PVA in solution, 0.033ml STMP was added, followed by 0.3 ml of APS and 0.0833ml NaOH. The solution was mixed for 1-2 seconds with a vortex machine at a low spin rate. 0.3 ml of TEMED per gram of PVA was then added, vortexed for 1-2 seconds, and immediately inserted into the vessel mold with a pipette, releasing the solution from the bottom of the mold upwards to prevent air bubbles. The grafts were dried overnight and rehydrated.

Results of our study indicate significantly improved production time and uniformity of the radical crosslinking method and show promising efficiency and consistency for large scale, patient-specific production of vascular grafts for *in vivo* applications after further testing of mechanical and cell adhesion properties. Future work includes testing solutions with different Resorcinol Diphenyl Phosphate (RDP) concentrations to improve cell adhesion properties and refining the APS and STMP + NaOH concentrations for optimal mechanical properties.

[1] Adelnia et al. (2022). Freeze/thawed polyvinyl alcohol hydrogels: Present, past and future. *European Polymer Journal.*

[2] Oh et al. (2023). *Mechanical Characterization of Poly(vinyl alcohol) and Resorcinol Diphenyl Phosphate Clay Blend Vascular Grafts. Materials Research Society Fall Meeting.*

[3] Zarket et al. (2021). Multilayer Tubes that Construct, Dilate, and Curl in Response to Stimuli. *Soft Matter.*

[4] Goldvaser, M et al (2022). *Poly(vinyl alcohol)-methacrylate with CRGD peptide: A photocurable biocompatible hydrogel. Journal of tissue engineering and regenerative medicine, 16(2), 140–150.*

Bioprinting Human Vasculature within a Collagen Gel

Ananya Anand[1*], Jerry Gu[2*], Zihan Jia[3*], Viraj Pahuja[4*], Shreyaa Sanjay[5*], Theodora Siu[6*], Jenny Dinh Nhu Zhang[7*], Brooklyn Ratel[8], Divleen Singh[9], Shi Fu[10], Huiting Luo[11], Miriam Rafailovich[12]

[1]*Johns Creek High School, Johns Creek, Georgia, 30022, [2]Princeton International School of Mathematics and Science, Princeton, New Jersey, 08540, [3]The Experimental High School Attached to Beijing Normal University, Beijing, China, 100032, [4]The Wheatley School, Old Westbury, New York, 11568, [5]West Windsor-Plainsboro High School North [6]Ward Melville High School, 380 Old Town Road, East Setauket, New York, 11733, [7]Renaissance International School Saigon, 74 Đ. Nguyễn Thị Thập, Bình Thuận, Quận 7, Hồ Chí Minh 700000, Vietnam

Angiogenesis, the formation of new blood vessels from pre-existing vasculature[1], facilitates wound healing, repair, and tissue regeneration[2]. The use of cell-delivery approaches—such as cell-loaded scaffolds or scaffold-free systems—to induce angiogenesis is thereby a potent area of study in wound healing research. However, an intense angiogenic response in the wound site is often associated with a higher risk of scar formation[3] and in more severe cases, keloid formation[4]. Our objective is to investigate a bioprinting model that enables precise regulation of the angiogenic process during wound healing.

This study explores the potential and application of bioprinting human blood vessels within collagen for improved wound healing. We used free-form printing to create vascular structures with human umbilical vein endothelial cells (HUVEC) stained with green fluorescent protein (GFP). These cells were suspended in a 3% gelatin gel and extruded through a syringe pump into a viscous collagen solution to give the researcher control over printing the blood vessels. Through repeated parameter testing of the pump, rheology of the gel, a proof-of-concept model using fibroblasts within the bioink, cell vitality assay, coupled with the ultimate use of HUVEC cells, a synthetic model of human vasculature was printed within a collagen gel.

Figure 1 illustrates the experimental setup of which the HUVEC-gelatin structure in the collagen gel was achieved. A singular vertical line of the gel/cell suspension was extruded onto each of the 3 wells as depicted. The 6-well plate was subsequently incubated at 37°C and 5% CO_2 before using an EVOS M7000
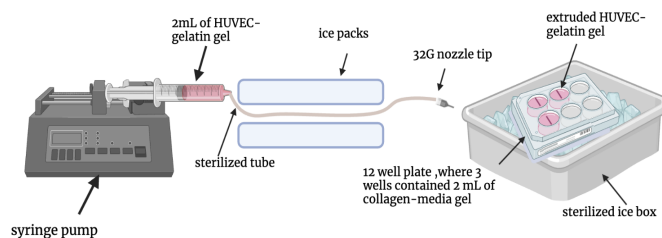

Figure 1. Procedure used to synthesize human vasculature in a collagen gel.

imaging microscope to assess whether the GFP-stained endothelial cells branched from the gelatin structure: a finding that could demonstrate the gel/cell suspension's ability to form structure akin to human vasculature. Additionally, the cell vitality assay—conducted by comparing HUVEC cells before extrusion, in the syringe, and after extrusion—provided data that further supports the possibility of synthesizing human vasculatures from HUVEC-gelatin structures within a collagen gel.

The current data and results gathered from the aforementioned experiments thus support this prospective method of synthesizing human vasculature from HUVEC-gelatin gel. This consequently provides promising results for the future plan to integrate these synthetic vasculatures into bioengineered skin grafts.

1

Cleveland Clinic. (2022, September 21). *What is angiogenesis?* Cleveland Clinic. https://my.clevelandclinic.org/health/articles/24206-angiogenesis
[2]DiPietro, L. A. (2016). Angiogenesis and wound repair: when enough is enough. *Journal of Leukocyte Biology*, *100*(5), 979–984. https://doi.org/10.1189/jlb.4mr0316-102r
[3]Lali, F., & Metcalfe, A. (2014, November 1). *The role of angiogenesis in wound healing, scarring and tissue regeneration*. The PMFA Journal https://www.thepmfajournal.com/features/post/the-role-of-angiogenesis-in-wound-healing-scarring-and-tissue-regeneration
[4]Nour, S., Imani, R., Chaudhry, G. R., & Sharifi, A. M. (2020). Skin wound healing assisted by angiogenic targeted tissue engineering: A comprehensive review of bioengineered approaches. *Journal of Biomedical Materials Research Part A*, *109*(4), 453–478. https://doi.org/10.1002/jbm.a.37105

Engineering a Reverse Thermo-Responsive Injectable Liquid Embolic Agent for Brain Aneurysm Treatment

Leah Abrahams[1*], Dhruva Bhat[2*], Shira Fisher[3*], Joshua Mu[4*], Catherine Suo[5*], Kimberly Wang[6*], Sarah Yagudayev[3*], Robert Wong[7], Miriam Rafailovich[7]

[*1]The Frisch School, [2]Foothill High School, [3]Yeshiva University High School For Girls (Central), [4]Illinois Mathematics and Science Academy, [5]Hong Kong International School, [6]Jericho Senior High School, [7]Department of Materials Science and Chemical Engineering, Stony Brook University, NY, 11794

Current treatments for brain aneurysms are unpredictable and have high mortality rates.[1] A new method uses F88 Pluronic polymer functionalized with dimethacrylate groups (F88DMA), crosslinked to form irreversible gels that can plug aneurysms. This project aimed to evaluate the mechanical, chemical, and biological properties of crosslinked F88DMA gels for aneurysm treatment.

To determine the fundamental properties of uncrosslinked gels, rheological analysis was conducted. At ~24.6°C, viscosity increase indicated micelle formation and differential scanning calorimetry confirmed this micelle formation at the same temperature **(Fig. 1B)**.

Crosslinking with ammonium persulfate (APS) and tetramethylethylenediamine (TEMED) was performed to analyze the gel mechanics of the crosslinked version. Rheological analysis with a single-frequency and temperature sweep revealed a correlation between F88DMA concentration and crosslinking time, shown by the x-value of concavity changes (**Fig.1A**). Lower concentrations resulted in longer crosslinking times, allowing for linear regression to guide the selection of F88DMA concentration based on desired crosslinking time.

Swelling experiments on crosslinked F88DMA samples investigated the effects of concentration, iohexol, static vs. flow conditions, and crosslinking temperatures. Mass swelling ratios were determined, and rheology was performed to correlate shear modulus with time. Initially, all gels swelled rapidly for three hours, then contracted over several days. Higher F88DMA concentrations led to greater swelling, while higher iohexol concentrations reduced swelling, however a combination of high iohexol and low F88DMA caused the gels to contract over time. Gels exposed to flowing saline (simulating blood flow) **(Fig.1C)** and those crosslinked below the micellization temperature showed reduced swelling.

To mimic cell adhesion in blood vessels, F88DMA hydrogels were immersed in fibrinogen before plating human umbilical vascular endothelial cells. Fibrinogen-treated gels showed significantly more well-shaped, adherent cells and supported greater proliferation **(Fig.1E)** compared to untreated gels **(Fig.1D)**. These results suggest fibrinogen enhances cell compatibility and proliferation on polymer gels, making them promising for aneurysm repair.

A stable procedure was developed to test injectability by drawing up the polymer, attaching it to a catheter, and injecting it into a model aneurysm. iohexol and simulated blood flow were added for realism. The results showed consistent gel strands inside the aneurysm, indicating a successful procedure suggesting an effective and sustainable treatment for brain aneurysms (**Fig.1F**). Future research will evaluate the long-term sustainability of F88DMA in the body, including its biocompatibility, biodegradability, and ability to withstand blood flow.
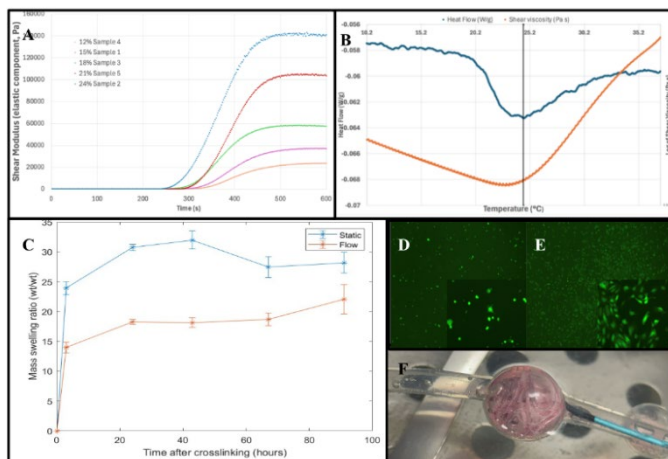
Fig. 1. (A) Elastic modulus vs. time for varying concentrations (B) Rheology and Differential Scanning Calorimetry Overlay for 18% F88DMA (C) Swelling graph of static vs. flow (D) EVOs imaging of fibrinogen treated cells (E) EVOS imaging of non-fibrinogen treated cells (F) A Successful injection trial into model aneurysm

[1] Taschner CA, Chapot R, Costalat V, Machi P, Courtheoux P, Barreau X, et al. Second-Generation Hydrogel Coils for the Endovascular Treatment of Intracranial Aneurysms: A Randomized Controlled Trial. Stroke. 2018;49(3):667-74.

Session IIIa: Theory and Simulation
Karin Hasegawa, Ziyuan Niu, Giorgios Kementzidis
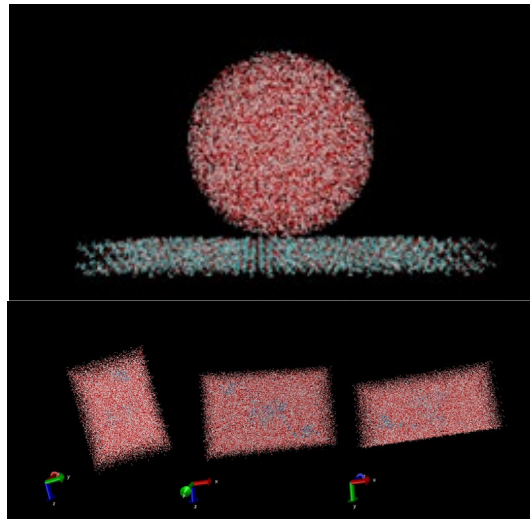
**Figure 2:** Solvated box of water around e-domain

An integrated *in silico* approach for AI-enhanced discovery of novel eIF4E inhibitors targeting drug-resistant ER+ breast cancer

Audrey Huang[1], Xingchuan Ma[2], Zeyu Yao[3], Karin Hasegawa[4], Yuefan Deng[4]

[1]Woodbridge High School, Irvine, CA 92604, [2]Portsmouth Abbey School, Portsmouth, RI, 02871, [3]Stamford American International School, Singapore 357684, [4]Department of Applied Mathematics and Statistics, Stony Brook University, Stony Brook, NY 11790

Eukaryotic translation initiation factor 4E (eIF4E) plays a critical role in regulating protein synthesis, with its overexpression particularly implicated in drug-resistant estrogen receptor-positive (ER+) breast cancer, a form of cancer known for its resistance due to numerous genetic and epigenetic aberrations [1,2]. Due to its interaction with the 5' cap structure of mRNA for the translation of oncogenes and survival proteins (Fig. 1), inhibiting the cap-eIF4E interaction has emerged as a promising target for drug development [3]. However, despite significant advances in our understanding of eIF4E, developing effective inhibitors remains a challenge due to protein dynamics and the need to avoid off-target effects.
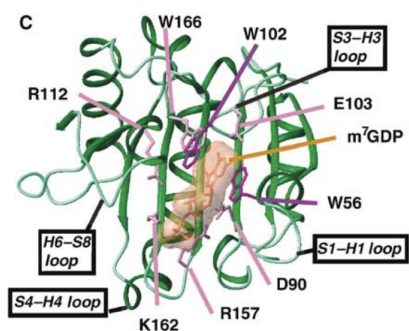
Figure 1: Binding of eIF4E to the mRNA cap (m7GTP)[5].

In this study, we propose an integrated *in silico* approach using AI-driven drug discovery techniques to identify novel inhibitors targeting both non-covalent and covalent binding interactions with eIF4E. For the discovery of non-covalent inhibitors, we prepared and preprocessed two comprehensive datasets from the CheMBL database: a general dataset and a targeted dataset. Using an autoencoder, we converted the SELFIES representations of the molecules into latent vectors. These latent vectors were then utilized in transfer learning to train a Wasserstein GAN with Gradient Penalty (WGAN-GP), a WGAN-GP paired with a Genetic Algorithm (GA), and a WGAN-GP paired with a Pareto-based Genetic Algorithm (PGA) on the datasets. Additionally, Neural Networks and Random Forests were trained as QSAR models to predict the pIC50, MW, and LogP of compounds in conjunction with the GA and PGA. The WGAN-GP models will generate 250,000 unique compounds each, with the generated compounds undergoing molecular docking simulations using AutoDock Vina. The top-ranked compounds from the docking studies will be further validated through molecular dynamics (MD) simulations to assess their binding stability and interaction dynamics with eIF4E.

For covalent inhibitors, we targeted lysine residues K106 and K108 on eIF4E, which are pivotal for maintaining the cap-binding site's integrity. We designed covalent inhibitors based on sulfuryl fluorides, featuring a carbon backbone substitution for fluoride, where the sulfur atom is in a +6 oxidation state, acting as an electrophilic center. The nitrogen from the lysine amino group, with an extra lone pair, can form a covalent bond with the sulfur by substituting the remaining fluoride in sulfuryl fluorides. Covalent docking was performed using Schrödinger Maestro and ICM-Pro, with visualization and interaction analysis facilitated by LigPlot.

[1] Fan, S. *et al.* Phosphorylated eukaryotic translation initiation factor 4 (eIF4E) is elevated in human cancer tissues. *Cancer Biology & Therapy* **8**, 1463–1469 (2009).

[2] Hanker, Ariella B., et al. "Overcoming Endocrine Resistance in Breast Cancer." *Cancer Cell*, vol. 37, no. 4, 13 Apr. 2020, pp. 496–513, https://doi.org/10.1016/j.ccell.2020.03.009.

[3] De Benedetti, A. & Graff, J. R. eIF-4E expression and its role in malignancies and metastases. *Oncogene* **23**, 3189–3199 (2004).

[4] Uttam, S., Wong, C., Price, T. J. & Khoutorsky, A. eIF4E-Dependent Translational Control: A Central Mechanism for Regulation of Pain Plasticity. *Frontiers in Genetics* **9**, (2018).

[5] Volpon, L., Osborne, M. J., Topisirovic, I., Siddiqui, N. & Borden, K. L. Cap-free structure of eIF4E suggests a basis for conformational regulation by its ligands. The EMBO J. 25, 5138–5149 (2006).

Molecular Dynamics and Conditional Generative Adversarial Network Prediction of the Spike Protein in SARS-CoV-2 at Various Temperatures and pH Levels

Ashley Jisue Hong[1], Ziyuan Niu[2], Giorgos Kementzidis[2], Yuefan Deng[2]

[1]*Punahou School, Honolulu, HI 96822,*
[2]*Stony Brook University, Department of Applied Mathematics and Statistics, Stony Brook, NY 11790*

As the COVID-19 pandemic remains globally without known definitive treatment, studies in SARS-CoV-2 continue to hold importance. A component of SARS-CoV-2 that plays a pivotal role in viral infection is the Spike Glycoprotein (S-protein), which facilitates membrane fusion and replication of host cell machinery through viral RNA injection.[1] Understanding the S-protein's structural mechanisms in diverse environmental conditions is critical for inhibiting infection and finding treatment methods.[2] Therefore, this study aims to use Molecular Dynamics (MD) and Machine Learning (ML) to predict the S-protein's properties better in varying pH and temperatures.

MD models movements of molecules and atoms through computer simulations. Though MD was used to analyze the S-protein, complications arose as existing MD methods required significant time and processing power. To increase our modeling efficiency, we trained ML models on MD simulation data to predict the S-protein's stability under varying temperatures and pH levels using three measurements: root-mean-square deviation (RMSD), solvent-accessible surface area (SASA), and protein-water hydrogen-bonds (HBPW). RMSD assesses stability through deviations between the protein's backbone and reference (initial) structures. SASA assesses stability through folding dynamics shown by surface area of the protein accessible to the solvent. HBPW assesses stability by the number of hydrogen bonds between the protein and water molecules.

MD simulation was conducted using the open-source software GROMACS with the CHARMM36 force field. The initial structure of the S-protein was obtained from the protein data bank (6VXX.pdb), and any missing loops in the 6VXX structure were completed using Robetta. The S-protein, comprising 1273 residues per chain, was placed in an explicit solvent. Simulation box for the SPC/E water models measured $21 \times 21 \times 21$ nm³ with periodic boundary conditions applied in all three Cartesian dimensions.

A Conditional Generative Adversarial Network (CGAN) for each RMSD, SASA, and HBPW was developed as this study's generative model for higher efficiency.[3] The model was programmed in Python and trained on 200 ns of MD simulation data. Model accuracy was summarized through Kernel Density Estimation (KDE) distribution comparison histograms of actual data and generated data, plot of generator and discriminator loss as a function of epochs, and Jensen–Shannon Divergence (JSD) plot of actual and generated data. The JSD between distributions is calculated using base 2 logarithms and is bounded by 1.

Figure 1. KDE distribution comparison histograms of actual and generated SASA data for pH 9, temperature 37°C at 45 epochs.

Our results showed significance as generated data distributions showed great similarities to actual data distributions. The model was also able to generate data in given conditions with great similarity to the actual data without training, as shown in Figure 1. Such results of this study can be applied to further SARS-CoV-2 studies, especially focusing on COVID-19 treatment and antiviral drug discovery targeting the S-protein by disrupting its structural integrity. Similarly, our model's accelerated running efficiency with the combination of CGAN and MD simulations can reduce the need for extensive MD simulations for other viral protein studies. Such broader applications can help types of drug discoveries beyond SARS-CoV-2.
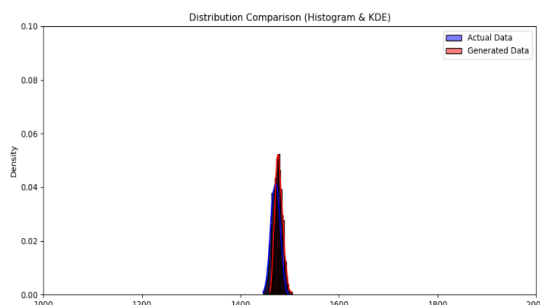
[1]Huang, Y., Yang, C., Xu, X., Xu, W., & Liu, S. (2020). Structural and functional properties of SARS-COV-2 spike protein: Potential antivirus drug development for covid-19. *Acta Pharmacologica Sinica, 41(9)*, 1141–1149. https://doi.org/10.1038/s41401-020-0485-4

[2]Xie, Y., Guo, W., Lopez-Hernadez, A., Teng, S., & Li, L. (2022). The pH Effects on SARS-CoV and SARS-CoV-2 Spike Proteins in the Process of Binding to hACE2. *Pathogens, 11*(2), 238. https://doi.org/10.3390/pathogens11020238

[3]Mert, A. (2022). Enhanced dataset synthesis using conditional generative adversarial networks. *Biomedical engineering letters, 13(1)*, 41–48. https://doi.org/10.1007/s13534-022-00251-x

Molecular Dynamics and Conditional Variational Autoencoder Prediction of the Spike Protein in SARS-CoV-2 at Various Temperatures and pH Levels

Marissa Huang[1], Georgios Kementzidis[2], Ziyuan Niu[2], Yuefan Deng[2]

[1]Woodbridge High School, Irvine, CA 92604, [2]Department of Applied Mathematics and Statistics, Stony Brook University, Stony Brook, NY 11790

The spike glycoprotein (S-protein) of SARS-CoV-2 plays a critical role in viral infection, facilitating the virus's entry into host cells [1]. As such, understanding the structural stability and denaturation mechanisms of the S-protein under different environmental conditions is crucial for developing strategies to inhibit viral infectivity. Molecular dynamics (MD) simulations are frequently used to model nanoscale interactions, such as those of the S-protein [2]. However, these simulations are computationally intensive and require significant time and processing power, underscoring the need for more efficient methods [3].

To address this, we aim to use machine learning (ML) models trained on MD simulation data to predict properties, such as stability, of the S-protein under varying temperatures and pH levels by examining three measurements: the backbone root-mean-square deviation (RMSD), solvent-accessible surface area (SASA), and protein-water hydrogen-bonds (HBPW). RMSD measures the deviation between the protein's backbone atoms and the initial structure. SASA is a measure of the surface area of the protein accessible to the solvent. HBPW quantifies the number of hydrogen bonds between the protein and water molecules.

MD simulations were conducted using GROMACS with the CHARMM36 force field. The initial S-protein structure (PDB: 6VXX) was retrieved from the Protein Data Bank, with missing loops in the 6VXX structure reconstructed using Robetta. The S-protein, which consisted of 1273 residues per chain, was placed in an explicit solvent. The cubic simulation box dimensions used for the SPC/E water models were $21 \times 21 \times 21$ nm³, and periodic boundary conditions were applied in all three Cartesian dimensions.

A Conditional Variational Autoencoder (CVAE) was developed for each of the three properties and trained on 200 ns of MD simulation data. The model's performance was evaluated using probability density functions showing the predicted and actual distributions, Jensen-Shannon (JS) divergence values bounded between 0 and 1, and plots of the loss values over the epochs.
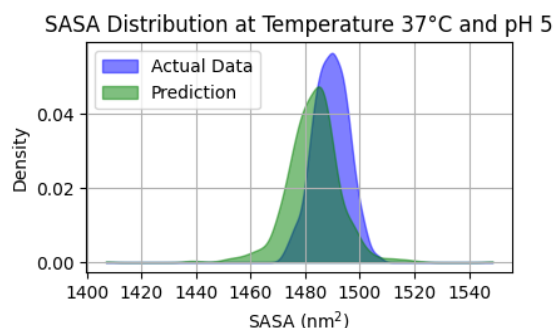

Figure 1: Distribution of SASA values predicted by CVAE model compared to actual distribution of data

The model was able to generate predictions for data it was not trained on. These predictions were plotted as probability density functions and found to be similar to the distributions of the actual data, as shown in Figure 1, which achieved a JS divergence value of 0.0942. This demonstrates a good start that we plan to refine through further strategies such as integrating a Recurrent Neural Network (RNN) and a Normalizing Flow (NF) into our architecture.

Our results can enhance viral protein dynamic studies by reducing the need for extensive MD simulations, potentially speeding up simulation efforts many times over. This can aid the development of antiviral drugs targeting the S-protein and its stability, leading to more effective COVID-19 treatments. Our approach can also be adapted to other viral protein studies to enhance drug discovery processes. Thus, these models present a powerful tool to help in the discovery and development of COVID-19 treatments and beyond.

[1] Huang, Y., Yang, C., Xu, X., Xu, W., & Liu, S. (2020). Structural and functional properties of SARS-CoV-2 spike protein: potential antivirus drug development for COVID-19. *Acta Pharmacologica Sinica*, *41*, 1141–1149. https://doi.org/10.1038/s41401-020-0485-4

[2] Hollingsworth, S. A., & Dror, R. O. (2018). Molecular Dynamics Simulation for All. *Neuron*, *99*(6), 1129–1143. https://doi.org/10.1016/j.neuron.2018.08.011

[3] Vlachakis, D., Bencurova, E., Papangelopoulos, N., & Kossida, S. (2014). Current State-of-the-Art Molecular Dynamics Methods and Applications. *Advances in Protein Chemistry and Structural Biology*, *94*, 269–313. https://doi.org/10.1016/b978-0-12-800168-4.00007-x
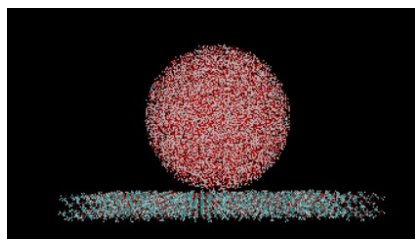
Molecular Dynamics of Fibrinogen Binding with PLA

Calvin Yu[1], Leo Pan-Wang[2], Brandon Qi[3], Ziyuan Niu[4], Miriam Rafailovich[4], Yuefan Deng[4]

[1]Weston High School, Weston MA, 02493; [2]The Peddie School, Hightstown NJ, 08520; [3]Davis Senior High School, Davis CA, 95618; [4]Stony Brook University, Stony Brook NY, 11794;

Fibrinogen is a protein produced in the liver that forms fibrin and is composed of two D domains connected to a central E-domain.[1] Recent studies seem to indicate that fibrinogen can bind to hydrophobic surfaces through strong hydrophobic interactions between the surface and the E and D domains, potentially causing fibrinogen to clump together.[2] Thrombin then cleaves the fibrinogen clump, forming a fibrin mesh that eventually becomes a blood clot in the circulatory system. Although blood clots are beneficial when preventing blood from leaving the system, clots have the potential to block blood flow within the system and stop circulation—thrombosis—creating ailments in patients such as strokes and heart disease.[3] Thus, it is crucial to understand the adhesion tendencies of fibrinogen on hydrophobic surfaces to better control clotting and reduce the number of health consequences caused by clotting or lack thereof. This research aims to analyze the interactions between the E-domain of fibrinogen and PLA, which is primarily hydrophobic.[4]

Before running simulations for fibrinogen, we utilized GROMACS to confirm PLA's relation to water by finding its contact angle via simulations. We did this by creating a water droplet of radius 5 nm with GROMACS commands and Python scripts. This water droplet was then put in the same system as our PLA sample separated by 0.8 nm and then ran to equilibrium. After the setup, a series of simulations found the contact angle to be between 76-81 degrees, confirming that PLA is hydrophobic. In future research, we hope further to explore the interactions between the water droplet and PLA to understand wettability, adhesion, and water's long-term effects on PLA.

Figure 1: Water droplet on PLA
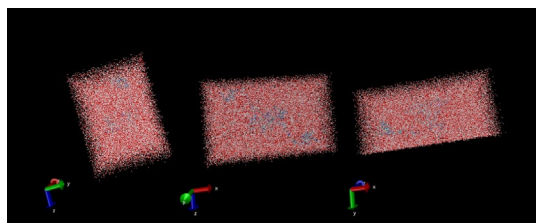
Figure 2: Solvated box of water around e-domain

The study utilized the molecular dynamics software GROMACS to simulate the binding of the E-domain to the PLA and VMD to visualize the interactions. The fibrinogen file was initially cleaned of all excess water molecules, and then a topology was generated for the file utilizing the CHARMM36 force field. Once the topology was successfully created, a water box with measurements 2 nanometers greater than those of the E-domain was generated around the molecule. The solvated box was then ionized by 0.1 mol Na and Cl ions. To finalize the setup, it was then run to equilibrium for the temperatures and pressure. Then, the entire system was placed onto PLA and the distance between the PLA and the E-domain and fibrinopeptides was measured.

[1] Köhler, S., Schmid, F., & Settanni, G. (2015). The internal dynamics of fibrinogen and its implications for coagulation and adsorption. *PLoS computational biology*, *11*(9), e1004346.

[2] Zhang, L., Casey, B., Galanakis, D. K., Marmorat, C., Skoog, S., Vorvolakos, K., ... & Rafailovich, M. H. (2017). The influence of surface chemistry on adsorbed fibrinogen conformation, orientation, fiber formation and platelet adhesion. *Acta biomaterialia*, *54*, 164-174.

[3] Raskob, G. E., Angchaisuksiri, P., Blanco, A. N., Buller, H., Gallus, A., Hunt, B. J., ... & Weitz, J. I. (2014). Thrombosis: a major contributor to global disease burden. Arteriosclerosis, thrombosis, and vascular biology, 34(11), 2363-2371.

[4] Kurokawa, N., Endo, F., Maeda, T., & Hotta, A. (2017). Electrospinning and surface modification methods for functionalized cell scaffolds. In Nanostructures for Novel Therapy (pp. 201-225). Elsevier.

Reinforcement Learning Based Simulated Annealing

Daniel Liang[1]*, Nathan Qiu[2]*, Emily Jiang[3]*, Ruichen Xu[4], Yuefan Deng[4]

[1]Ward Melville, [2]Canyon Crest Academy, [3]Shenzhen College of International Education, [4]Stony Brook University

In general, simulated annealing (SA) is a meta-heuristic algorithm by approximating the global optimum of a function to solve optimization problems, for both discrete and continuous problems. SA is an extension of conventional gradient descent, where worse solutions are probabilistically accepted to escape local optima. The "temperature" determines the probability of accepting worse solutions, and the "energy" assesses how good a solution is. The performance of the SA algorithm is dependent on the neighbor proposal distribution and the temperature annealing schedule. The Neural SA algorithm is an improvement of SA by regarding SA from a reinforcement learning perspective, as introduced in the paper "Neural Simulated Annealing" (Correia, Worrall, and Bondesan 2022). It also frames the proposal distribution as a trainable policy using equivariant neural networks. In the paper, the Neural SA performs better than ordinary SA algorithms by evaluating its results on several different benchmarks including Rosenbrock's function, the Knapsack problem, the Binpacking problem, and the Travelling Salesperson problem. The study claims that Neural SA is generalizable, robustly scalable to larger problems, and computationally efficient.

However, although the Neural SA introduced in the paper is supposedly generalizable, robustly scalable, and computationally efficient, its performance is often worse than standard commercial solvers. This severely limits its potential of being used in real world applications. In this paper, we significantly improve upon the performance of Neural SA and truly demonstrate its generalizability on continuous problems, while retaining its beneficial qualities of robust scalability and computational efficiency.

Firstly, we introduce modifications to the state parameters, by adding a parameter that corresponds to the immediate gain or change in cost from the previous to the current state. With this change, the model is able to more effectively learn which actions lead to better solutions, and we observe a corresponding increase in performance for almost all problems and number of items (see figure 1). We find that for the smaller SA chains, specifically $m = 1$ and 2 (where m denotes the length of the SA chain), the original Neural SA performs better than our modified Neural SA. However, for $m = 5$ and 10, we observe that our model has better performance. This is due to our model taking longer to converge than the original Neural SA algorithm because of the additional parameter.

Item number	SA (KNAP)	Neural SA PPO (KNAP)	RL SA PPO (ours) (KNAP)	OR Tools (KNAP)	SA (BIN)	Neural SA PPO (BIN)	RL SA PPO (ours) (BIN)	OR Tools (BIN)
50	18.43	19.69	19.78	20.12	30.38	27.32	27.24	26.71
100	36.81	39.54	40.04	40.41	60.66	53.53	53.29	53.91
200	50.89	55.03	55.34	57.65	121.27	105.63	105.43	109.19
500	126.92	138.14	139.40	144.14	302.84	259.08	261.94	267.63
1000	254.45	277.41	279.09	289.01	605.23	512.66	521.14	N/A
2000	507.72	554.32	558.50	577.28	1209.72	1017.88	1038.43	N/A

Figure 1 - Cost for Knapsack and Binpacking Problem for m = 10, Bigger is Better for Knapsack, Smaller is better for Bikepacking

Furthermore, we observe that our model achieves significantly better results than the original Neural SA on the Rosenbrock function (see figure 2). Furthermore, for the continuous Rosenbrock function, we observe a very significant increase in performance for the longer SA chains (+*35.7%* for $m = 10$).

For our main innovative change to increase performance and demonstrate generalizability, we use LSTMs (long short term memory) neural networks instead of multilayer perceptron neural networks. With LSTMs, we can include the entire replay of previous state parameters in the reinforcement learning state. This allows the model to more effectively learn which actions allow for more exploration to find global optima, and which actions minimize the energy function, both of which are crucial for simulated annealing. Furthermore, we demonstrate generalizability by removing the problem specific state parameters for continuous problems. We then train on one continuous problem (ex: Rosenbrock), and evaluate on another continuous problem (ex: Lennard Jones). Our results indicate that our model performs well, is robustly scalably, and generalizable to continuous problems, demonstrating the potential of our model to be used in a variety of real world applications.

m	SA	Neural SA PPO	RL SA PPO (ours)
1	0.321	0.308	0.291
2	N/A	0.196	0.196
5	N/A	0.127	0.096
10	N/A	0.084	0.058

Figure 2 - Cost for Rosenbrock Problem, Lower is Better

Correia, A., Worrall, D., & Bondesan, R. (2022). Neural Simulated Annealing. In *Arxiv*. https://arxiv.org/pdf/2203.02201

Simon J.D. Prince. (2023). *Understanding Deep Learning*. MIT Press.

Sequential backmapping: Stepwise reconstruction of all-atomic configurations from coarse-grained structures

[1]Erin Wong, [2]Jack Nicholson, [2]Georgios Kementzidis, [2]Yuefan Deng

[1]Great Neck South High School, Great Neck, NY 11020, [2]Department of Applied Mathematics and Statistics, Stony Brook University, Stony Brook, NY 11794

Molecular dynamics (MD) simulation is a *computationally intensive* technique that predicts the movement of the atoms of a system in order to study the changes in conformational state over time. However, traditional all-atomic (AA) MD simulations are only feasible for relatively small molecules with few atoms, under short simulation times [1]. Coarse graining (CG) addresses these computational limitations by predicting the movement of a group of atoms, effectively representing the atoms' individual movements with that of a coarse-grained "bead" [2]. Besides making more complex simulations possible, CG also allows for multi-scale modeling (MSM), which integrates multiple models spanning various spatial and temporal scales to fully understand a systems' behavior. In MSM, CG is paired with another technique, backmapping, which restores the system's configuration to a more fine-grained scale upon completion of CG simulation[3]. This step, however, is complicated: one CG configuration could correspond to many AA structures. Current highest-performing deep learning methods are either inflexible, restricted to a specific method of CG, or not generalizable to more complex systems. Thus, this study sought to implement a flexible and efficient end-to-end backmapping method applicable to most types of CG and systems of varying complexity.

Unlike current methods, which aim to backmap CG structures in a single "step", from CG to AA, we propose a sequential method of backmapping: CG structures are backmapped to an intermediate- scale, Cα CG—which coarse-grains based on the α-carbons of a polypeptide—before being further backmapped to their AA structures (Figure 1). We hypothesize that this end-to-end method will improve upon the performance of previous backmapping methods since the inclusion of a validated intermediate structure places necessary constraints on the distribution of structures from which the ultimate AA configuration is sampled from. Our algorithm comprises two previously published, high-performing conditional variational autoencoders, CGVAE[4] and GenZProt[5] (Figure 1).
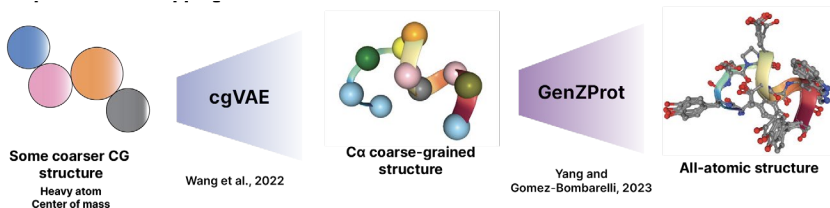
Figure 1. Architecture of the sequential backmapping algorithm. CGVAE backmaps input CG structure into a its Cα CG representation, which is then further backmapped by GenZProt into its AA configuration.

The CGVAE and GenZProt models were both trained and tested, reproducing the results reported by their respective authors. To benchmark the effectiveness of our new approach, we chose the first thirty-six residues of eIF4E—a mRNA cap-binding protein whose overexpression is linked to breast cancer—for its complexity (5890 atoms) and medical relevance. The benchmarking dataset consisted of trajectories for three simulations of eIF4E, each 1001 frames long, as well as an all-atomic topology file., Both models were trained using parallel GPUs, wrapped in the PyTorch class Fully Sharded Data Parallel, to account for the size of eIF4E. After individual model training, we will train our sequential model and compare its performance with that of the individual models to validate the utility of our proposed method.

1. Hollingsworth, S. A., & Dror, R. O. (2018). Molecular dynamics simulation for all. Neuron, 99(6), 1129–1143. https://doi.org/10.1016/j.neuron.2018.08.011
2. Kmiecik, S., Gront, D., Kolinski, M., Wieteska, L., Dawid, A. E., & Kolinski, A. (2016). Coarse-Grained Protein Models and Their Applications. Chemical Reviews, 116(14), 7898–7936. https://doi.org/10.1021/acs.chemrev.6b00163
3. Ayton, G. S., Noid, W. G., & Voth, G. A. (2007). Multiscale modeling of biomolecular systems: In serial and in parallel. Current Opinion in Structural Biology, 17(2), 192–198. https://doi.org/10.1016/j.sbi.2007.03.004
4. Wang, W., Xu, M., Cai, C., Miller, B. K., Smidt, T., Wang, Y., Tang, J., & Gomez-Bombarelli, R. (2022). Generative Coarse-Graining of Molecular Conformations. Proceedings of the 39th International Conference on Machine Learning, 23213–23236. https://proceedings.mlr.press/v162/wang22ag.html
5. Yang, S., & Gómez-Bombarelli, R. (2023). Chemically Transferable Generative Backmapping of Coarse-Grained Proteins (No. arXiv:2303.01569). arXiv. http://arxiv.org/abs/2303.01569

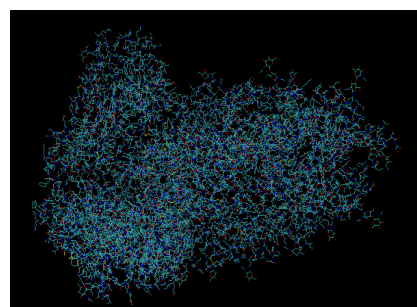# Binding Dynamics of SARS-CoV-2 Spike Glycoprotein to Polylactic Acid

Reilin Lyu[1*], Rochelle Sun[2*], Karin Hasegawa[3], Yuefan Deng[3], Miriam Rafailovich[3]

[1]*Williamsville East High School, Buffalo, NY 14221; [2]Beijing National Day School, Beijing, 100039; [3]Stony Brook University, Stony Brook NY, 11794*
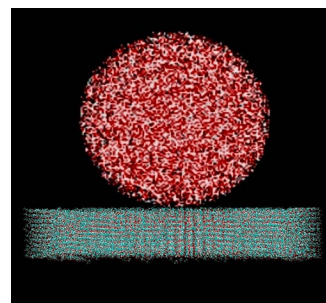
Among the most prominent features of the SARS-CoV-2 virion is the spike glycoprotein (*S*) that protrudes from the viral capsid. This glycoprotein mediates virus entry into cells as well as its adsorption to surfaces. Adsorption of the virus to surfaces using *S* is of particular interest, as the molecular dynamics properties of the protein-surface interaction can determine a particular surface's utility as a virucidal material as well as its potential for transmission of the adsorbed virus. The interactions between *S* and numerous surfaces have already been studied, including, notably, polystyrene[1]. We aim to carry out a similar molecular dynamics study between *S* and a surface of polylactic acid (PLA).

There were two main approaches used in initial analysis of the *S*/PLA interaction - *in silico* and *in vitro*. For the *in silico* analysis GROMACS software was used, with the crystal *S* structure obtained from the Protein Data Bank (PDB: 6VXX) and PLA surface section generated using AVOGADRO and LigParGen, to create a MD simulation of the interaction. This allows for analysis by quantifying the binding intensity by counting the number of atomic contacts, as well as calculating the binding force as a function of time. As for the *in vitro* approach, H1N1 virus was substituted for SARS-CoV-2 due to laboratory restrictions; these are plated with PLA and left at room temperature (297K) for an arbitrary amount of time. Adsorption in the *in vitro* approach is analyzed by counting the number of viruses remaining on the surface after washing with water.

Figure 1. The SARS-CoV-2 spike protein, visualized by Visual Molecular Dynamics (VMD)[2]

We have worked to verify the results obtained from these two approaches, using a GROMACS simulation of the *S*/PLA interaction in a droplet of water. After the removal of crystal waters from the structure, the topology was generated using GROMACS based on CHARMM36 force field. The PLA substrate model was created and simulations of S-protein interaction with PLA were performed. S-protein binding affinity with the PLA surface varied depending on temperature. The final, adsorbed structure of *S* after the simulation is compared to its crystal structure through RMSD analysis to quantify conformational changes before and after adsorption. In addition, the contact angle of the simulated nanoscopic water droplet is compared to known macroscopic values for water on polylactic acid to validate the simulation.

Figure 2. Water droplet and PLA interaction, visualized by VMD[2]

[1]Sahihi, M., & Faraudo, J. (n.d.). Molecular dynamics simulations of adsorption of SARS-CoV-2 spike protein on polystyrene surface. American Chemical Society Publications, 62(16). https://doi.org/10.1021/acs.jcim.2c00562?ref=pdf

[2]Humphrey, W., Dalke, A., & Schulten, K. (1996). Visual Molecular Dynamics. Journal of Molecular Graphics, 14, 33-38.

ProLiDE: A comprehensive AI-driven approach with multi-source biological data integration for enhanced drug discovery and optimization

Zeyu Yao[1], Karin Hasegawa[2], Yuefan Deng[2]

[1]Stamford American International School, Singapore 357684, [2]Stony Brook University, Stony Brook, NY 11790

The integration of computational techniques in drug discovery has significantly advanced the prediction of protein-ligand interactions, drug efficacy, and safety [1-3]. However, existing models often fail to fully integrate the vast amount of biological and chemical data necessary for accurate in vivo predictions of drug candidates' behavior [4]. A major challenge lies in consolidating diverse datasets—ranging from successful and failed drug trials to post-translational modifications and binding site dynamics—into a unified system. Additionally, current models often fall short in addressing the complex pharmacokinetics and pharmacodynamics within the human body. To address these challenges, we propose developing an advanced AI model that integrates diverse data on protein-ligand interactions to evaluate drug candidates' potential for specific targets, predicts their pharmacokinetics and pharmacodynamics, and assesses the likelihood of adverse effects and off-target interactions. We developed automated scripts to extract and standardize data from various sources, integrating this data into a centralized database. Quantitative parameters were normalized, and machine learning algorithms were utilized. Binding site prediction tools and molecular docking simulations identified potential binding sites and calculated affinities. Scoring functions were developed to integrate binding affinities with drug-likeness and ADMET properties, and high-throughput virtual screening and toxicity prediction models ranked drug candidates based on efficacy, specificity, and off-target effects.
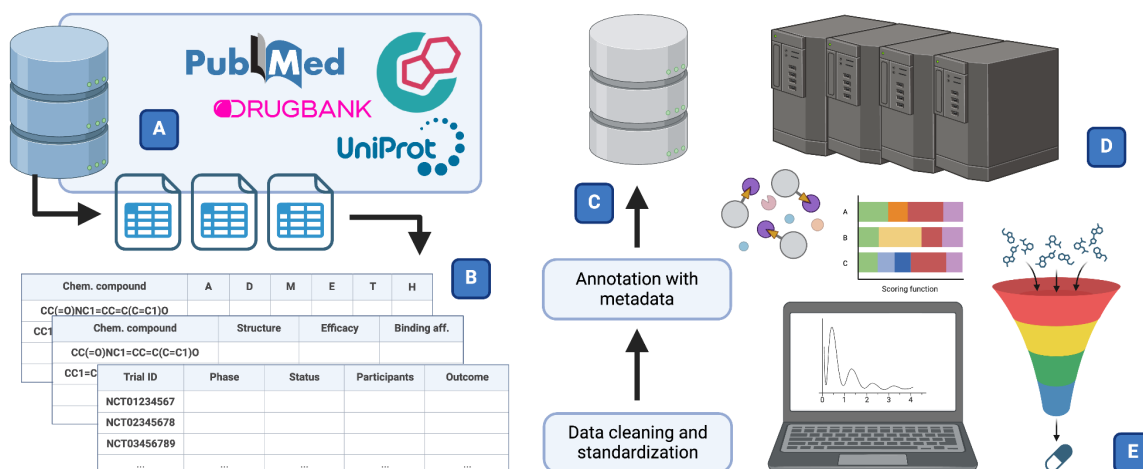
Figure 1. Workflow of ProLiDE. (A) Data collection from public databases such as PubMed, DrugBank, and UniProt. (B) Integration and structuring of collected data into standardized formats. (C) Annotation with metadata for comprehensive analysis. (D) Computational processing and analysis of annotated data. (E) Application of scoring functions to evaluate data and identify promising drug candidates.

[1]Sadybekov, A.V., and Katritch, V. (2023). Computational approaches streamlining drug discovery. Nature 616, 673–685. https://doi.org/10.1038/s41586-023-05905-z.

[2]Sliwoski, G., Kothiwale, S., Meiler, J., and Lowe, E.W. (2013). Computational Methods in Drug Discovery. Pharmacological Reviews 66, 334–395. https://doi.org/10.1124/pr.112.007336.
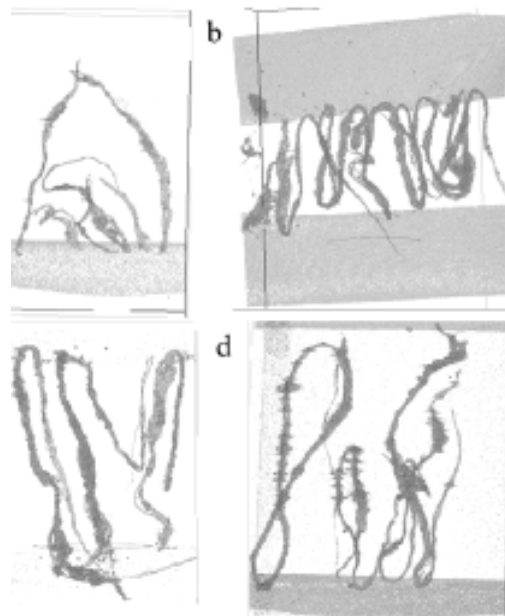
[3]Soham Choudhuri, Manas Yendluri, Poddar, S., Li, A., Mallick, K., Mallik, S., and Ghosh, B. (2023). Recent Advancements in Computational Drug Design Algorithms through Machine Learning and Optimization. Kinases and Phosphatases 1, 117–140. https://doi.org/10.3390/kinasesphosphatases1020008.

[4]Kong, W., Midena, G., Chen, Y., Athanasiadis, P., Wang, T., Rousu, J., He, L., and Aittokallio, T. (2022). Systematic review of computational methods for drug combination prediction. Computational and Structural Biotechnology Journal 20, 2807–2814. https://doi.org/10.1016/j.csbj.2022.05.055.

Session IIIb:
CT Segmentation
Karin Hasegawa

Using Landmark Detection to Identify Maturation Stage of Cervical Vertebrae in Cone Beam Computed Tomography Scans

Aaryan Vira[1], Karin Hasegawa[2], Dr. Yuefen Deng[2]

[1]North Shore High School, Glen Head, NY 11579; [2]Department of Applied Mathematics and Statistics, Stony Brook University, Stony Brook, NY 11790

Understanding the skeletal maturity of orthodontic patients is crucial to predicting the optimal timing for craniofacial treatment and other orthodontic treatments. However, chronological age is not an accurate metric to predict skeletal maturity. Cervical vertebral maturation (CVM) is a commonly used method to predict the skeletal matsuration of patients. In this method, the shapes of the second, third, and fourth cervical vertebrae (C2, C3, and C4) are analyzed via computed tomography (CT) scans and fit with the six stage CVM chart[1] (Figure 1). This method is widely considered one of the most accurate, safe, and easy to use methods to understand skeletal maturity. However, the process is extremely subjective and can be impacted by factors such as the knowledge and experience of the professional analyzing the CT scans[2].

Figure 1: The 6 maturation stages of the cervical vertebrae[1]

To minimize the subjectivity of CVM and increase the efficiency of the evaluation by automating the process, recent research has focused on developing machine learning (ML) models to identify the CVM of a patient given CT scans. ML models are able to accomplish tasks by being trained and optimized using datasets. Previously, automatic CVM classification task has been performed based on lateral cephalometric images, which are 2D images and showed a remarkable performance[2]. However, the rise of 3D scans with use of Cone Beam Computed Tomography (CBCT) in dentistry and orthodontic practices has made past ML models for CVM identification more obsolete[3]. Therefore, the aim of the present study is to develop an ML model that can accurately identify CVM in dental CBCT scans. This study was reviewed and approved by an Institutional Review Board (IRB) at Stony Brook University

A total of 77 CBCT scans of the cervical vertebrae were obtained from the Stony Brook School of Dental Medicine. Each scan was annotated by an orthodontic expert with 18 landmarks at the different vertices of the C2, C3, and C4 vertebrae[1]. The xy coordinate positions of each of these landmarks are notated and were used by the model for training landmark detection. Ground truth heatmaps, which are used as training labels, were also generated from the landmarks in the CBCT scans[4]. Based on recent ML research with CBCT analysis, the model was developed using U-Net architecture. The U-Net architecture model is crucial in landmark detection due to its ability to capture fine details and contextual information through its encoder-decoder system and skip connections. This makes it highly effective for precise identification and localization of landmarks, which is essential for the classification of CVM in the CBCT scans. The training of the model is currently performed on the Seawulf Super Computer and the results will be reported in a future presentation.
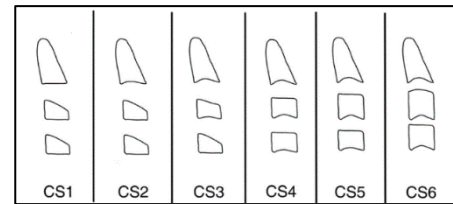
[1] Szemraj-Folmer, A., Wojtaszek-Słomińska, A., Racka-Pilszak, B., & Kuc-Michalska, M. (2021). Duration of the pubertal growth spurt in patients with increased craniofacial growth component in sagittal and vertical planes—retrospective and cross-sectional study. *Clinical Oral Investigations*, 1-8.

[2] Amasya, H., Yildirim, D., Aydogan, T., Kemaloglu, N., & Orhan, K. (2020). Cervical vertebral maturation assessment on lateral cephalometric radiographs using artificial intelligence: comparison of machine learning classifier models. *Dentomaxillofacial Radiology*, *49*(5), 20190441.

[3] Ajami, M., Tripathi, P., Ling, H., & Mahdian, M. (2022). Automated detection of cervical carotid artery calcifications in cone beam computed tomographic images using deep convolutional neural networks. *Diagnostics*, *12*(10), 2537.

[4] Stern, A., Sharan, L., Romano, G., Koehler, S., Karck, M., De Simone, R., ... & Engelhardt, S. (2021, February). Heatmap-based 2d landmark detection with a varying number of landmarks. In *Bildverarbeitung für die Medizin 2021: Proceedings, German Workshop on Medical Image Computing, Regensburg, March 7-9, 2021* (pp. 22-27). Wiesbaden: Springer Fachmedien Wiesbaden.

Plant Root Morphology Analysis and 3D Printed Dental Models Dimensional Accuracy Evaluation for Clear Aligners via Computed Tomography and Image Processing Tools

Ava Zhou[1*], Sichen Liu[2*], Aaron Sloutski[3], Andy Lin[3], Justin Burzachiello[3], Yuefan Deng[3], Miriam Rafailovich[3]

[1] Bellport High School, NY, 11719 [2] Shanghai Foreign Language School [3] Stony Brook University, NY, 11794

Quantification of botanical morphometrics, such as volume, is necessary for examining the results of scientific developments in agriculture, ecology, and forestry. However, young roots and shoots often exhibit complex, multi-scale geometric structures on the level of micrometers to centimeters which cannot accurately be studied by hand without introducing significant error. Therefore, advanced imaging techniques, like x-ray-based computed tomography (CT), must be used to accurately represent them for later quantitative and qualitative analysis[1].

VTJ's VEDA-CORE CT machine was used to analyze Arabidopsis thaliana (AT) plants treated with varying concentrations of RT-EPS (EPM) to assess EPM's effectiveness in promoting root growth, which aids in soil erosion resistance[2]. Four AT samples were grown for three weeks in soil with different EPM levels (0, 12.5, 125 mg/kg) and then replanted in sand for another three weeks. Particularly, the control group was split when replanted: half remained as control, and half were replanted in 125 mg/kg EPM. Then, AT root samples were fixed by tapes on styrofoam, and CT scanning was performed in 5 steps: warm up, detector calibration, location adjustment of object, geometry alignment, and final CT scan.

Figure 1. 3D reconstruction volume viewer in ImageJ of AT grown in (a) 0 mg/kg EPM, (b) 12.5 mg/kg EPM, (c) 125 mg/kg EPM, (d) orginally 0 then 125 mg/kg EPM

By utilizing ImageJ software, visualization of how X-rays of varying intensities shine through the samples and 3D reconstruction images formed by filtered back-projection algorithms were generated. Plant root volume was quantitatively assessed using ImageJ, providing statistical evidence of increased root volume in AT when treated with varying concentrations of EPM.

Similarly, the rapid development of three-dimensional (3D) printing technologies has revolutionized the production of 3D models for clear aligners, offering unprecedented precision and customization. Several variables throughout the production process can impact the accuracy and clinical utility of these models. Among them, previous studies have reported that print orientation affects dimensional accuracy of the prints[3], but with conflicting results.
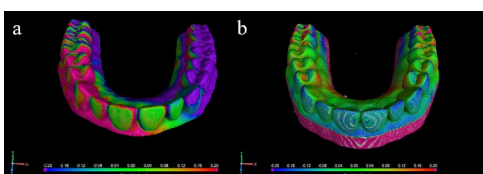

Figure 2. The deviation between modeling source file and (a) horizontally-printed dental model, (b) vertically-printed dental model in a color-coded scheme
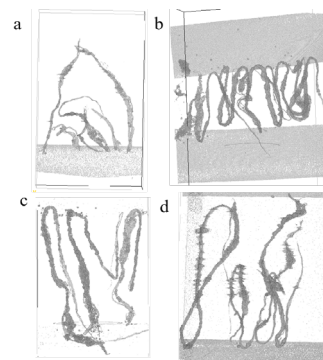
In this project, CT scanning was conducted on a vertically printed dental model and a horizontally printed dental model to generate precise 3D images. Subsequently, VGSTUDIO MAX was utilized to quantify the deviation of the CT-scanned prints from the original STL file used in their creation. Best-fit alignment techniques were applied to compare the modeling source file with the vertically and horizontally printed models. The deviation between these models was illustrated using a color-coded scheme. It was observed that both models exhibited shrinkage compared to the original modeling source file. Preliminary analysis indicates that the vertically-printed model demonstrates less accuracy than the horizontally-printed model. Additional models are currently in production, and final results will be updated in due course.

---

[1] Piovesan, A., Vancauwenberghe, V., Van De Looverbosch, T., Verboven, P., & Nicolaï, B. (2021). X-ray computed tomography for 3D plant imaging. Trends in Plant Science, 26(11), 1171–1185. https://doi.org/10.1016/j.tplants.2021.07.010

[2] Staudt, A. K., Wolfe, L. G., & Shrout, J. D. (2011). Variations in exopolysaccharide production by Rhizobium tropici. *Archives of Microbiology*, *194*(3), 197–206. https://doi.org/10.1007/s00203-011-0742-5

[3] Boyer, R. A., et al. "Effect of Print Orientation on the Dimensional Accuracy of Orthodontic Aligners Printed 3-Dimensionally." Am J Orthod Dentofacial Orthop, vol. 160, no. 5, 2021, pp. 732–742.e1.
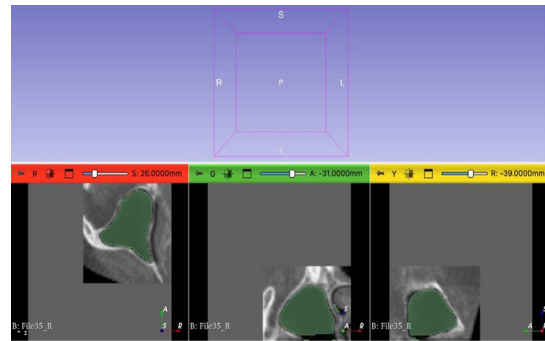
Deep Learning-Based CT Volumetry for Maxillary Sinus Segmentation in Patients with Mucus Infections and Mucosal Retention Cysts

Niranjana Sankar[1], Thomas Lin[2], Karin Hasegawa[3], Yuefan Deng[3]

[1]*Monta Vista High School, Cupertino, CA,* [2] *The Stony Brook School, Stony Brook, NY,* [3]*Stony Brook University, Stony Brook, NY*

Accurate 3D segmentation of the maxillary sinus region is crucial for oral surgeries and treatment applications[1]. Cone-beam computed tomography (CBCT) images prove very helpful in diagnosis of maxillary sinus infections and detecting mucous retention cysts (MRC) through segmentation methods (Fig. 1). Understanding the differences between MRC and maxillary sinus infection CBCT scans help improve accurate diagnoses. However, manual and semi-automatic segmentation methods of CBCT images are time-consuming and often not reliable. Recently, convolutional neural networks and deep learning methods have been applied and proved to perform exemplary in 3D image segmentation. A dataset with images of 40 healthy patients, 15 patients with MRC, and 61 patients with a mucous infection were acquired from the Stony Brook Dental School. Images were annotated by dental students and validated for precision by the experts. After evaluation, the images were cropped and padded before using data augmentation techniques such as random flips. The images were

Figure 1: Sample segmentation by 3D UNet machine learning model of a healthy patient's maxillary sinus region CBCT scan

divided into 3 subsets: training, validation, and testing with a 85 to 15 training-validation split. A 3D U-Net model and a deep dilated segmentation network (DilatedSegNet), were tested as these models recorded high performance for medical image segmentation in previous studies. A 3D U-Net model uses multiple convolutional layers following a an encoder-decoder architecture [2]. A DilatedSegNet is an encoder-decoder network that uses a pre-trained ResNet50 as the encoder to extract feature maps which are concatenated through 4 decoder blocks to predict the segmentation[3]. The performance of the model was evaluated in 3 metrics: average loss, dice similarity coefficient (DSC), intersection over union (IoU). For healthy patients, the 3D U-Net model recorded an average loss of 0.132, DSC of 0.841, and IoU of 0.729 while the DilatedSegNet recorded an average loss of 0.119. The proposed models provide a more time-efficient and precise method for automatic segmentation which can allow for accurate and immediate generation of 3D models for virtual treatment planning and diagnosis in oral applications.

[1] Çiçek, Ö., Abdulkadir, A., Lienkamp, S.S., Brox, T., Ronneberger, O. (2016). 3D U-Net: Learning Dense Volumetric Segmentation from Sparse Annotation. In: Ourselin, S., Joskowicz, L., Sabuncu, M., Unal, G., Wells, W. (eds) Medical Image Computing and Computer-Assisted Intervention – MICCAI 2016. MICCAI 2016. Lecture Notes in Computer Science(), vol 9901. Springer, Cham. https://doi.org/10.1007/978-3-319-46723-8_49

[2] Dreizin D, Nixon B, Hu J, Albert B, Yan C, Yang G, Chen H, Liang Y, Kim N, Jeudy J, Li G, Smith EB, Unberath M. A pilot study of deep learning-based CT volumetry for traumatic hemothorax. Emerg Radiol. 2022 Dec;29(6):995-1002. doi: 10.1007/s10140-022-02087-5. Epub 2022 Aug 16. PMID: 35971025; PMCID: PMC9649862.

[3] Tomar, N.K., Jha, D., Bagci, U. (2023). DilatedSegNet: A Deep Dilated Segmentation Network for Polyp Segmentation. In: Dang-Nguyen, DT., *et al.* MultiMedia Modeling. MMM 2023. Lecture Notes in Computer Science, vol 13833. Springer, Cham. https://doi.org/10.1007/978-3-031-27077-2_26

Session IV: Robotics
Shi Fu, Fumi Honda, Khiem Phi
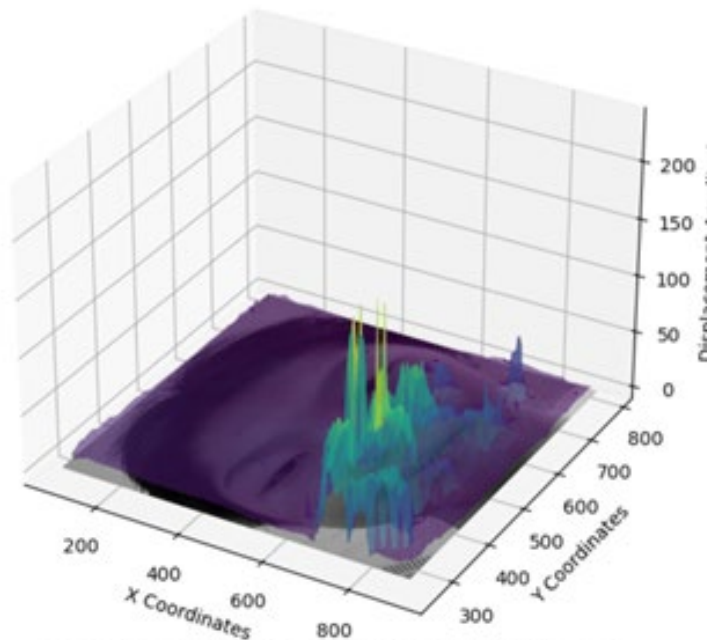
Figure 3. 3D bilinear interpolation
topography map of displacement

Face Digital Image Speckle Correlation (DISC) Application as a Non-Invasive, Accessible Tool to Detect Acoustic Neuroma

Corey Zhang[1], Leah Song[2], Jerry Gu[3], Shreyaa Sanjay[4], Zihan Jia[5], Eugene Jiang[6], Shi Fu[7], Miriam Rafailovich[7]

[1] Eastlake High School, Sammamish, WA 98074, [2] Maclay School, Tallahassee, FL 32312, [3] Princeton International School of Mathematics and Science, Princeton, NJ 08540, [4] West Windsor-Plainsboro High School North, Plainsboro Township, NJ 08536, [5] The Experimental High School Attached to Beijing Normal University, Xicheng District, China, 100032, [6] Department of Biology, Pre-Medicine/Pre-Medical Studies, Stony Brook University, NY 11790, [7] Department of Materials Science and Engineering, Stony Brook University, NY 11790

Acoustic neuroma, a benign tumor on the vestibulocochlear nerve, often causes hearing loss and facial asymmetry, with traditional diagnosis often complex and costly. To address these challenges, our project aims to develop a face digital image speckle correlation (DISC) application for iOS to facilitate real-time diagnosis by detecting facial asymmetry through advanced image processing techniques. This approach provides a non-invasive, accessible tool for patients and doctors[1].

We hypothesize that the DISC application will facilitate the diagnosis of acoustic neuroma by standardizing and streamlining the process of photo-taking and cropping. This ensures that patients are consistently positioned, aiding doctors in accurately identifying facial asymmetry, thus enhancing diagnostic accuracy and accessibility.

Figure 1. Grayscale images of the subject in a neutral expression (left) and a smirk (right).

For image processing and heatmap application, a Python script in a Jupyter Notebook managed image acquisition, preprocessing, and speckle correlation analysis. Utilizing OpenCV, we performed edge detection, contour detection, and region of interest extraction. The user interface, developed with Swift and Apple's CoreML library, applied a mask to ensure correct user positioning during photo capture. Both images were converted to grayscale and downscaled to 10 by 10 pixels for easier processing (Figure 1).
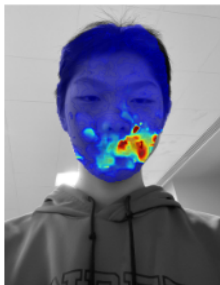

Figure 2. Heatmap overlay on a grayscale image of the subject's face, highlighting areas of significant vector displacement associated with facial asymmetry.

Tests on research project members demonstrated the DISC application's effectiveness in generating heatmaps, accurately identifying facial asymmetry by highlighting stronger vector displacements in areas of facial movement, such as a smirk (Figure 2). Bilinear interpolation, used to calculate displacement at intermediate points within a planar face mesh, highlighted variations in facial movement, indicating potential asymmetry associated with acoustic neuroma (Figure 3).

The DISC application shows significant promise as a preliminary diagnostic tool for acoustic neuroma by effectively detecting facial asymmetry. By integrating Python and OpenCV for image processing with Swift and CoreML for facial segmentation, we have developed a robust and user-friendly platform. The deployment on Azure ensures scalability and reliability. Future enhancements will focus on OpenCV integration into Xcode to interlink all GUI elements.

Figure 3. 3D bilinear interpolation topography map of displacement

In conclusion, the DISC application offers a novel approach for diagnosing acoustic neuroma through the detection of facial asymmetry, by standardizing the photo-taking process and providing real-time analysis, facilitating early detection and prompt medical consultation, thereby ultimately improving patient outcomes.
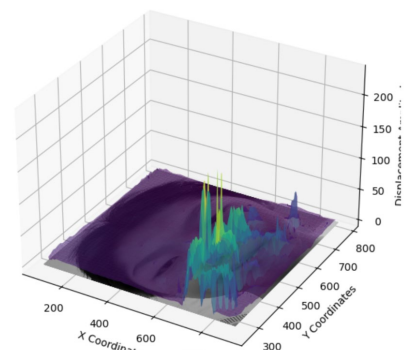
---

[1]Bhatnagar, Divya, et al. "An Analysis of Facial Nerve Function in Patients with Vestibular Schwannomas Using Digital Image Speckle Correlation." Journal of Neuroscience and Neuroengineering 3.1 (2014): 62-71.
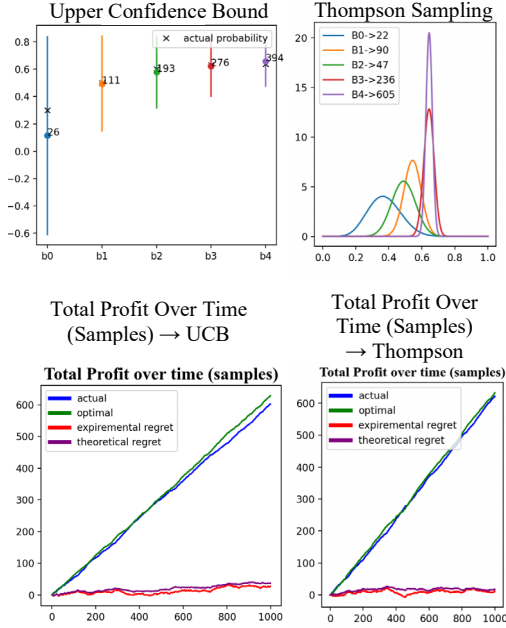
Demonstration Acquisition System for Complex Manipulation Tasks

Ishita Banerjee[1], Sadie Seulal[2], Dibyendu Das[3], Fumi Honda[3], Nilanjan Chakraborty[3]

[1]Academy for Math Science and Engineering, Morris Plains, NJ, 07866 [2]South Side High School Rockville Centre, NY, 11570, [3]Stony Brook University, Stony Brook, NY, 11790

This research aims to provide users with the ability to teach various robots complex manipulation tasks through demonstrations so that these robots can help those with disabilities who cannot complete these tasks themselves. The system takes in a demonstration performed by a user and generates a plan based

on screw interpolation that follows the underlying geometric constraints from the user demonstration. This plan is then carried out in the background, failing if the joint limits are reached in the execution[1].

In the current setup, the workspace is organized into a 2D grid divided into 16 regions; each region can be equated to an arm. To minimize the number of total demonstrations needed, the user is advised to perform the next demonstration in the area that the robot feels it will perform the most poorly. To determine the success rates of the regions, a number of samples determined by Hoeffding's inequality is generated from each region. However, if the environment were to grow in area or dimension, the number of samples would become immense, and the algorithm would become computationally expensive. The research being implemented is aimed at decreasing the total number of samples taken given an environment so that the environment can be expanded and still maintain a reasonable runtime.

Figure 1. Graphs produced by algorithms to observe and compare

In order to perform the minimum amount of demonstrations, the algorithm only needs to know the region in which the robot believes it will perform the worst. Bandit algorithms can be adopted to help decrease the exploration of successful regions. This research explores and compares different bandit algorithms to determine the demonstration point in the context of the worst arm. Before incorporating the algorithm into the robotic system, the algorithms were tested on binomial bandits. Consequently, these implementations lead to the creation of graphs that allow the comparison of the performance of different algorithms (Figure 1).

With this process completed, these algorithms were implemented into the robot to generate heat maps and test their performance. To achieve the overarching goal of aiding the general population with our system, the mechanism must be easily usable. Along with the bandit algorithm and heat map being generated, a user interface is being further improved in order for the average user to be able to be able to communicate with the robot. This transformation entails seeing the heat map, the most optimal point for the next demonstration, and a new feature such as voice recognition (Figure 2).

Figure 2. Extended UI with a sketch of the top view of Baxter, voice command, and the heat map with green (successful task instances), red (failed task instances), black (demonstrations), and blue (the next demonstration) dots. (Not to scale)

[1]Mahalingam, D., & Chakraborty, N. (2022). Human-guided planning for complex manipulation tasks using the screw geometry of motion. arXiv. https://arxiv.org/pdf/2209.05672

Utilizing Machine Learning to Inform Tomato Harvesting in Containerized Vertical Farming

Megan Chan [1], Khiem Phi [2], Nilanjan Chakraborty [2]

[1] Great Neck South High School, Great Neck, NY 11020, [2] Stony Brook University, Stony Brook, NY 11794

The planet's population is growing rapidly with an estimated population of 9.8 billion by 2050 [1]; at the same time, the resources needed to feed the planet's population are rapidly diminishing, with amounts of water and arable land decreasing at an accelerated rate due to climate change. Thus, vertical farming, the agricultural process of growing crops vertically instead of horizontally, is being used to conserve space and resources as it has a higher crop yield per square foot of land.

In Mahalingam et al., 2023, using only RGBD camera images and one human demonstration, collaborative robots, or cobots, were successfully utilized in vertical farming to automate two key farming operations: transplantation of saplings and the harvesting of grown plants [2]. However, this current technology does not include consideration of the timing of harvest; that is, the current technology does not take into account whether a crop is diseased, ripe, or unripe for harvesting. Thus, this study aims to utilize computer models to inform harvest time by classifying tomato crops as diseased, ripe, or unripe.

Three machine learning models—support vector machine (SVM), XGBoost (XGB), and convolutional neural networks (CNN) were developed, and their accuracies in classifying the tomato images were compared to select an optimal model. As inputs, 1922 tomato images were extracted from the Harvesting Dataset on Roboflow and split into training (70%) and testing (30%) subsets. The models output 0 for diseased, 1 for ripe, and 2 for unripe. CNN had the best performance in accurately classifying the tomatoes with the highest test accuracy of 78.12%. This was followed by XGB with an accuracy of 74.48% and SVM with an accuracy of 39.93%. The CNN model was selected as the optimal model.

Still, this CNN model only gives one label for each image. When integrated with the cobots, the RGBD camera on the robots' hands used to obtain inputs for the CNN model would retrieve images with multiple tomatoes. It would be inaccurate to label an image with multiple tomatoes of different categories only one category (e.g. an image with two ripe tomatoes and one unripe tomato cannot simply be labeled automatically). Each tomato needs to be considered as one input to the CNN model rather than one image with multiple tomatoes considered as one input.

Thus, the next step of this study is to use the foundational model YOLO-World, a large AI model that can detect an object based on descriptive text, and the RGBD camera images and the keywords "diseased tomato," "ripe tomato," and "unripe tomato" as inputs to the model to get the bounding box coordinates of each tomato, their labels, and confidence scores. The bounding box coordinates can be used to crop and resize the robot's camera images to single tomatoes as the appropriate input for the CNN model. Furthermore, the labels and confidence scores can be used as input features in another machine learning model which can be combined with the CNN model for a better informed final output (Figure 1).
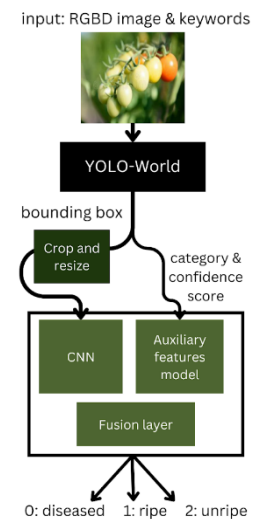
Figure 1. Model pipeline for tomato classification.

[1] UN Department of Economic and Social Affairs. (2017). World population projected to reach 9.8 billion in 2050, and 11.2 billion in 2100. Welcome to the United Nations. https://www.un.org/en/desa/world-population-projected-reach-98-billion-2050-and-112-billion-2100

[2] Mahalingam, D., Patankar, A., Phi, K., Chakraborty, N., McGann, R., & Ramakrishnan, I. (2023). Containerized vertical farming using cobots. https://arxiv.org/abs/2310.15385

Session V:
Materials Under
Extreme Conditions

Abhinav Sharma, Huiting Luo,
Shi Fu, Yongseok Kim, Hongyeon Lee

Figure 2. 2D (top) and 3D (bottom) AFM height images of W-1OTf-5Cl (left) and W-1OTf-15Cl (right)
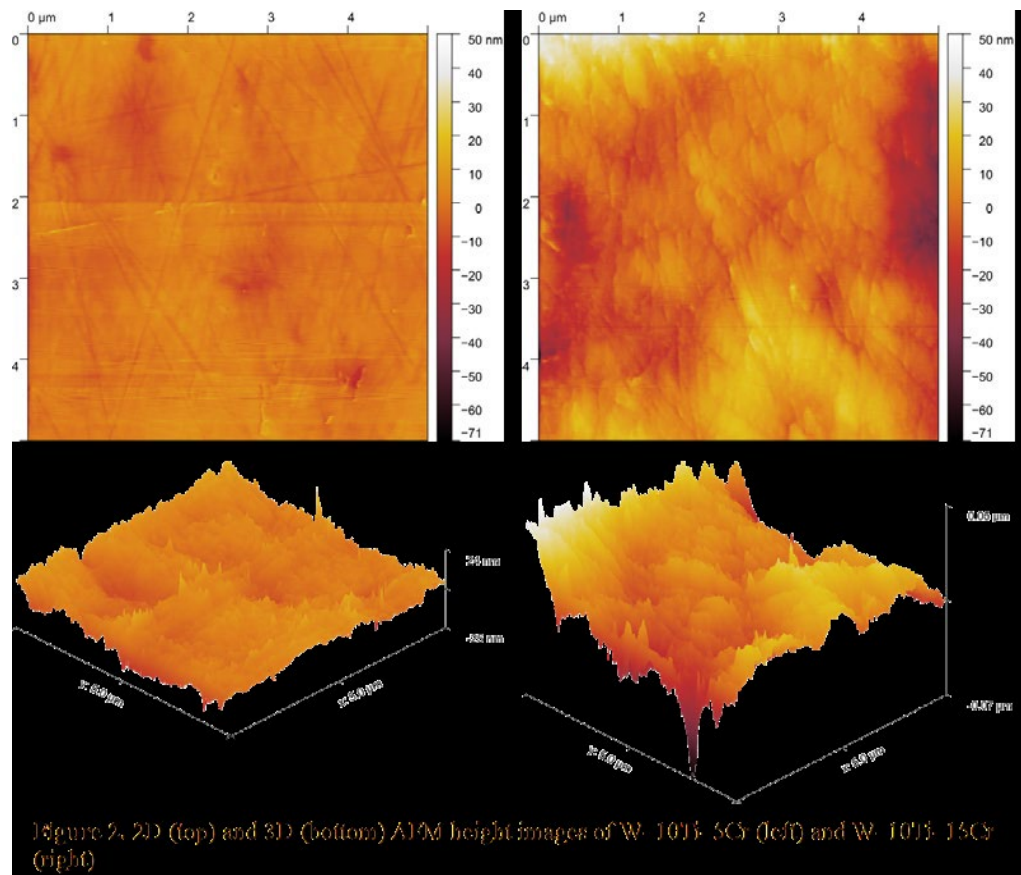
Silica Aerogels: A Review of Synthesis and Application in Hydrogen Storage

Brianna Zheng[1], Seohee Park[2], Leo Pan-Wang[3], Yongseok Kim[4], Hongyeon Lee[4], Shi Fu[5], Huiting Luo[5], Miriam Rafailovich[5]
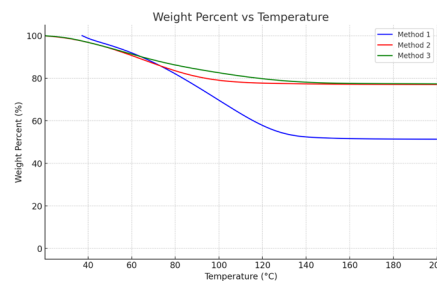[1]*BASIS Independent Silicon Valley, San Jose, CA 95126, [2]Dwight School Seoul, Seoul, South Korea, 03919, [3]Peddie High School, NJ 08520, [4]Chungnam National University, Daejeon, South Korea, [5]Department of Materials Science and Chemical Engineering, Stony Brook University, Stony Brook, NY 11794*
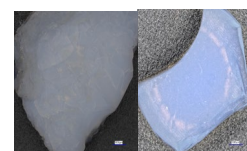
Developing efficient hydrogen storage technologies is vital for cultivating sustainable energy solutions. Hydrogen is considered a promising alternative to traditional fossil fuels due to its ability to be produced from various domestic resources and its production of only water vapor as a byproduct in fuel cells[1]. However, hydrogen's low volumetric energy density and embrittlement necessitate adsorption-based storage, which enables storage at lower pressures and near-ambient temperatures. Aerogels, ultralight, three-dimensional, highly porous materials characterized by low density and a large specific surface area, have emerged as superior adsorbents for storage[2]. While carbon aerogels have previously been identified to possess several desirable structural features for hydrogen storage, this study aims to investigate the synthesis of silica aerogels utilizing supercritical CO_2 drying and to evaluate their efficacy in hydrogen adsorption, addressing the global demand for clean and sustainable energy sources.

Aerogels are made by replacing the liquid in a gel with air. A sol solution with a 1:7:4:0.01:0.01 molar ratio of tetraethyl orthosilicate (TEOS) to ethanol (EtOH) to water (H_2O) to hydrochloric acid (HCl) to ammonium hydroxide (NH_4OH) was prepared. To create a sample size of 240 mL, 75 mL of TEOS, 135 mL of EtOH, and 300 μL of 36.5-38.0% HCl diluted with 12.5 mL of deionized (DI) water were spun in a beaker on a hot plate at 400 rpm and 40°C for 30 minutes, followed by an additional 10 minutes with the insertion of 400 μL of 28.0-30.0% NH_4OH diluted with 12.5 mL of DI water. After gelling in silicone molds for 4 hours and a three-day aging process, submerging the gels in EtOH, DI water, and EtOH for 24 hours each, the alcogels' quality was tested using Fourier-transform infrared spectroscopy (FTIR). The peaks at approximately 1080 cm^{-1}, 970 cm^{-1}, 800 cm^{-1}, and 455 cm^{-1} are all characteristic of hydrogels, confirming the presence of the Si-O asymmetric stretching vibration in siloxane, Si-O stretching vibration in the silanol group, the Si-O symmetric wagging vibration, and the Si-O-Si bending vibration, respectively.

The qualified alcogels were subjected to the supercritical drying process, which removes the EtOH solvent and preserves the aerogel's porous structure by eliminating capillary action that could shrink or collapse the gel. The final weight percentage from the thermogravimetric analysis (TGA) of our aerogels determined the amount of residual liquid, either EtOH or air moisture, in each of the three samples made using different supercritical drying methods. Our last method, as shown in Fig.01, achieved a weight percentage of 74.09%, compared to the lowest trial of 49.24%, as well as an expected appearance (Fig.02), proving to be the most successful. This method

Fig.01. Thermogravimetric Analysis of Three Aerogel Samples

utilized a metal cage to maximize the surface area for CO_2 diffusion, maintained high temperatures above 30°C throughout both holding and purging processes to prevent the condensation of EtOH, and applied quick purging to enhance the release of EtOH. Scanning electron microscopy (SEM) was used to confirm porosity. Future steps involve performing Raman spectroscopy on our aerogels and applying them to hydrogen adsorption techniques.electron microscopy, (SEM) was used to confirm porosity. uture steps involve performing Raman spectroscopy on our aerogels and applying them to hydrogen adsorption techniques.

Fig.02. Aerogels from Method 1 & 3 (left to right)

[1] Meda, Ujwal Shreenag, et al. "Challenges Associated with Hydrogen Storage Systems due to the Hydrogen Embrittlement of High Strength Steels." *International Journal of Hydrogen Energy*, vol. 48, no. 47, 1 June 2023, pp. 17894–17913, www.sciencedirect.com/science/article/abs/pii/S036031992300530X, https://doi.org/10.1016/j.ijhydene.2023.01.292. Accessed 6 Aug. 2024.

[2] Franco, Paola, et al. "Porous Aerogels and Adsorption of Pollutants from Water and Air: A Review." Molecules, vol. 26, no. 15, 23 July 2021, pp. 4440–4440, www.ncbi.nlm.nih.gov/pmc/articles/PMC8347855/, https://doi.org/10.3390/molecules26154440. Accessed 6 Aug. 2024

Assessing the Impact of Polydispersity on the Thickness of Polystyrene Thin Films to Adapt a Monodisperse Polystyrene Machine Learning Model

Dhruva Bhat[1*], Dvita Bhattacharya[2*], Isabelle Chan[3*], Aditi Kiran[4*], Eli Krasnoff[5*], Brenna Ren[6*], John Jerome[7], Miriam Rafailovich[8]

[1]Foothill High School, [2]Kent Place School, [3]Michael E. DeBakey High School for Health Professions, [4]BASIS Independent Fremont, [5]The Loomis Chaffee School, [6]The Harker School

Spin-coated polystyrene thin films have a variety of industrial applications including biomedical device production, electronics manufacturing, and nanomaterial synthesis, with film thickness affecting their mechanical, electrical, and thermal properties [1]. A previous study by Wang et al. utilized curve-fit machine learning to produce a 3-dimensional manifold relating molecular weight (MW), solution concentration, and film thickness of spin-coated monodisperse polystyrene samples [2]. Although polydisperse polystyrene is more frequently utilized in industrial applications due to its ease of production and affordability, the curve-fit model's applicability to polydisperse polystyrene has yet to be fully assessed. This study aims to evaluate the accuracy of the curve-fit model applied to polydisperse polystyrene thin films; examine the correlation between the ratio of monodisperse samples and thickness of the resultant thin-film; and adjust the curve-fit model to the polydisperse mixtures by relating the model's prediction error to the ratio of the monodisperse samples.
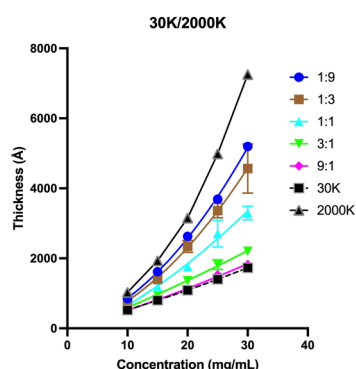
Pure polystyrene stock solutions of MWs 30K, 50K, 200K, 311K, 650K, and 2000K were made at concentrations of 10, 15, 20, 25, and 30 mg/mL. Artificial polydisperse samples were then created by mixing the combinations 30K/50K, 30K/200K, 30K/311K, 30K/650K, and 30K/2000K for each of the following ratios: 1:9, 1:3, 1:1, 3:1, and 9:1. Silicon wafers were cleaved from 100 index silicon circles, cleaned under nitrogen gas, and dipped in hydrofluoric acid to ensure hydrophobicity. Three wafers were then spin-coated with polystyrene solution for 30.0 seconds at a rate of 2500 rotations per minute and acceleration of 1000 rotations per minute squared for each MW combination and ratio. In addition to the polydisperse samples, monodisperse control wafers were created for each of the MWs at 10 mg/mL and 30 mg/mL. Ellipsometry was conducted on each sample to determine the thickness in angstroms of the polystyrene film, and average thickness values for each ratio were plotted against concentration in comparison to control monodisperse.

Fig 1. Concentration vs Thickness graph for 30K/2000K

The weighted average MW and film thickness for each sample were then inputted into Wang et al.'s model, which returned critical concentrations consistently lower than the actual concentration. The graph of thickness vs. concentration for each ratio was plotted, and the thicknesses were skewed more towards the lower MW of 30K (Fig. 1). A linear relationship was also determined between the percent of 30K MW in the polydisperse solution and the percent of the distance between the thickness of 30K to 2000K MW polystyrene at each concentration for each ratio, which had percentages significantly lower than the predicted

relationship (Fig. 2). Future research will involve quantifying the correlation between the concentration of the lower MW in the polydisperse mixture and the impact on the polydisperse polystyrene thin film's thickness, as well as determining the driving factor of this impact. Furthermore, it will be necessary to test the correlation of the concentration of the lower MW to the deviation in thickness in polystyrene solutions with more than two monodisperse MWs. Finally, once the requisite data is collected to determine each monodisperse polymer's impact on film thickness, the curve-fit model must be adjusted for its error in predicted thickness based on pure weighted average MW rather than adjusted weighted average MWs.
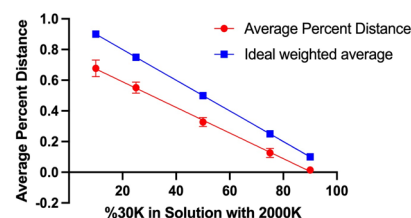
[1] Kumar, S., & Aswal, D. K. (1970, January 1). Thin film and significance of its thickness. SpringerLink. https://link.springer.com/chapter/10.1007/978-981-15-6116-0_1#:~:text=Thickness%20is%20one%20of%20the,electrical%2C%20etc.%2C%20depends.

[2] Wang, A.C., Chen, S.Z., Xie, E. et al. Utilizing machine learning to model interdependency of bulk molecular weight, solution concentration, and thickness of spin coated polystyrene thin films. MRS Communications 14, 230–236 (2024). https://doi.org/10.1557/s43579-024-00527-6

Microstructural Analysis of Mechanically-Alloyed Tungsten-Titanium-Chromium

Silas Dorsky[*1], Jhen-Bahn Benjamin Li[*2], Daniel Lim[*3], Sylvie Liu[*4], Brandon Qi[*5], Bowen Tian[*6], Philip Colman[*7], Michael Lotwin[*8], Abhinav Sharma[8], Miriam Rafailovich[8], David Sprouster[8]

*Authors contributed equally and have been sorted alphabetically

[1] The High School for Math, Science and Engineering at City College of New York, NY 10031, [2] Northern Valley Regional High School at Demarest, NJ 07627, [3] Staten Island Technical High School, NY 10306, [4] Hefei Thomas School, Anhui, China, [5] Davis Senior High School, CA 95616, [6]College Station High School, TX 77845, [7] Department of Chemistry, Lehman College of the City University of New York, NY 10468, [8] Department of Materials Science and Chemical Engineering, Stony Brook University, NY 11794

Rising global energy demands, in conjunction with increased awareness of the climate crisis, have instituted a need for reliable, clean energy, which can be sourced through nuclear fusion power. However, it is necessary to develop materials resistant to the extreme radiation doses and high-temperature environments intrinsic to nuclear fusion reactors. Tungsten has been proposed to meet these criteria, but recent research has shown that tungsten can become brittle under neutron irradiation [1]. Alternatively, mechanically-alloyed tungsten derivatives, such as tungsten-titanium-chromium (W–Ti–Cr), possess unique characteristics that mitigate some of the radiation defects and stem grain recrystallization at high temperatures, allowing for increased phase stability [2]. The objective of this research is to analyze the microstructural properties of mechanically-alloyed W–Ti–Cr samples with varying concentrations of chromium.

Three specimens (W–Ti–Cr with 10% Ti by concentration and 5%, 10%, and 15% Cr by concentration) were sintered in a vacuum atmosphere at a heating rate of 50 °C/min before reaching 1200 °C, where they were held for 15 minutes before cooling down. To prepare for microstructural characterization, the samples were sequentially polished with SiC polishing paper at grits P800, P1200, and P2400, then fine polished with diamond

Figure 1. XRD patterns of W–Ti–Cr specimens
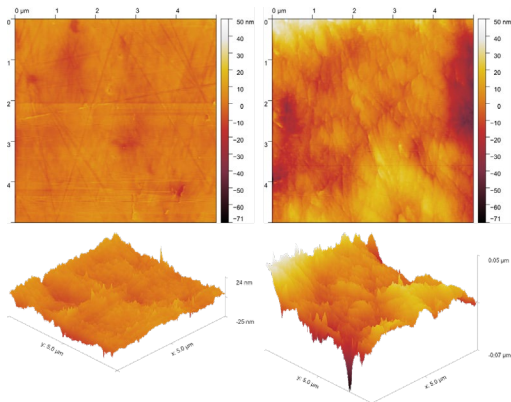
Figure 2. 2D (top) and 3D (bottom) AFM height images of W–10Ti–5Cr (left) and W–10Ti–15Cr (right)

suspension solutions of sizes 15 μm, 9 μm, 3 μm, and 1 μm. The samples were then ultrasonicated in isopropanol for 5 minutes and analyzed using X-ray diffraction (XRD) at a wavelength of 1.5418 angstroms and atomic force microscopy (AFM) at a 5 μm by 5 μm field of view. XRD results (Figure 1) were further examined using TOPAS Rietveld refinements and quantitative phase analysis, while AFM images (Figure 2) were segmented using Trainable Weka Segmentation in FIJI and Watershed Segmentation in Gwyddion to determine average grain size.

XRD analysis indicated the materials were multi-phase, with minor titanium and surface contamination from the SiC polishing. TOPAS refinements revealed that as chromium concentration within the samples increased, lattice parameters systematically contracted and crystallite sizes decreased. Additionally, diffraction peaks from a chromium phase were not observed, indicating that the chromium was effectively incorporated within the tungsten host matrix as a substitutional dopant and potentially concentrated at grain boundaries. Lateral force imaging from AFM show evidence that chromium was segregated at grain boundaries with clear depressions in the force traces across grain boundaries. In future studies, the stability of the grain size and chemical alloying distribution after neutron irradiation and high-temperature exposures will be investigated, and XRD and AFM methods will be utilized to quantify changes post-exposure.

[1] Katoh, Y., Snead, L., Garrison, L., Hu, X., Koyanagi, T., Parish, C., Edmondson, P., Fukuda, M., Hwang, T., Tanaka, T., & Hasegawa, A. (2019). Response of unalloyed tungsten to mixed spectrum neutrons. Journal of Nuclear Materials, 520, 193–207. https://doi.org/10.1016/j.jnucmat.2019.03.045

[2] Olynik, N., Cheng, B., Sprouster, D. J., Parish, C. M., & Trelewicz, J. R. (2022). Microstructural Transitions during Powder Metallurgical Processing of Solute Stabilized Nanostructured Tungsten Alloys. Metals, 12(1), 159. https://doi.org/10.3390/met12010159

Microstructural Analysis of Ultra-High Temperature Ceramics: Tungsten Carbide and Vanadium Carbide

Silas Dorsky[*1], Jhen-Bahn Benjamin Li[*2], Daniel Lim[*3], Sylvie Liu[*4], Brandon Qi[*5], Bowen Tian[*6], Philip Colman[*7], Michael Lotwin[*8], Abhinav Sharma[8], Miriam Rafailovich[8], David Sprouster[8]

*Authors contributed equally and have been sorted alphabetically

[1] The High School for Math, Science and Engineering at City College of New York, NY 10031, [2] Northern Valley Regional High School at Demarest, NJ 07627, [3] Staten Island Technical High School, NY 10306, [4] Hefei Thomas School, Anhui, China, [5] Davis Senior High School, CA 95616, [6] College Station High School, TX 77845, [7] Department of Chemistry, Lehman College of the City University of New York, NY 10468, [8] Department of Materials Science and Chemical Engineering, Stony Brook University, NY 11794

Nuclear fusion is capable of providing large-scale clean energy to meet global demands. A primary issue with implementing nuclear fusion is finding durable materials that can withstand the extreme conditions of a fusion reactor. Ultra-high temperature ceramics (UHTCs) have emerged as promising candidates with unique thermal and electrical properties [1] for potential applications as plasma-facing materials. However, microstructural properties such as grain size and grain boundary density can reduce a material's ability to shield against neutron irradiation [2]. Hence, the objective of this research is to analyze the microstructural characteristics of two potential UHTC materials, tungsten carbide (WC) and vanadium carbide (VC), fabricated through direct current sintering with and without silicon carbide (SiC) additives.

Four specimens (WC, WC with 4% SiC by concentration, VC, and VC with 4% SiC by concentration) were sintered in a vacuum atmosphere at a heating rate of 50°C/min before reaching 1900°C, where they were held at a constant temperature for 15 minutes before cooling down. To prepare for microstructural characterization, the samples were sequentially polished with SiC polishing paper with grits P800, P1200, and P2400, then fine polished with diamond suspension solutions of sizes 15 μm, 9 μm, 3 μm, and 1 μm. The samples were then ultrasonicated in isopropanol for 5 minutes and analyzed using X-ray diffraction (XRD) at a wavelength of 1.5418 angstroms and atomic force microscopy (AFM) at a 5 μm by 5 μm field of view. XRD results (Fig. 1) were further examined using TOPAS Rietveld refinements and quantitative phase analysis, while AFM images (Fig. 1) were segmented using Trainable Weka Segmentation in FIJI and Watershed Segmentation in Gwyddion to determine mean grain size.

XRD analysis revealed the materials fabricated were single-phase, with minor surface contamination from the SiC polishing. TOPAS refinement determined similar lattice parameters and coherent mean crystallite sizes for the WC and VC specimens as well as their SiC-containing counterparts. Segmentation data for the AFM images showed similar mean grain sizes. These results demonstrate the stability of the UHTC microstructure for processing and point to potential research investigating changes in mean grain size and grain boundary characteristics after high-temperature exposure and extreme radiation damage.

---
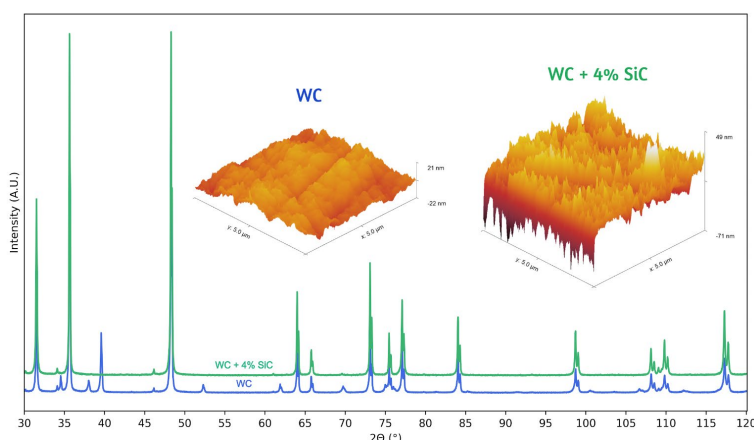
[1] Wyatt, B. C., Nemani, S. K., Hilmas, G. E., Opila, E. J., & Anasori, B. (2023). Ultra-high temperature ceramics for extreme environments. Nature Reviews Materials. https://doi.org/10.1038/s41578-023-00619-0

[2] Zinkle, S., & Snead, L. (2014). Designing radiation resistance in materials for fusion energy. Annual Review of Materials Research, 44(1), 241–267. https://doi.org/10.1146/annurev-matsci-070813-113627

Session VI: Clean Energy Generation

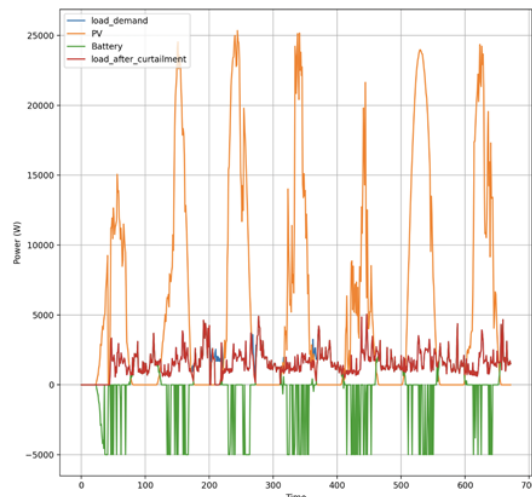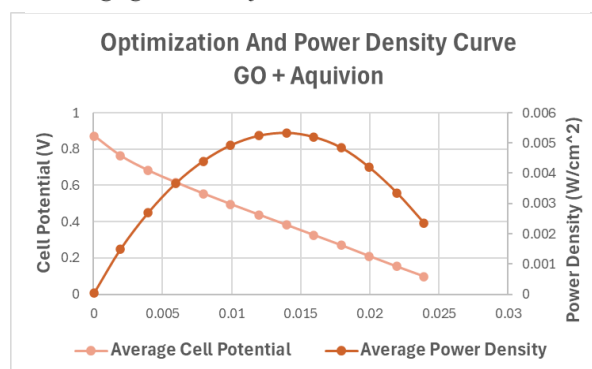## Haoyan Fang, Md Farabi Rahman, Chaofan Lin, Eliana Matsil, Zimin Jiang

Figure 1 - Power of load, PV production, battery charging/ discharging, and load after curtailment over time

Optimization of Aquivion Proton Exchange Membrane Fuel Cells with Synthesized Graphene Oxide

Indus Boddu[1,2], Dylan Deng[1,3], Maya Puterman[1,4], Rebecca Isseroff[1], MD Farabi Rahman[1], Miriam Rafailovich[1],

[1]Stony Brook University, Stony Brook, NY 11790, [2]High Technology High School, Lincroft, NJ 07738, [3]Westview High School, San Diego, CA 92129, [4]Ramaz Upper School, New York, NY 10075

Proton Exchange Membrane Fuel Cells (PEMFCs) have become a subject of research interest for properties including clean emissions, high power density, and high portability.[1, 2] However, fuel cells (FCs) have a low individual power output. In addition, the platinum catalyst that causes hydrogen to split into protons and electrons is subject to carbon monoxide (CO) poisoning due to the reverse gas shift reaction, degrading FC performance.[3] This study aims to improve the power output of Aquivion, a new PEMFC membrane, using the integration of graphene oxide (GO)-based electrolyte solutions.

Graphene oxide, consisting of sheets of carbon atoms studded with carboxyl, hydroxyl, and epoxy functional groups, has been studied for its electronic and optical properties and monolayer structure. This study tested the effects of integrating graphene oxide, partially reduced graphene oxide (prGO), and metallized GO onto an Aquivion membrane to enhance the power output of a PEMFC.
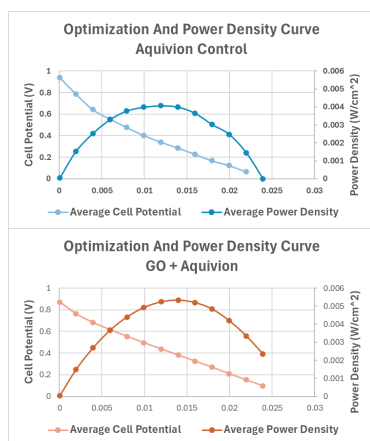

Fig 1. Optimization and

This study was conducted using an optimal hydrogen flow rate of 129 SCCM. Solutions diluted 1:2 in distilled water were deposited onto a hydrated Aquivion membrane by either dipping or spraying. Spraying ~205 µL of solution (four drops) on each side of the membrane was optimal for enhancing power output for a duration of at least four consecutive tests. A comparison between 1 mg/ml GO and different degrees of reduction of prGO concentrations was done on various membranes to determine the base solution that would provide the optimal power output with integrated nanoparticles. The 18 mM prGO sample provided a power increase of 22.8% over the control, the best of the pRGO samples. However, the unreduced GO sample proved to be the most effective, with a power increase of 28.0% greater than the control (Fig 1). Additionally, GO metallized with platinum was tested on Aquivion but diminished the power output, possibly because some platinum precipitated out and disrupted the proton exchange. GO metallized with a mixture of nickel, copper, manganese, cobalt, and iron was also tested but resulted in a power increase of only 9% over the control (Fig 2.).

Our findings demonstrate that graphene oxide successfully increases the power output of Aquivion FCs. Future work includes testing the effects of GO functionalized with individual catalytic metal nanoparticles, investigating various temperatures and humidity levels, and examining different levels of partial GO reduction on Aquivion FC.
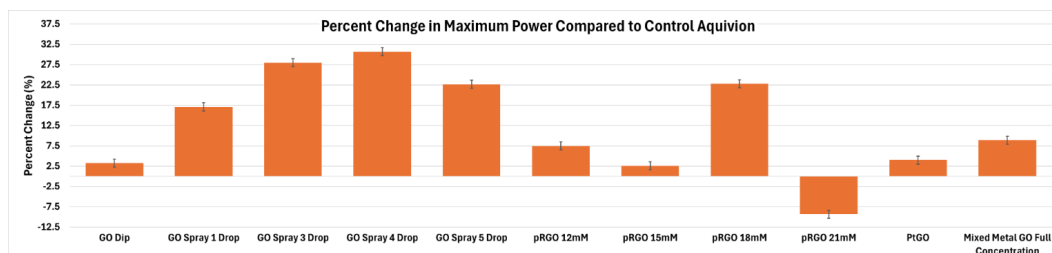
Fig. 2: Analyzing the Power Output Enhancement of Various Aquivion Treatments.

[1]Tellez-Cruz, M. M., Escorihuela, J., Solorza-Feria, O., & Compañ, V. (2021). Proton Exchange Membrane Fuel Cells (PEMFCs): Advances and Challenges. *Polymers*, *13*(18), 3064. https://doi.org/10.3390/polym13183064

[2]Lin Chen, Yongwen Ren, Faying Fan, Tianyuan Wu, Zhe Wang, Yaojian Zhang, Jingwen Zhao, Guanglei Cui, Artificial frameworks towards ion-channel construction in proton exchange membranes, Journal of Power Sources, Volume 574, 2023, 233081, ISSN 0378-7753, https://doi.org/10.1016/j.jpowsour.2023.233081.

[3]A. Rodrigues, J. C. Amphlett, R. F. Mann, B. A. Peppley and P. R. Roberge, "Carbon monoxide poisoning of proton-exchange membrane fuel cells," *IECEC-97 Proceedings of the Thirty-Second Intersociety Energy Conversion Engineering Conference (Cat. No.97CH6203)*, Honolulu, HI, USA, 1997, pp. 768-773 vol.2, doi: 10.1109/IECEC.1997.660236.

Enhancing AEM Fuel Cell Performance Using Partially Reduced Graphene Oxide

Eva Jain[1], Amanda Liu[2], Ella Wunderlich[3], Evan Xie[4], Oluomachi Uwakwe[5], Haoyan Fang[5], Farabi Rahman[5], Miriam Rafailovich[5]

[1]Tesla STEM High School, Redmond, WA 98053, [2]Redlands High School, Redlands, CA 92374, [3]Pingry School, Basking Ridge, NJ 07920, [4]Deerfield Academy, Deerfield, MA, 01342 [5]Department of Materials Science and Chemical Engineering, Stony Brook University, Stony Brook, NY 11794

Alkaline Exchange Membrane Fuel Cells (AEMFC) are at the forefront of research in sustainable and renewable energy systems. AEMFCs are of interest due to their higher power output compared to proton exchange membrane hydrogen fuel cells. Thus far, their widespread use is limited by their short lifespan and the requirement of pure oxygen conditions[1]. Current efforts aim to improve their power efficiency and stability, with a particular focus on addressing challenges such as the migration of Platinum (Pt) ions across the Anion Exchange Membrane (AEM), which rapidly degrades fuel cell performance[2].

In this study, we explored the use of graphene-based materials, including graphene oxide (GO) and partially reduced graphene oxide (prGO) at various concentrations (6, 12, 15, 18, and 21 mmol $NaBH_4$), to enhance AEMFC performance. We hypothesized that adding prGO to the AEM would improve fuel cell efficiency due to graphene's high electrical conductivity and large surface area[3]. GO, prepared by Hummer's method, was dissolved in distilled water and partially reduced with $NaBH_4$ to create the prGO at different concentrations. XRD results showed 21mmol reduction prGO had a more oxidized degree compared to the 12mmol prGO. As shown in Figure 1(a), after air-spraying prGO solutions onto Sustainion membranes, we found that the 12 mmol prGO sample exhibited the best performance, achieving a maximum power density of 0.604 W/cm^2, a 48.8% increase over the control sample. As the concentration of $NaBH_4$ increased beyond 12 mmol, we saw a progressive decrease in the maximum power density. Comparing the performance of prGO with GO, we saw that the 12 mmol prGO sample outperformed the GO sample by 92 mW/cm^2. Additionally, we examined fuel cell performance when only the anode or the cathode was coated with 12 mmol prGO. The anode-only sample demonstrated slightly higher performance compared to the cathode-only sample as seen in Figure 1(b), with the anode-only sample having an 18.23% increase over the control sample while the cathode-onl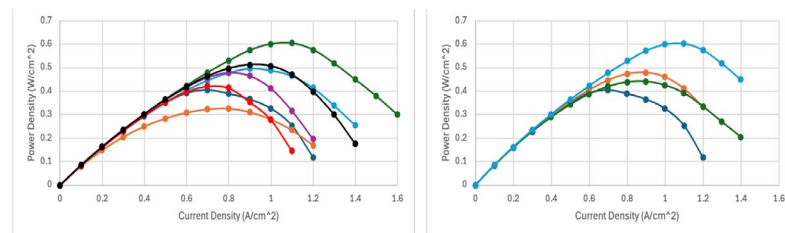y sample only had an 8.87% increase. However, the highest performance was achieved when both sides of the Sustanion membrane were sprayed, indicating a positive synergistic effect. Our study suggests that prGO, particularly at the 12 mmol concentration, is a promising material for enhancing the performance of AEMFCs, leading to significant improvements in peak power density. These findings could contribute to the proliferation of AEMFCs as a viable method of sustainable energy generation, with potential applications spanning the transportation industry, spacecraft development, and beyond.

Figure 1. (a) Power density curve for various prGO concentrations. (b) Power density curve for 12 mmol prGO membranes

(1) Ramaswamy, N.; Mukerjee, S. Alkaline Anion-Exchange Membrane Fuel Cells: Challenges in Electrocatalysis and Interfacial Charge Transfer. *Chemical Reviews* **2019**, *119* (23), 11945–11979. https://doi.org/10.1021/acs.chemrev.9b00157.

(2) Raut, A.; Fang, H.; Lin, Y.; Fu, S.; Sprouster, D.; Ryuichi Shimogawa; Frenkel, A. I.; Bae, C.; Douglin, J. C.; Jaana Lillojad; Kaido Tammeveski; Zeng, Z.; Stoyan Bliznakov; Rafailovich, M.; Dekel, D. R. Migration and Precipitation of Platinum in Anion-Exchange Membrane Fuel Cells. *Angewandte Chemie* **2023**, *135* (37). https://doi.org/10.1002/ange.202306754.

(3) Somya Samantaray; Mohanty, D.; Santosh Kumar Satpathy; Hung, I-Ming. Exploring Recent Developments in Graphene-Based Cathode Materials for Fuel Cell Applications: A Comprehensive Overview. *Molecules* **2024**, *29* (12), 2937–2937. https://doi.org/10.3390/molecules29122937.

Improving Proton Exchange Membrane Fuel Cells by Thiol-Capped Silver Nanoparticles

Yuchen Bai[*1], Hongfan Deng[*2], Evan Ji[*3], Cynthia Qian[*4], Farabi Rahman[5], Haoyan Fang[5], Miriam Rafailovich[5]

[1] *Experimental High School Attached to Beijing Normal University, Beijing, China, 100032,* [2] *Hefei Thomas School, Hefei, China, 230088,* [3] *Del Norte High School, CA 92127,* [4] *Jericho High School, NY 11753,* [5] *Department of Materials Science and Chemical Engineering, Stony Brook University, Stony Brook, NY 11794*

Hydrogen fuel cells have emerged as a sustainable and clean energy source, generating electricity through the electrochemical reaction between hydrogen and oxygen, emitting water vapor as a sole byproduct. This technology has been proposed as a resolution to the impact of carbon emissions on climate change[1]. Proton exchange membrane fuel cells (PEMFCs) are a type of fuel cell that transports H^+ from the anode to the cathode across a proton exchange membrane (PEM). PEMFCs have been noted for their low operating temperatures and high power densities[2]. However, since existing PEMFCs use platinum (Pt) catalysts to enhance efficiency, the cost of Pt materials limits their commercialization. Furthermore, carbon monoxide (CO) binding with Pt catalysts, due to inevitable CO impurities in hydrogen gas, also leads to fewer active sites on the catalysts, lowering cell efficiency. To mitigate this, the incorporation of non-Pt group catalysts into the fuel cell system has been proposed to reduce the dependency on Pt. Therefore, this study aims to investigate octanethiol-stabilized silver nanoparticles (AgNPs) as a CO-resistant catalyst in PEMFCs and test the impact of AgNPs at different thiol stabilization levels on PEMFC efficiency.

AgNPs were synthesized using the Brust-Schiffrin method. During the synthesis, 200, 400, or 600 μL of octanethiol (200th, 400th, 600th respectively) were added. The thiol molecules surrounded the AgNPs, forming stable Ag–S–C links, which prevented agglomeration and maintained their functional properties. Transmission electron microscopy (TEM) images of the 200th AgNP samples (Figure 1) confirmed their quasi-spherical shapes and normal size distributions, with an average diameter of 2.7 ± 0.8 nm. However, TEM images of the 400th and 600th AgNPs demonstrated agglomeration, likely caused by incomplete reduction of Ag salt in the synthesis process or oxidation of AgNPs after synthesis. X-ray diffraction (XRD) analysis of all samples (Figure 2) showed reflections at 38.1, 44.3, 64.4, and 77.3 degrees, which aligns with AgNP peaks in literature[3], representing the diffraction from (111), (200), and (220) planes of silver; the peak at 32.1 degree indicated the presence of silver oxide (Ag_2O). The 200th nanoparticles' XRD spectra showed the highest peak intensity ratio of AgNP to Ag_2O, which supported the TEM results.

Isothermal data of AgNPs at each thiol stabilization level, collected with a Langmuir-Blodgett trough (LBT), were analyzed to determine the surface pressures at which AgNP monolayers start to form. Deposition of 200th, 400th, and 600th AgNP monolayers on Nafion-117 membranes at 5 and 10 mN/m surface pressures was then completed using the LBT. The resulting six nanoparticle-deposited membranes were characterized for their PEMFC performances at a fuel cell test station. Results (Figure 3) demonstrated 22.2% and 44.4% maximum power density enhancements (vs. the control) for the 200th AgNPs deposited at 5 mN/m and 10 mN/m pressures, respectively, and no significant enhancement by the 400th or 600th AgNPs at either pressure, as predicted by the TEM and XRD analyses.

This study derived a method of applying thiol-stabilized AgNPs on Nafion membranes in a PEMFC for power density and durability enhancements, and disproved the use of excessively high concentrations of octanethiol in the synthesis of AgNPs to increase their catalytic activities. Future research will investigate the 200th AgNPs deposited at higher monolayer formation pressures (15 mN/m, 20 mN/m, etc.) toward improved catalytic activities in a PEMFC. CO poisoning resistance capabilities of the 200th AgNPs will also be studied.
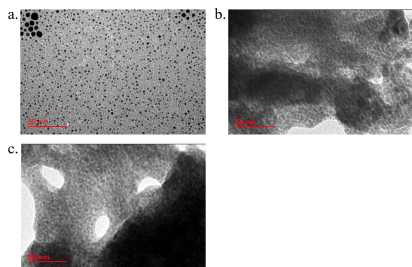
Figure 1. TEM images of (a) 200th (b) 400th (c) 600th AgNPs
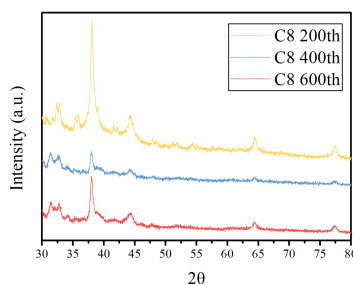
Figure 2. XRD spectra of AgNPs at different thiol stabilization levels
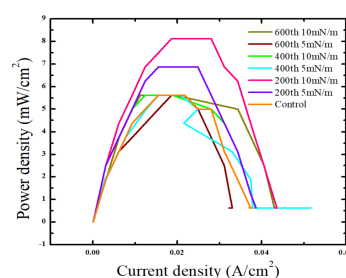
Figure 3. Polarization curves of AgNPs-deposited Nafion membranes

[1] Edwards, P. P., et al. "Hydrogen and Fuel Cells: Towards a Sustainable Energy Future." *Energy Policy*, vol. 36, no. 12, Dec. 2008, pp. 4356–4362, doi:10.1016/j.enpol.2008.09.036.

[2] O'Hayre, Ryan. *Fuel Cell Fundamentals*. 3rd ed., Wiley, 2016.

[3] Anandalakshmi, K., et al. "Characterization of Silver Nanoparticles by Green Synthesis Method Using Pedalium Murex Leaf Extract and Their Antibacterial Activity." *Applied Nanoscience*, vol. 6, no. 3, May 2015, pp. 399–408, doi:10.1007/s13204-015-0449-z

Microgrid Design for Energy-Independence in the Shinnecock Nation

Vinav Shah*, Nathan Qiu*, Emily Jiang*, Zihan Jia*, Eliana Matsil, Daniel Arnoldi, Chaofan Lin,
Zimin Jiang, Peng Zhang, Miriam Rafailovich

A microgrid is an independent electric grid with onsite energy generation and storage that can operate both independently from or connected to the centralized main grid. Customers who install microgrid technology can save their energy costs while gaining a reliable source of backup power in the event of a main grid outage and also reduce greenhouse gas emissions if the microgrid uses renewable energy sources such as solar or wind. In this project, we worked with the Shinnecock Indian Nation to establish an off the grid-energy system for hunter shelters, temporary housing aimed at addressing housing for homeless members of the Shinnecock Nation.

Addressing the issue of energy poverty, a solar array was installed on the reservation, which provides energy for the two hunter homes. Without the capability for energy storage, however, the houses are still dependent on external lines for energy in a low-production environment. The nation hopes to offset the cost of purchasing external energy, achieve energy sovereignty, and have a resilient power source with the implementation of a full microgrid with islanding capabilities. Our project focuses on the development of an independent microgrid system for the Shinnecock Indian Nation in Southampton, New York.

By constructing the microgrid, we aim to design a system that can help us achieve complete off-the-grid operation for the Shinnecock Microgrid so that the system can choose the best combination at the different weather conditions. In detail, the system can optimize microgrid energy storage configuration to minimize energy curtail (wasted energy) in order to decide between difference energy storage by collecting the real consumption voltage from the home and do estimation about the sources of consumption and decide the solution to cope with them. In addition to this, the system can also determine how to develop an integrated hydrogen energy/battery storage system to generate energy when in need. This is the key for the off-the-grid operation of the home as the energy is produced.

We used an open source model paired with the energy grid optimizer Gurobi. First, we formulated our own objectives and constraints mathematically. We then implemented these objectives and constraints into the program. Running the simulations allowed us to obtain the optimal configuration for distribution of batteries and hydrogen fuel cells. Finally, we evaluated the feasibility of such a solution by graphing the variables involved in the problem including PV production, load demand, and battery charging/discharging (figure 1). Finally, we continued to formulate slightly modified objectives to arrive at

Figure 1 - Power of load, PV production, battery charging/ discharging, and load after curtailment over time

the optimal solution. This study will play an important role in real life. Firstly, it shows the feasibility of establishing an off-the-grid energy system for the Shinnecock Reservation using the existing solar array and a hydrogen storage system, which serves as the basic model for achieving energy independence. By doing so, the solar array can potentially meet the energy demands of the homes, especially during months with lower sunlight, the project supports the goal of grid-independence for the Shinnecock Nation. In this case, the home can run on itself and being crucial to have resilience against power outages and reliance on external energy sources. Besides, the implementation of a solar-to-hydrogen system promotes the use of renewable energy, reducing the carbon footprint and environmental impact of the community. This aligns with global efforts to transition to sustainable energy sources.
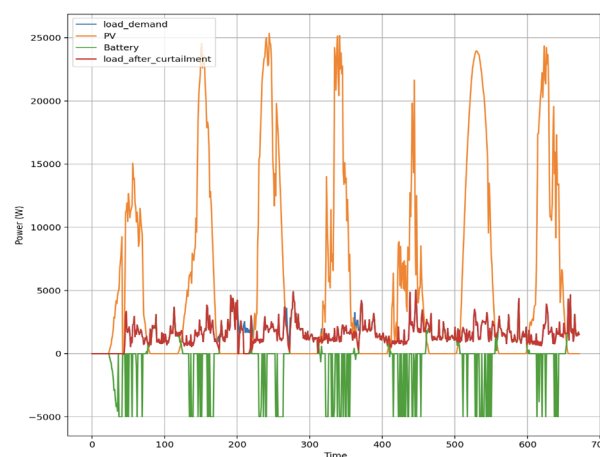
Arnoldi, D., Matsil, E., & Harris, M. (2024). Solar-to-Hydrogen Microgrid Evaluation for Hunter Homes of Shinnecock Nation. *Journal of Undergraduate Chemical Engineering Research*, *13*(9). https://drive.google.com/file/d/1NNqSUM5MvlixmIl91v7mOS509gyu8TvB/viewNarum, D., Ganion, J., & Carter, D. (2019). *Developing a Low-Carbon Microgrid on Tribal Lands: A Case Study*. https://bluelakerancheria-nsn.gov/wp-content/uploads/2017/08/11_459.pdf

Session VII: Nanocomposites

Yiwei Fang
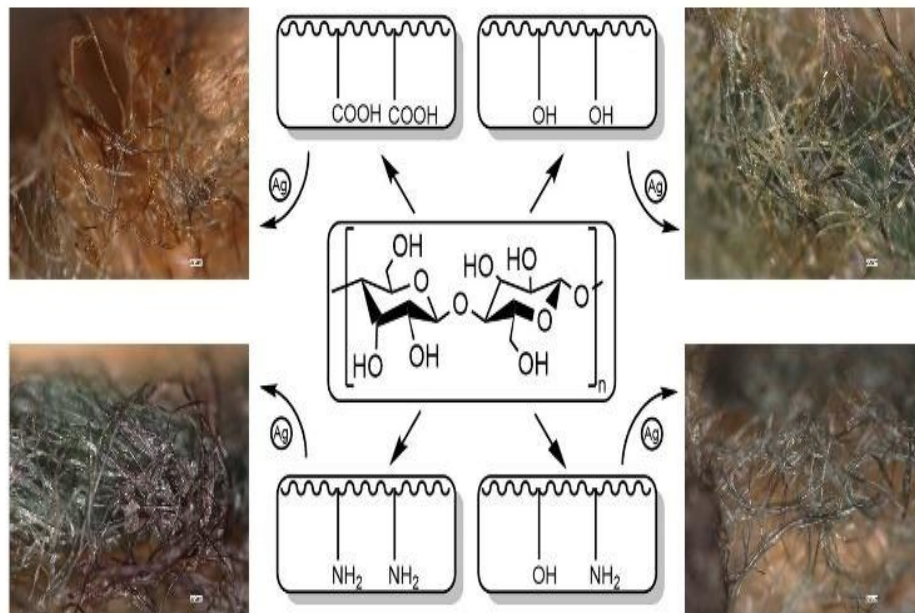
Compatibilizing Recycled Polymer Blends

Damien Crowley[1], Brianna Zheng[2], Katherine Martinez[3], Allen Bethancourt[3], Yiwei Fang,[3] Miriam Rafailovich[3]
[1]*Wantagh High School, Wantagh, NY 11793*,[2]*BASIS Independent Silicon Valley, San Jose, CA 95126*,[3]*Stony Brook University, Stony Brook, NY 11794*

Mixed sorting of plastics at recycling facilities limits the capacity for recycling, because many synthetic organic compounds are incompatible with others at the molecular level, resulting in high interfacial tensions and immiscible blends. Consequently, less than 9% of United States plastic is recycled annually[2]. While research has displayed blend enhancement by organoclays, phyllosilicates functionalized with organic molecules, and silica-coated cellulose nanofibers (sCNF) and microfibers (sCMF), phase separation in nanocomposites still poses extensive limitations for recycling competence[3]. Thus, this study aims to understand the mechanical and interfacial impact of adding organoclay, clay combined with RDP, a flame retardant, sCMF, and sCNF to commonly recycled nanocomposite blends, exploring potential solutions to polymer incompatibility. We hypothesized that organoclay application would decrease interfacial tension while sCNF and sCMF treatment would enhance mechanical strength.

50-gram blends of 35 g polylactic acid (PLA) and 15 g polystyrene (PS) were composited with various copolymers (e.g., C-20A, C-30B, acryl-sCMF, sCMF, RDP-clay) at various concentrations (1%, 3%, 5%) in a Brabender at 180°C and molded into necessary formats for experimentation (rectangular prisms, dog bones, notched). Differential scanning calorimetry was initially conducted on the control, C-20A, and C-30B samples, revealing slight convergence in polymer glass transition (T_g) temperature: C-20A induced a -0.41°C alteration in T_g compared to the control while the C-30B displayed a -1.13°C change, two statistically insignificant modifications. Dynamic mechanical analysis revealed that C-30B also boosted amalgam elasticity. Transmission electron microscope (TEM) imaging qualified these results, however, because C-20A was found at the PLA-PS interfaces more than C-30B, which was commonly in the PLA domain. Sample impact strength findings demonstrated clay-induced brittleness, while sCMF and sCNF results were insignificant within error (Figure 1). Tensile testing imitated these conclusions.

Similar compounding of PLA and polycaprolactone (PCL) occurred next, and impact strength testing revealed PCL sample superiority (Figure 1). Additionally, sCNF, especially when concentrated at 3%, improved impact strength significantly (+95.5 ± 15.13 (J/m)) (Figure 1). Tensile testing also displayed PCL's augmentation of PLA ductility. Future work includes TEM imaging of PLA:PCL composites, analysis of PLA:PCL tensile data, surface tension analysis using Young's contact angle, scanning electron microscopy, and RDP-clay sample experimentation and analysis.
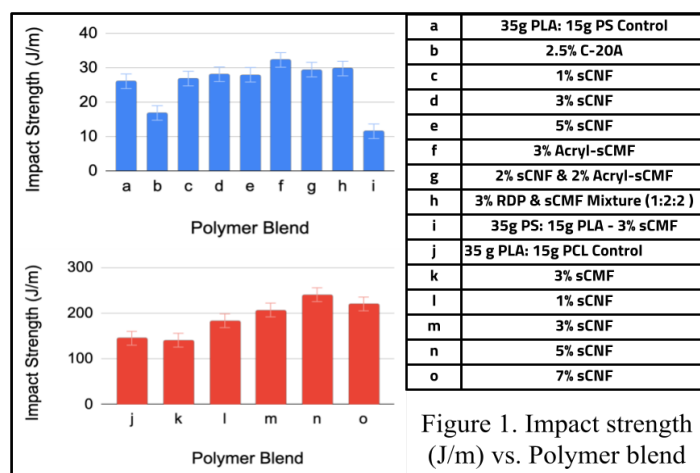

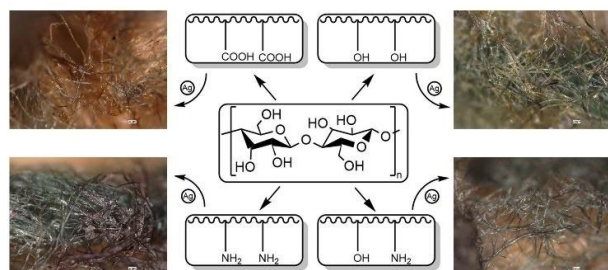|	
a	35g PLA: 15g PS Control
b	2.5% C-20A
c	1% sCNF
d	3% sCNF
e	5% sCNF
f	3% Acryl-sCMF
g	2% sCNF & 2% Acryl-sCMF
h	3% RDP & sCMF Mixture (1:2:2)
i	35g PS: 15g PLA - 3% sCMF
j	35 g PLA: 15g PCL Control
k	3% sCMF
l	1% sCNF
m	3% sCNF
n	5% sCNF
o	7% sCNF

Figure 1. Impact strength (J/m) vs. Polymer blend

[1]Bourtsalas, Yepes, I. M., & Tian, Y. (2023). U.S. plastic waste exports: A state-by-state analysis pre- and post-China import ban. *Journal of Environmental Management*, *344*, 118604. https://doi.org/10.1016/j.jenvman.2023.118604
[2]Dorigato, A. (2021). Recycling of polymer blends. *Advanced Industrial and Engineering Polymer Research*, *4*(2), 53–69. https://doi.org/10.1016/j.aiepr.2021.02.00

Sustainable Fabrication of Silver Nanoparticles on Functionalized Cotton Fibers
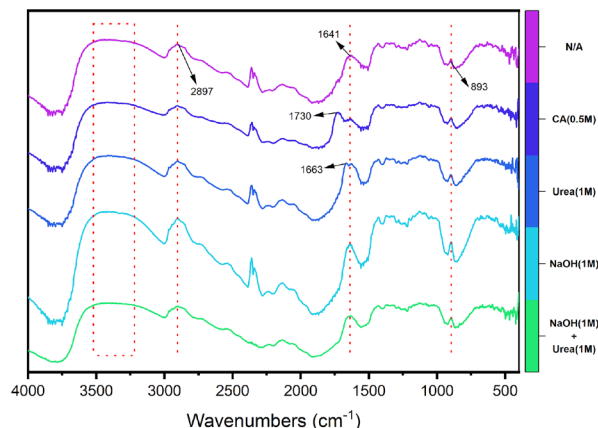
Runjing Guo[1], Gary Halada[2], Michael Cuiffo[2]

[1]The Experimental High School Attached to Beijing Normal University, Beijing, China 100032; [2]Department of Materials Science and Chemical Engineering, Stony Brook University, Stony Brook, NY, 11790

Figure 1. Digital Microscopy of Ag NPs Coated Cotton Fibers

The synthesis of silver nanoparticles in natural fibers has become a promising green field[1]. The antimicrobial properties of Ag NPs make them suitable for potential usage in wearable medical devices designed to monitor various human body conditions. This study researched a series of functional group modifications of cellulose aiming to make the whole process of Ag NPs synthesis green, safe, and effective.

In this study, 25 pieces of 0.5cm×0.5cm square cotton cloths were treated differently with citric acid (0.5M) solution, NaOH (1M) solution, Urea (1M) solution, and Urea (1M), NaOH (1M) mixed solution for 0.5 hours to chemically deweave cotton cloths down to fibers. After drying out, the samples were soaked in a 50ml solution with 0.25g lecithin and 0.5g urea for 24 hours as the reduction process. Then, the solutions were switched to 0.1M AgNO$_3$ for another 24 hours to synthesize Ag NPs.
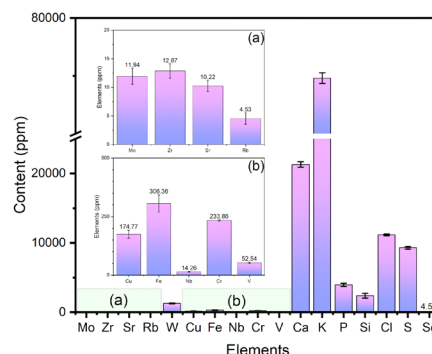
Various methods of characterization and analysis were conducted on the samples, including Optical and Digital Microscopy, Elemental Analysis, Fourier Transform Infrared Spectroscopy (FTIR), X-ray Photoelectron Spectroscopy (XPS), X-ray Fluorescence (XRF), and Scanning Electron Microscopy (SEM).

Figure 2. XRF of Cotton Cloth

Figure 1 shows the Digital Microscopy of Ag NPs coatings on cotton fibers. It is evident that silver particles are covering the fibers well. Figure 2 shows the XRF of cotton cloth to check the contaminations on cotton fibers. Figure 3 is the FTIR spectrum in DRIFTS mode, showing the chemical modification of functional groups on different samples.

Future works could focus on testing the functional properties of Ag NPs coated cotton fibers, including conductivity, thermal stability, cell toxicity, and encapsulation of Ag NPs coating.

Figure SEQ Figure * ARABIC 3. FTIR of Deweaved Cotton Fibers

[1] Barani, H., Montazer, M., Samadi, N., & Toliyat, T. (2012). In situ synthesis of nano silver/lecithin on wool: Enhancing nanoparticles diffusion. *Colloids and Surfaces B: Biointerfaces*, *92*, 9–15. https://doi.org/10.1016/j.colsurfb.2011.10.062

Session VIII: Anti-Bacterial Devices
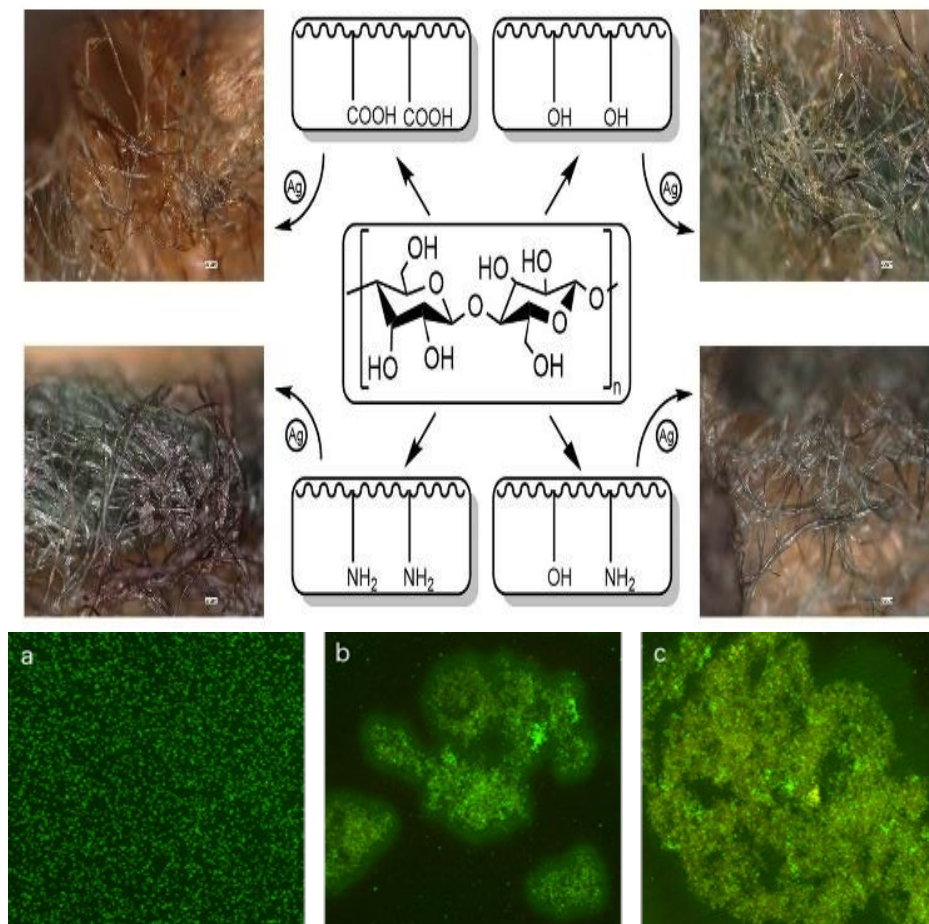
Abdelhameed Mahmoud, Shi Fu, Zoe Katevadis

Figure 1. Live/dead stain image of (a) E.coli, (b) E.coli mixed with GO, (c) E.coli mixed with pRGO

An Innovative Injectable, Retrievable, and Sustainable Drug Delivery System for Endodontic Therapy

Aadi Bordia[1*], Candy Deng[2*], Eli Krasnoff[3*], Linda Liang[4*], Brenna Ren[5*], Mira Setia[6*], Zoe Katevatis[7*], Abdel H. Mahmoud[7], Aaron Sloutski[8], Miriam Rafailovich[8]

[1]*Archimedean Upper Conservatory, [2]YK Pao School, [3]The Loomis Chaffee School, [4]Experimental High School Attached to Beijing Normal University, [5]The Harker School, [6]New Providence High School, [7]Stony Brook School of Dental Medicine, NY 11790, [8]Department of Materials Science and Engineering, Stony Brook University, NY 11790*

Endodontic treatment failures, commonly caused by *Enterococcus faecalis*, pose a significant challenge in dental treatment[1]. Addressing this issue requires the implementation of a novel intracanal medicament with antimicrobial efficacy, high injectability and retrievability, stability, sustained drug release, and optimal pH. While calcium hydroxide remains the predominant medicament, it lacks sufficient antimicrobial efficiency against *E. faecalis*, has poor flowability and retrievability, does not provide sustained release, and has a high pH. This study aims to investigate the potential of a mixture of calcium hydroxide and salicylic acid (CASA) encapsulated in thermoreversible hydrogels (F127-DMA) as an injectable and retrievable intracanal medicament with strong antibacterial efficacy and sustained and controlled drug release.

CASA was prepared by mixing calcium hydroxide and salicylic acid at a 1:6 ratio, respectively, then added to F127-DMA and UV-crosslinked using Lithium phenyl (2,4,6-trimethylbenzoyl) phosphinate (LAP). The injectability and retrievability of the hydrogel were assessed using a rheometer and a clear root canal model. Chemical characterization was determined through RAMAN and FT-IR spectroscopy. The pH of F127-DMA/CASA hydrogels was measured, and solubility was assessed. Additionally, this study examined swelling, degradation, and crosslinking efficiency to evaluate hydrogel performance over time. A goniometry test was also conducted to assess the surface wettability of the hydrogels. The antimicrobial effects of the hydrogel were investigated using a biofilm model with *E. faecalis*, *Streptococcus mutans* (a leading cause of caries), and fibrinogen, which previous studies have shown to aid the growth of *E. faecalis* [3][4]. Biofilm effects were quantified using RAMAN spectroscopy on stainless steel wafers.

F127-DMA/CASA (1:6) possessed optimum solubility, stability, and crosslinking ability. Additionally, encapsulation of CASA in F127-DMA made its viscosity consistently low. We confirmed that the hydrogel was injectable and retrievable in root canal models. RAMAN and FT-IR analyses of CASA paste reveal the presence of co-crystals, including calcium salicylate and other salts, explaining its improved drug performance. The optimal formulation exhibited near-neutral pH over three days, superior crosslinking efficiency (80.9%), and the lowest swelling ratio over 14 days. CASA significantly decreased the contact angle of F127-DMA/CASA, enhancing hydrophilicity. This improvement aids in better absorption of inflammatory exudate in the root canal system, offering additional therapeutic benefits.

Our findings offer valuable insights into using F127-DMA/CASA hydrogels as an intracanal medicament for endodontic treatments. With its effective antimicrobial properties, flowability, retrievability, stability, hydrophilicity, and controlled release, F127-DMA/CASA hydrogels meet essential requirements, making it a promising alternative to calcium hydroxide in root canal treatments.
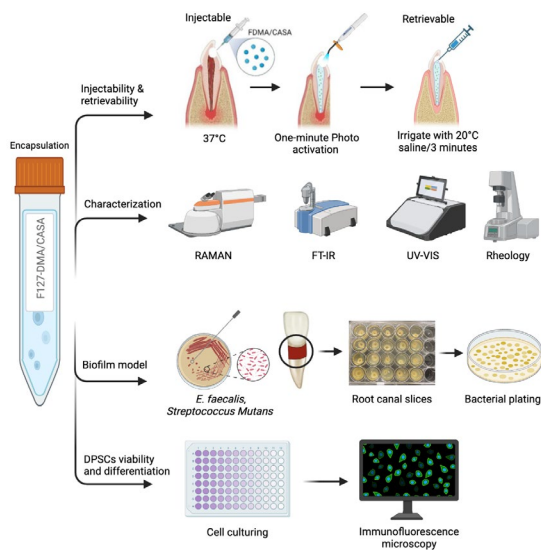
[1] Alghamdi, Faisal, and Marwa Shakir. "The Influence of Enterococcus Faecalis as a Dental Root Canal Pathogen on Endodontic Treatment: A Systematic Review." Cureus, U.S. National Library of Medicine, 13 Mar. 2020, www.ncbi.nlm.nih.gov/pmc/articles/PMC7152576/.

[2] Matsumoto-Nakano, Michiyo. "Role of Streptococcus Mutans Surface Proteins for Biofilm Formation." The Japanese Dental Science Review, U.S. National Library of Medicine, Feb. 2018, www.ncbi.nlm.nih.gov/pmc/articles/PMC5884221/.

[3] Sillanpää, Jouko, et al. "A Family of Fibrinogen-Binding Mscramms from Enterococcus Faecalis." Houston Methodist Scholars, Society for General Microbiology, 19 June 2015, scholars.houstonmethodist.org/en/publications/a-family-of-fibrinogen-binding-mscramms-from-enterococcus-faecali.

[4] Wang, Qian-Qian, et al. "Prevalence of Enterococcus Faecalis in Saliva and Filled Root Canals of Teeth Associated with Apical Periodontitis." International Journal of Oral Science, U.S. National Library of Medicine, Mar. 2012, www.ncbi.nlm.nih.gov/pmc/articles/PMC3412659/.

Effects of graphene oxide and partially reduced graphene oxide on Escherichia Coli and Staphylococcus aureus

Sichen Liu[1], Anastasiia Bezugla[2], Ariel Khavulya[3], Tavan Bhatia[4], Shi Fu[4], Rebecca Isseroff[5], Stephen Walker[5], Miriam Rafailovich[5]

[1]Shanghai Foreign Language School, Shanghai, China [2]American International School - Salzburg, Salzburg, Austria [3]Rambam Mesivta, NY [4]Cornell University, NY [5]Stony Brook University, NY

Escherichia coli (E.Coli) and Staphylococcus aureus (S.A.) are common bacterial species and leading causes of infectious diseases, especially dangerous among the elderly[1]. Treatment of infections is becoming difficult due to antimicrobial resistance. Previous literature has shown that Graphene oxide (GO) and partially reduced graphene oxide (pRGO) display antibacterial properties.[2] GO is composed of single or bilayer strongly oxidized carbon nanosheets, and pRGO is made by partially reducing GO, increasing the electrical conductivity by removing some functional groups while still retaining water solubility.

Experimental results in this research suggest otherwise. When GO or pRGO solutions were added into E. Coli and S.A. solutions in a 1:1 ratio and incubated, no obvious increase in the number of dead cells was observed in a live/dead stain using an EVOS Microscope (Fig.1, 2). However, in the mixtures of E. Coli and GO/pRGO, large clumps of E. Coli were observed under transmitted light microscopy .

Thus, the authors speculate that GO and pRGO may promote the formation of biofilms in these bacteria. To measure the extent of the biofilm production, a crystal violet assay was
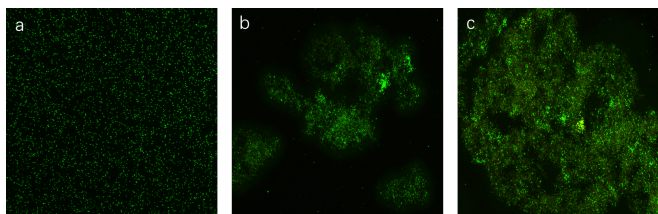

Figure 1. Live/dead stain image of (a) E.coli, (b) E.coli mixed with GO, (c) E.coli mixed with pRGO
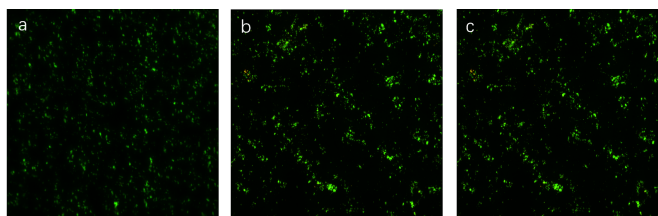

Figure 2. Live/dead stain image of (a) S.aureus, (b) S.aureus mixed with GO, (c) S.aureus mixed with pRGO
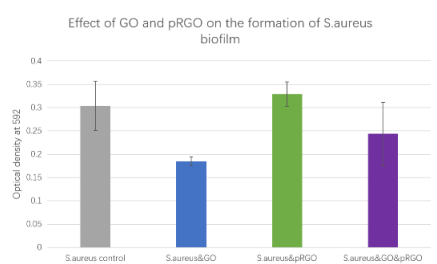

Figure 3. Effect of GO and pRGO on the formation of E.coli biofilm
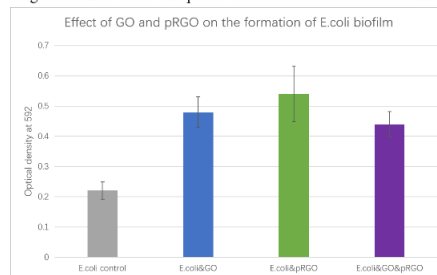

Figure 4. Effect of GO and pRGO on the formation of S.aureus biofilm

conducted. The violet absorbance intensity of four identical samples of each of the two bacteria incubated with GO and pRGO was measured, with a higher absorbance indicating greater formation of biofilm. As seen in Figure 3, both GO and pRGO enhance biofilm formation in E. coli. In contrast, GO inhibits biofilm formation in S. aureus (Fig. 4), whereas pRGO does not exhibit a significant effect on biofilm formation in this bacterium.

Further experiments will be done to test if GO and pRGO are pro-bacterial by forming biofilms to protect the bacteria from external threats. E. coli will be cultured in a 6-well tissue culture plate for two days: two samples in phosphate-buffered saline (PBS), two in a 1:1 mixture of GO and pRGO, one in GO, and one in pRGO. Each sample will be divided and treated with either PBS or ampicillin to determine whether the biofilm provides resistance to ampicillin.

[1] Poolman, J. T., & Anderson, A. S. (2018). *Escherichia coli* and *Staphylococcus aureus*: leading bacterial pathogens of healthcare associated infections and bacteremia in older-age populations. *Expert Review of Vaccines*, *17*(7), 607–618. https://doi.org/10.1080/14760584.2018.1488590

[2] Iman Sengupta, Proma Bhattacharya, Monikangkana Talukdar, Sudarsan Neogi, Surjya K. Pal, Sudipto Chakraborty, Bactericidal effect of graphene oxide and reduced graphene oxide: Influence of shape of bacteria, Colloid and Interface Science Communications,Volume 28,2019,Pages 60-68,ISSN 2215-0382, https://doi.org/10.1016/j.colcom.2018.12.001.

Session IX: Molecular Models for Thrombosis

Adam Hansen, Kao Li, Peining Wang
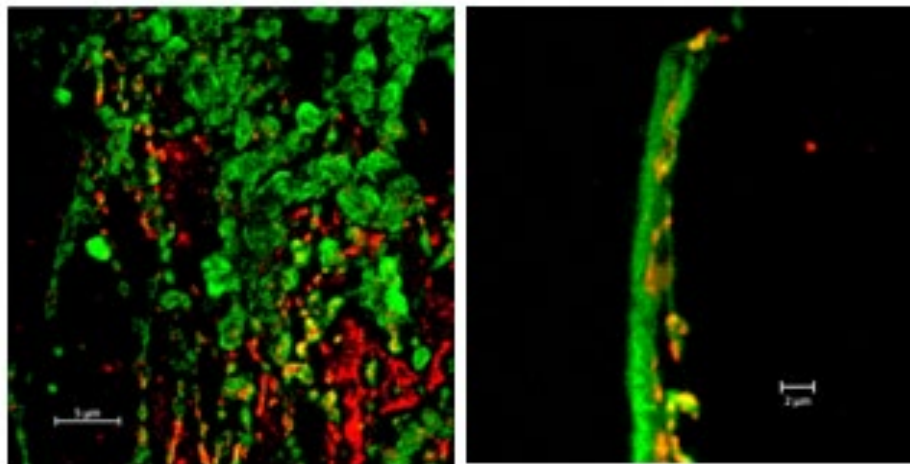
Utilizing Machine Learning to Analyze the Effects of PI3K Inhibitor TGX-221 on Shear-Mediated Platelet Kinematics and Adhesion

Aryan Agahtehrani[1*], Isabelle Chan[2*], Vincent Lo[3*], Jawaad Sheriff [4], Peining Wang[4], Xiaotian Wang[4], Miriam Rafailovich[5]

[1]*duPont Manual High School, Louisville, KY, 40208; [2]Michael E. DeBakey High School for Health Professions, Houston, TX, 77030; [3]Evergreen Valley High School, San Jose, CA, 95135; [4]Department of Biomedical Engineering, Stony Brook University, NY 11794, Department of Materials Science and Chemical Engineering, Stony Brook University, Stony Brook, NY 11794*
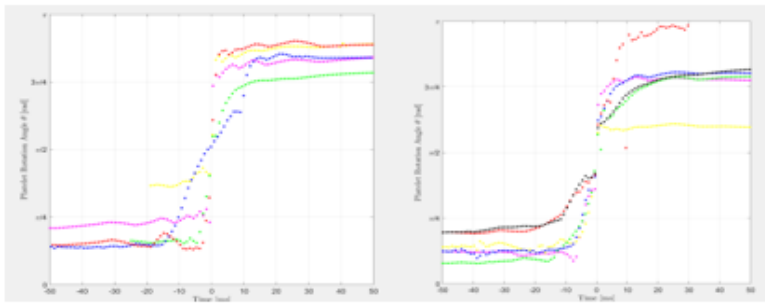
Figure 1. Differences in angular position of platelets in relation to time between platelets treated with PI3K inhibitor (A) and without inhibitor (B)

Platelets are cell fragments ranging from 3-4 micrometers in diameter that play an integral role in initializing the wound healing process through clot formation and bleeding inhibition. When vascular injury occurs, von Willebrand factors (vWF) are released, promoting adhesion of platelets to the wound surface and allowing aggregation into blood clots1. Initially, platelets are weakly tethered to vascular walls on their edge, in which the phospholipids on the inner leaflet of the platelet membrane move to the outer leaflet. Shear stress then causes them to 'flip' before adhering firmly to the vWF-coated surface, suggesting that flipping is a key precursor to platelet activation and aggregation. However, the exact mechanisms of this process are not clearly understood and are rarely studied on the scale of individual platelets2. It is crucial to characterize platelet and vascular surface interaction, which can aid in the future development of critical clot-regulating medication. We investigated the impact of the inhibition of the PI3K receptor on platelet activity by treating GFP with the drug TGX-221, a permeable inhibitor of PI3K, before undergoing shear stress. The PI3K receptor is essential to cell regulation, and a previous study showed that the inhibition of PI3K could prevent the activation and adhesion of platelets as well as pro-coagulant platelet formation in COVID-19 patients3. Thus, inhibiting PI3K could be a promising strategy to prevent the onset of thrombosis in patients with COVID-19 and other diseases.

We simulated an in vitro environment via custom microchannels of 1 mm length and 100 um diameter composed of polypropylene to replicate the conditions found in human blood vessels. Initially, the microchannels were coated with vWF, and gel-filtered platelets (GFP) were then flowed under shear conditions of 15 dynes/cm2, which is within the typical range found in the body. Upon analysis of platelet flipping videos and using a semi-unsupervised learning system (SULS), a graph of the rotational angle vs time graph of a flip can be created (Figure 1). After removing outliers and denoising the data, the peak velocity of the platelet can be determined by implementing a polyfit regression. Peak velocity is an important characterization of platelet activity, aiding in describing and predicting trends in shear-mediated platelet morphology change and aggregation. By comparing platelet flow with and without TGX-221, we found that without the PI3K receptor, platelets flipped significantly faster – peak velocity increased by 49.28% after inhibition using the drug – and were less adherent to the surface. These results agree with previous literature and serve as a promising sign for the future of drug development for regulating thrombosis, thus necessitating further sampling and research in future works.

1 Ruggeri Z. M. (2007). The role of von Willebrand factor in thrombus formation. Thrombosis research, 120 Suppl 1(Suppl 1), S5–S9. https://doi.org/10.1016/j.thromres.2007.03.011

2 Sheriff, J., Wang, P., Zhang, P., Zhang, Z., Deng, Y., & Bluestein, D. (2021). In vitro measurements of shear-mediated platelet adhesion kinematics as analyzed through machine learning. *Annals of Biomedical Engineering*, *49*(12), 3452–3464. https://doi.org/10.1007/s10439-021-02790-3

3Khezri, M. R., Varzandeh, R., & Ghasemnejad-Berenji, M. (2022). The probable role and therapeutic potential of the PI3K/AKT signaling pathway in SARS-CoV-2 induced coagulopathy. *Cellular & Molecular Biology Letters*, *27*(1). https://doi.org/10.1186/s11658-022-00308-w

Partially Reduced Graphene Oxide as a Promoter of Thrombin Activity and Fibrinogen Clot Formation

----
Jennifer Gao[1*], Emily Zhang[2*], Rebecca Isseroff[3], Miriam Rafailovich[3]

[1] Shanghai Pinghe School, Shanghai, China, [2] Roy C. Ketcham High School, Poughkeepsie, NY 12603 United States, [3] Stony Brook University, Stony Brook, NY 11790

Approximately 40% of trauma-related deaths worldwide are due to bleeding[1], highlighting the need to create a topical dressing that would enhance the rapid clotting of deep cuts and/or wounds. Previously it was shown that partially reduced graphene oxide (pRGO), a one-atom thick carbon sheet with fewer oxygen-containing functional groups than graphene oxide (GO), enhanced the ability of the enzyme microbial transglutaminase to crosslink gelatin. Since thrombin catalyzes fibrinogen clot formation, we sought to enhance its enzymatic activity[2] with prGO as well.

A 1 mg/mL GO solution was reduced with sodium borohydride ($NaBH_4$) to obtain 10, 12, 15, 20 and 25mM reductions of pRGO. Fibrinogen (4 mg/ml) was clotted with thrombin (1 u/ml) and a thromboelastograph quantified the viscoelastic properties of the sample including the angle of the tangent to the clotting curve, which indicates the rate of clot formation; and the maximum amplitude (MA), which shows the strength of the clot. The addition of 15 mM pRGO significantly enhanced thrombin's activity in all aspects; compared to the control it improved the MA of the clot by 71%, whereas GO decreased it by 6%. GO improved the initial clotting rate by 17% but pRGO boosted it by 63%. pRGO reduced clotting time by 60%, while GO reduced clotting time by 27%.
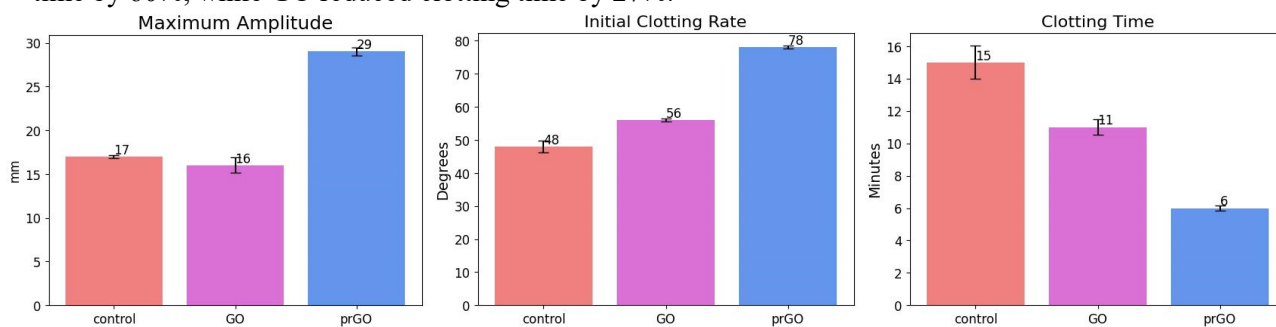

Figure 1. MA, Angle, and Clotting times of control, GO, and prGO

Testing the various reduction degrees of 10mM, 12mM, 15mM, 20mM, and 25mM, demonstrated that 20mM exerted the most significant enhancement, increasing the initial clotting rate by 147%, enhancing the clot strength by 154%, and decreasing the clotting time by 60%. To derive the optimal reduction degree for a pRGO promoter, the mean of the extremums was taken to be 19.2 mM.

Halving the amount of thrombin in the control resulted in close to half of the initial clotting rate as compared to full thrombin control. However, halving the amount of thrombin while adding 20 mM prGO
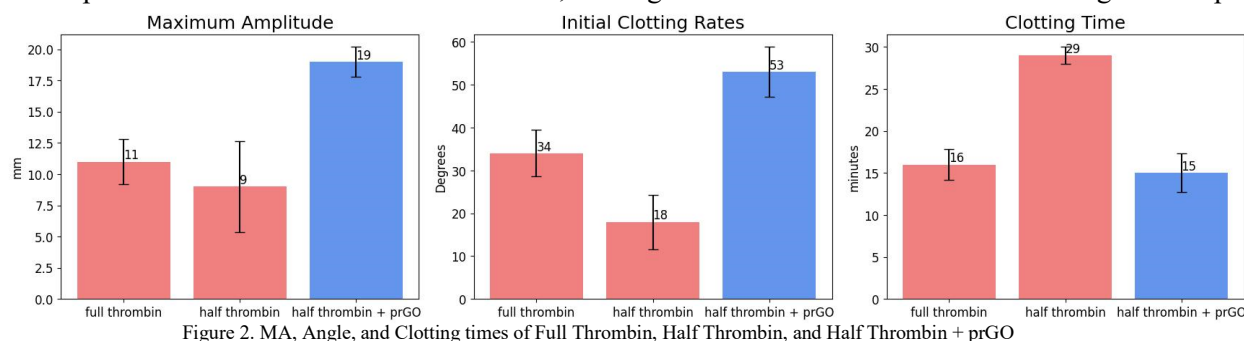

Figure 2. MA, Angle, and Clotting times of Full Thrombin, Half Thrombin, and Half Thrombin + prGO

(*Figure 2*) nearly triples the initial clotting rate of halved thrombin and even speeds the clotting rate by 56% as compared to the full thrombin control.

Future work includes conducting X-ray Photoelectron Spectroscopy characterization on GO and prGO reductions and testing prGO activity on a clot-dissolving enzyme.

---

[1] https://www.dhs.gov/science-and-technology/news/2022/05/19/st-helps-stop-bleed-fast

[2] Isseroff, R., Reyes, J., Reddy, R., Williams, N., & Rafailovich, M. (2019). The Effects of Graphene Oxide and Partially Reduced Graphene Oxide on the Enzymatic Activity of Microbial Transglutaminase in Gelatin. *MRS Advances*, *4*(15), 879–887. doi:10.1557/adv.2019.89
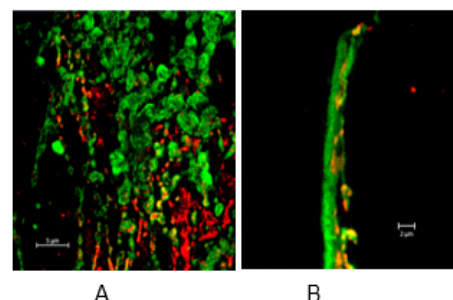
Differential Impacts of Hyperglycemia and P12 Inhibition on Fibrin Formation and Thrombosis

Aryan Agahtehrani[1], Isabelle Chan[2], Payton Fromm[3], Vincent Lo[4], Hunter Maguire[5], David Sun[6], Dylan Wang[7], Xinyu You[8], Calvin Yu[9], Nikita Karnik[10], Cathy Reyes[11], Jonathan Xavier[12], Adam Hansen[13], Miriam Rafailovich[14]
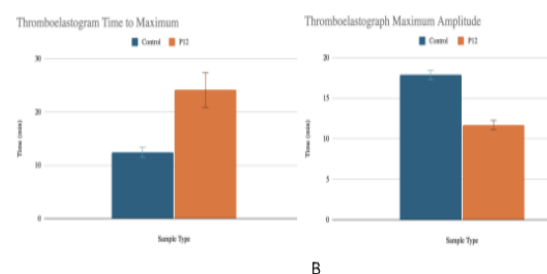
[1]duPont Manual High School, KY, 40208; [2]Michael E. DeBakey High School for Health Professions, TX, 77030; [3]St. John's the Baptist Diocesan High School, NY, 11794; [4]Evergreen Valley High School, CA, 95135; [5]Garden City High School, NY, 11530; [6]Joseph A. Gregori High School, CA, 95356; [7]Trinity Preparatory School, FL, 32766, [8]Western Reserve Academy, OH, 44236; [9]Weston High School, MA, 02493;[10]Carnegie Mellon University, PA, 15213; [11]Suffolk County Community College, NY, 11784; [12]Western New England University, MA, 01119; [13]Department of Materials Science and Chemical Engineering, Stony Brook University, Stony Brook, NY 11794

Fibrinogen, a hexameric homodimer composed of two sets of three polypeptide chains[1], is a vital protein produced by the liver. During clotting, prothrombin, after enzyme-mediated conversion into thrombin[2], cleaves fibrinopeptides A and B from fibrinogen's Aα and Bβ chains, generating fibrin monomers which polymerize into long fibers and promote aggregation of platelets into blood clots[3]. Coagulation, though integral to wound healing and hemorrhage control, is harmful when thrombosis occurs, resulting in serious, adverse patient outcomes. Hyperglycemia is known to promote thrombosis via increased platelet activity and decreased presence of fibrinolytic inhibitor PAI-I[4]. Additionally, hyperglycemic conditions mediate fiber formation directly by increasing thrombin-antithrombin complex activity[5]. P12, a fibronectin-derived peptide, has shown promise in reducing thrombogenicity during fibrinogen's polymerization onto various mediums[6], suggesting possible future biomedical and therapeutic applications. This experiment aimed to evaluate the effect of P12 as an antithrombotic agent and glucose as a promoter of clot formation. To begin, fibrinogen was applied to polystyrene-coated silicon wafers under high glucose conditions. Confocal

Figure 1. Confocal images of fibrin on polystyrene surface with glucose (A) and without (B)

Figure 2. Comparison of time to maximum (A) and maximum amplitude (B) between control and P12 group.

microscopy imaging of wafers showed fibrinogen, dyed fluorescent red, surrounding fibrin, dyed fluorescent green, demonstrating continuous fibrin polymerization (Figure 1). This was confirmed by immunofluorescent imaging after a 488 actin stain, where fibers produced by glucose-treated fibrinogen were significantly elongated. Thromboelastography was also used to determine that maximum amplitude values, representing peak clot strength, were greater in solutions of fibrinogen, thrombin, and 130 mg/dL glucose versus 70 mg/dL, reaching 23.73 mm and 19.93 mm respectively (Figure 2). Conversely, P12 decreased the amplitude value to 11.7 mm from a control of 17.9 mm, while also increasing the time taken to reach maximum clot strength. This indicates that P12 inhibits fiber formation and thus, thrombosis. This conclusion was further validated with fluorescent microscopy, in which shorter fibers formed in cells treated with P12. The study's promising results in regard to the effect of glucose and P12 on thrombolytic processes necessitate future research

[1] Kattula, S., Byrnes, J. R., & Wolberg, A. S. (2017). Fibrinogen and Fibrin in Hemostasis and Thrombosis. *Arteriosclerosis, thrombosis, and vascular biology*, *37*(3), e13–e21. https://doi.org/10.1161/ATVBAHA.117.308564

[2]Krishnaswamy S. (2013). The transition of prothrombin to thrombin. *Journal of thrombosis and haemostasis : JTH*, *11 Suppl 1*(0 1), 265–276. https://doi.org/10.1111/jth.12217 [3]Soria J, Mirshahi S, Mirshahi SQ, et al. Fibrinogen alphaC domain: its importance in physiopathology. *Res Pract Thromb Haemost*. 2019;3(2):173-183.   10.1111/j.1749-6632.2001.tb03517.x

[4]Batten, L.; Sathyapalan, T.; Palmer, T.M. Molecular Mechanisms Linking Diabetes with Increased Risk of Thrombosis. *Int. J. Mol. Sci.* 2023, *24*, 17465. https://doi.org/10.3390/ijms242417465

[5]Undas, A., Wiek, I., Stêpien, E., Zmudka, K., & Tracz, W. (2008). Hyperglycemia is associated with enhanced thrombin formation, platelet activation, and fibrin clot resistance to lysis in patients with acute coronary syndrome. *Diabetes care*, *31*(8), 1590–1595. https://doi.org/10.2337/dc08-0282

[6]Doilidov, A., El-Saieh, S., Faria, S., & Lo, P. (2023). The Effect of P12 Peptide on Fibrinogen Fiber Formation and Endothelial Cell Attachment on Polystyrene. Journal of Undergraduate Chemical Engineering Research, 19-23.

Impact of Surface Hydrophobicity on Fibrinogen Adsorption and Thrombosis Development

Aryan Agahtehrani*[1], Isabelle Chan*[2], Vincent Lo*[3], Payton Fromm[4], Hunter Maguire[5], David Sun[6], Dylan Wang[7], Daniel You[8], Calvin Yu[9], Nikita Karnik[10], Cathy Reyes[11], Jonathan Xavier[12], Adam Hansen[13], Miriam Rafailovich[13], Jawaad Sheriff[14], Peining Wang[14]

[1]duPont Manual High School, KY, 40208; [2]Michael E. DeBakey High School for Health Professions, TX, 77030; [3]Evergreen Valley High School, CA, 95135; [4]St. John's the Baptist Diocesan High School, NY, 11794; [5]Garden City High School, NY, 11530; [6]Joseph A. Gregori High School, CA, 95356; [7]Trinity Preparatory School, FL, 32766, [8]Western Reserve Academy, OH, 44236; [9]Weston High School, MA, 02493; [10]Carnegie Mellon University, PA, 15213; [11]Suffolk County Community College, NY, 11784; [12]Western New England University, MA, 01119; [13]Department of Materials Science and Chemical Engineering, Stony Brook University, [14]Department of Biomedical Engineering, Stony Brook University, NY 11794

Figure 1. AFM image of fibrinogen placed on polystyrene surface
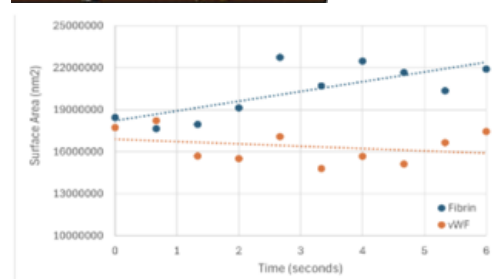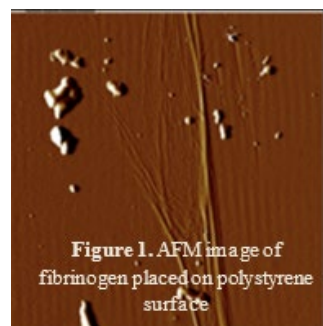

Fig 2. Comparison of platelet activation on different surfaces

Fibrinogen is a liver-produced protein native to the human circulatory system[1]. Recent studies suggest that strong interactions between fibrinogen's hydrophobic D and E regions and hydrophobic surfaces expose the molecule's alpha-C domains, recruit soluble fibrin to the surface, and result in fiber growth[2,3]. The hydrophobic nature of medical devices in contact with blood plasma promotes clot formation, enhancing fibrinogen adsorption and fibrin formation in the area of application with significant health consequences[4]. This study, aiming to evaluate surface chemistry required to initialize thrombosis, involved creating testable thin film polymer coatings on silicon wafers with substrates such as polystyrene, which were then irradiated with UV-ozone to increase their hydrophilicity. Contact angle goniometry was used to quantify surface properties, and results demonstrated decreased fiber formation as UV exposure–and thus hydrophilicity–increases. Additionally, surface thrombosis was studied via *in vitro* simulation of platelet activation and adhesion under shear stress. Polypropylene microchannels of 1 mm in length and 100 μm in diameter with a contact angle of 80.3° were used to simulate small blood vessels. A fibrinogen solution was then applied to the microchannel surface and atomic force microscopy was used to assess fiber formation, which averaged 1.15 μm in width and 258.83 nm in height, within the typical range for fibrin. Fibrinogen was then perfused through the microchannel, coating inner surfaces with fibrin. Samples of gel-filtered platelets obtained from adult whole blood samples were flown through microchannels at a speed of 15 dynes/cm^2 and analyzed to determine activation and degree of adherence. Results indicated that platelets' surface area grew at a greater rate when attached to fibrin in comparison to von Willebrand factors (vWF), glycoproteins that assist in initializing clot formation in vascular wounds (Figure 2). Additionally, it was found that a higher percentage of platelets stuck to the microchannel surface in fibrin samples than in vWF-coated samples, measuring 33.02% and 16.16%, respectively. This experimentation demonstrates the importance of surface chemistry with respect to fiber formation and thrombosis. Introducing foreign materials into the bloodstream presents a significant health risk via increased platelet aggregation, requiring further investigation.

1 Kattula, S., Byrnes, J.R., & Wolberg, A. S. (2017). Fibrinogen and fibrin in hemostasis and thrombosis. Arteriosclerosis, Thrombosis, and Vascular Biology, 37(3). https://doi.org/10.1161/atvbaha.117.308564

2 Zhang, L., Casey, B., Galanakis, D. K., Marmorat, C., Skoog, S., Vorvolakos, K., Simon, M., & Rafailovich, M. H. (2017). The influence of surface chemistry on adsorbed fibrinogen conformation, orientation, fiber formation and platelet adhesion. Acta Biomaterialia, 54, 164–174. https://doi.org/10.1016/j.actbio.2017.03.002

3 Galanakis, D. K., Protopopova, A., Li, K., Yu, Y., Ahmed, T., Senzel, L., Heslin, R., Gouda, M., Koo, J., Weisel, J., Manco-Johnson, M., & Rafailovich, M. (2022). Novel characteristics of soluble fibrin: Hypercoagulability and acceleration of blood sedimentation rate mediated by its generation of erythrocyte-linked fibers. *Cell and Tissue Research*, *387*(3), 479–491. https://doi.org/10.1007/s00441-022-03599-9

4 McFadden, E. P., Stabile, E., & Regar, E. (2005). Late thrombosis in drug-eluting coronary stents after discontinuation of antiplatelet therapy. ACC Current Journal Review, 14(2), 46. https://doi.org/10.1016/j.accreview.2004.12.106

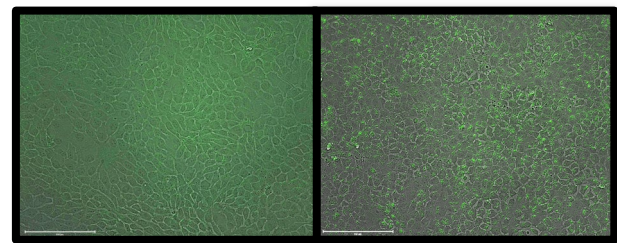# The Role of Viral Infections in Modulating Cell Surface Thrombosis

Aryan Agahtehrani*[1], Isabelle Chan*[2], Payton Fromm*[3], Vincent Lo*[4], Hunter Maguire*[5], David Sun*[6], Dylan Wang*[7], Daniel You*[8], Calvin Yu*[9], Nikita Karnik*[10], Cathy Reyes*[11], Jonathan Xavier*[12], Adam Hansen[13], Miriam Rafailovich[14]

[1]duPont Manual High School, KY, 40208; [2]Michael E. DeBakey High School for Health Professions, TX, 77030; [3]St. John's the Baptist Diocesan High School, NY, 11794; [4]Evergreen Valley High School, CA, 95135; [5]Garden City High School, NY, 11530; [6]Joseph A. Gregori High School, CA, 95356; [7]Trinity Preparatory School, FL, 32766, [8]Western Reserve Academy, OH, 44236; [9]Weston High School, MA, 02493; [10]Carnegie Mellon University, PA, 15213; [11]Suffolk County Community College, NY, 11784; [12]Western New England University, MA, 01119; [13]Deptt of Mat Sci and Chem Eng, Stony Brook University, Stony Brook, NY 11794
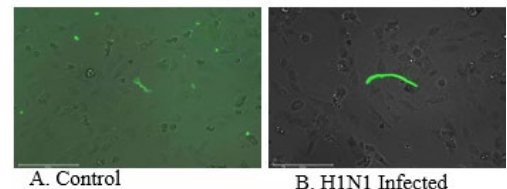
Fibrinogen, consisting of two sets of three polypeptide chains, is a hexameric homodimer produced by the liver[1] that can strongly adsorb to hydrophobic surfaces. Once adsorbed, fibrinogen may polymerize into large fibers in the absence of thrombin due to distortion of adsorbed monomers, exposing the molecule's alpha-C domains. However, P12, a fibronectin-derived protein, bonds specifically on the αC domain, preventing the polymerization of fibrin[2]. Coagulation upon injury is necessary to prevent excessive bleeding and initiate wound healing. However, thrombosis, coagulation within blood vessels, presents a health risk when circulation slows or ceases. Acute infection is postulated to increase thrombosis by intensifying lipid droplet synthesis[3], increasing the hydrophobicity of bodily environments, and promoting the formation of fibers. During the COVID-19 pandemic, infected patients experienced severe, extensive blood clotting[4], bringing viral-induced thrombosis to the forefront of medical research.

A. Healthy MDCK

B. H1N1-infected MDCK

Figure 1. Lipid formation on healthy and infected

A. Control

B. H1N1 Infected

C. H1N1 infected with P12

Figure 2. Fibrin formation on HUVEC cells under different conditions

This study, aiming to simulate viral infection in blood vessels, involved infecting canine kidney (MDCK) cells to model general cellular response to fibrinogen as well as human endothelial (HUVEC) cells which create a human vascular environment for fibrinogen interaction. The MDCK cells were infected with the H1N1 virus in a cell culture medium. After 24 hours of virus co-culturing, the supernatant was collected, and the cells were fixed by adding a fluorescent lipid stain to the cells (Figure 1). The supernatant and fibrinogen were added into HUVEC cells which then were used to analyze the fibrin formation.
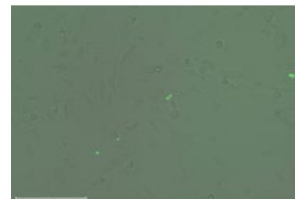
After immunofluorescent staining, increased lipid deposition was seen in infected cells. Additionally, fibrin synthesized within the infected medium was enlarged and elongated compared with controls (Figure 2). This study highlights the crucial impact of viral infection on endothelial cells and its potential to induce abnormal blood clotting. Further experimentation is required to elucidate underlying mechanisms and confirm experimental findings.

[1] Kattula, S., Byrnes, J. R., & Wolberg, A. S. (2017). Fibrinogen and Fibrin in Hemostasis and Thrombosis. *Arteriosclerosis, thrombosis, and vascular biology*, *37*(3), e13–e21. https://doi.org/10.1161/ATVBAHA.117.308564

[2] Niemeyer, A. P., Kroese, L. J., & Bretthauer, M. (2017). Fibrinogen adsorbed on hydrophobic surfaces induces platelet clustering. Acta Biomaterialia, 61, 169-181. https://doi.org/10.1016/j.actbio.2017.07.064

[3] ACS. (n.d.). Effectiveness of P12: Potential anti-thrombogenic drug for COVID-19. Retrieved August 5, 2024, from https://acs.digitellinc.com/p/s/effectiveness-of-p12-potential-anti-thrombogenic-drug-for-covid-19-46617

[4] Bosch, M., Sweet, M. J., Parton, R. G., & Pol, A. (2021). Lipid droplets and the host-pathogen dynamic: FATal attraction?. *The Journal of cell biology*, *220*(8), e202104005. https://doi.org/10.1083/jcb.202104005

[5] National Heart, Lung, and Blood Institute. "COVID-19 and the Blood." NHLBI, NIH, 11 July 2023, www.nhlbi.nih.gov/covid/blood. Accessed 5 Aug. 2024.

Session X:
# Tissue Engineering
Shi Fu, Jessica Hofflich, Peining Wang

Determining the Correlation between Aging and Cellular Mechanics

Ananya Anand[1*], Jerry Gu[2*], Zihan Jia[3*], Viraj Pahuja[4*], Shreyaa Sanjay[5*], Theodora Siu[6*], Jenny Dinh Nhu Zhang[7*], Brooklyn Ratel[8], Divleen Singh[8], Shi Fu[8], Huiting Luo[8], Miriam Rafailovich[8]

[1]*Johns Creek High School, Johns Creek, GA, [2]Princeton International School of Mathematics and Science, Princeton, NJ, [3]The Experimental High School Attached to Beijing Normal University, Beijing, China, [4]The Wheatley School, Old Westbury, NY, [5]West Windsor-Plainsboro High School North, NJ, [6]Ward Melville High School, East Setauket, NY, [7]Renaissance International School Saigon, 74 Đ. Nguyễn Thị Thập, Bình Thuận, Quận 7, Hồ Chí Minh 700000, Vietnam, [8]Stony Brook University, Stony Brook, NY*

The mechanical behavior of a cell is both a consequence and regulatory factor of biological function and cellular architecture. Researchers globally are investigating the forces that cells generate and sustain within their environment to provide a cellular-level perspective on pathologies among other pressing research questions[1]. Cellular Traction Forces (CTFs) are critical to the physiology of cells, through their structural support, and facilitation of migration within tissues. [2] These aforementioned features have been associated with aging due to gradual physiological cellular decay and warrants further investigation to expand etiological understanding[3].

This study investigates this correlation on both a macroscopic and microscopic level. Macroscopically, fibroblasts from three distinct age groups - neonatal, young, and mature cells - are placed within a collagen-media solution and once the collagen gelled, it was rimmed. Over the next 9 hours, and ultimately at the 24-hour mark, imaging was conducted to observe the cellular gel contraction as a reflection of the CTFs. The results displayed in Figure 1, highlight that the young and mature cells produced a similar trend in gel area rate,
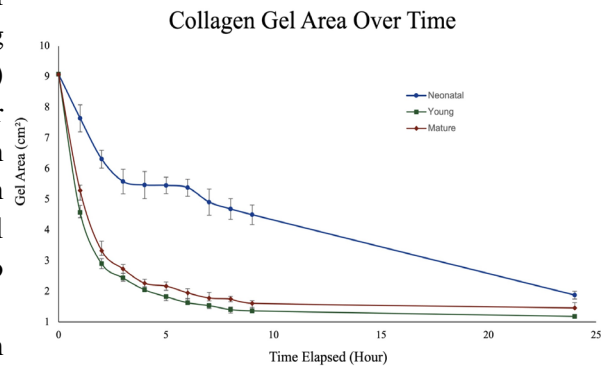
Figure 1: Collagen Gel Area over Time for Neonatal, Young, and Mature Cells
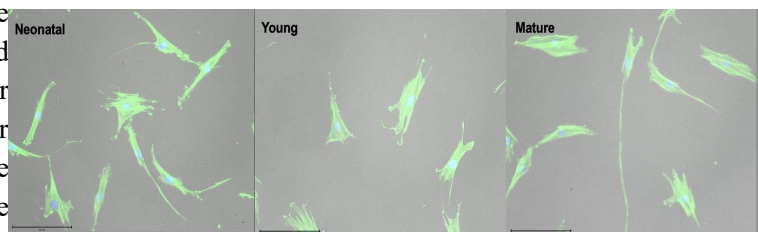
Figure 2: EVOS Images of Neonatal, Young, and Mature Fibroblasts GFP and DAPI

whereas the neonatal cells demonstrated a smaller rate of decrease of the gel area. Microscopically, fibroblasts incorporated with green and red fluorescent beads were plated atop mtG-crosslinked-gelatin alongside DMEM, and the CTFs are visualized through the observation of bead displacement during EVOS imaging. Additionally, for further biomechanic understanding, testing for cell proliferation, cell morphology, and cell modulus through Atomic Force Microscopy (AFM) was conducted. Cell modulus, the biophysical property that describes the cell elasticity and measures their resistance to strain[4]. The neonatal, young, and mature cells had moduli of 1, 1.264, and 2.022 respectively. We found that the mature cells had the greatest modulus and resistance to deformation. Morphological analysis was also conducted as seen in Figure 2, displaying a physical difference within the distinct cell types such that the neonatal and mature cells have a more slender and elongated structure compared to the young cells which had a more condensed and compact shape. Future applications include conducting further study on cell displacement and obtaining a quantifiable measurement of CTFs.

Moeendarbary, E., & Harris, A. R. (2014). *Cell mechanics: Principles, practices, and prospects*. Wiley interdisciplinary reviews. Systems biology and medicine.

[2]Wang, J. H.-C. (2010, June 1). Cell Traction Forces (ctfs) and CTF microscopy applications in Musculoskeletal Research. Operative techniques in orthopaedics.

[3]Designing the stem cell microenvironment for guided connective tissue regeneration - bogdanowicz - 2017 - annals of the New York Academy of Sciences - Wiley Online Library. (n.d.).

[4]Guz, N., Dokukin, M., Kalaparthi, V., & Sokolov, I. (2014, August 5). If cell mechanics can be described by elastic modulus: Study of different models and probes used in indentation experiments. Biophysical journal.

Effects of Titanium Dioxide Nanoparticles on UV-Exposed Human Dermal Fibroblasts

Aryan Agahtehrani*[1], Isabelle Chan*[2], Payton Fromm*[3], Vincent Lo*[4], Hunter Maguire*[5], David Sun*[6], Dylan Wang*[7], Daniel You*[8], Calvin Yu*[9], Nikita Karnik*[10], Cathy Reyes*[11], Jonathan Xavier*[12], Adam Hansen[13], Miriam Rafailovich[14]

[1]duPont Manual High School, KY, 40208; [2]Michael E. DeBakey High School for Health Professions, TX, 77030; [3]St. John's the Baptist Diocesan High School, NY, 11794; [4]Evergreen Valley High School, CA, 95135; [5]Garden City High School, NY, 11530; [6]Joseph A. Gregori High School, CA, 95356; [7]Trinity Preparatory School, FL, 32766, [8]Western Reserve Academy, OH, 44236; [9]Weston High School, MA, 02493;[10]Carnegie Mellon University, PA, 15213; [11]Suffolk County Community College, NY, 11784; [12]Western New England University, MA, 01119; [13]Department of Materials Science and Chemical Engineering, Stony Brook University, Stony Brook, NY 11794
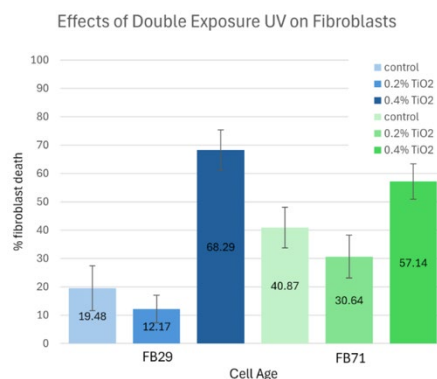*Authors are equal contributors

Fibroblasts (FB) are human dermal cells that secrete collagen proteins integral to maintaining the extracellular matrix (ECM). Age of FBs significantly affects collagen production and ECM integrity, as older cells synthesize less collagen and less readily maintain a functional ECM structure[1]. Upon exposure to ultraviolet (UV) radiation, dermal FBs exhibit reduced actin filament integrity and are known to undergo morphological changes resulting in reduced collagen synthesis[2] and destruction via apoptosis[3]. Titanium dioxide (TiO_2) nanoparticles (NPs) are widely used in sunscreens and other cosmetic products for their UV-B radiation absorbance and reflectance characteristics[4]. This research aims to assess the effectiveness of titanium dioxide NPs in reducing damage caused by UV radiation to human dermal FBs.
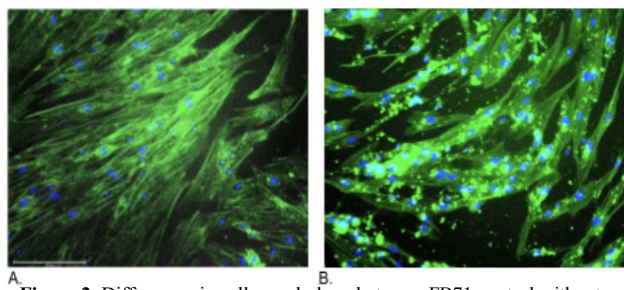

Figure 1. Cell death after double exposure to UV light at various titanium dioxide concentrations

This study utilized rutile TiO_2 NPs with an average diameter of 50 nm to examine the impact of 0.2% and 0.4% concentrations of TiO_2 on the morphology and survival of FB cells under single and double exposures to UV radiation at an intensity of 7 J/cm^2. Human FB cells aged 19, 29, 62, and 71 with passage numbers ranging from 7 to 8 were cultured, treated with or without TiO_2 NPs, and subsequently subjected to none, single, or double exposure to UV light. Cell counts were then conducted, quantifying cell viability post-UV exposure for each of the exposed samples to determine what effect TiO_2 NPs had on UV-induced cellular damage.

Figure 2. Differences in cell morphology between FB71 control without UV exposure (a) and FB71 0.4% TiO_2 UV double exposure (B).

Data indicated that cell viability decreased with 0.2% and 0.4% TiO_2 treatment alone (without UV) for all cell groups. After single UV exposure following 0.4% TiO_2 treatment, younger FBs showed greater or stable survival compared with UV exposure alone, whereas older FBs experienced lower survival rates. Survival after double UV exposure increased with 0.2% TiO_2 treatment; conversely, 0.4% TiO_2 groups experienced greater death after double UV exposure than control samples (Figure 1).

Upon immunofluorescence staining and imaging, UV-exposed FBs exhibited altered morphology, being less elongated with a lower aspect ratio. At high TiO_2 concentrations, a more subtle but parallel change in conformation occurred, and TiO_2 NPs were absorbed in significant quantities (Figure 2). The study highlights the differential impact of TiO_2 NPs on FBs of varying ages and their potential to modulate cellular responses to UV radiation. Further experimentation is required to elucidate underlying mechanisms and confirm findings.

[1] Zhang, J., Yu, H., Man, M., & Hu, L. (2023). Aging in the dermis: Fibroblast senescence and its significance. Aging Cell, 23(2). https://doi.org/10.1111/acel.14054
[2] Yamaba, H., Haba, M., Kunita, M., Sakaida, T., Tanaka, H., Yashiro, Y., & Nakata, S. (2016). Morphological change of skin fibroblasts induced by UV Irradiation is involved in photoaging. Experimental dermatology, 25 Suppl 3, 45–51. https://doi.org/10.1111/exd.13084
[3] Rehemtulla, A., Hamilton, C., Chinnaiyan, A., & Dixit, V. (1997). Ultraviolet Radiation-induced Apoptosis Is Mediated by Activation of CD-95 (Fas/APO-1). The Journal Of Biological Chemistry, 41(272), 25783-25786. https://doi.org/10.1074/jbc.272.41.25783
[4] Ghamarpoor, R., Fallah, A., & Jamshidi, M. (2023). Investigating the use of titanium dioxide (tio2) nanoparticles on the amount of protection against UV irradiation. Scientific Reports, 13(1). https://doi.org/10.1038/s41598-023-37057-5

# Evaluating the Effect of TiO2 on Angiogenesis and Anastomosis During Wound Healing on Mice Models

Leah Song[6*], Corey Zhang[9*], Ananya Anand[1*], Jerry Gu[2*], Zihan Jia[3*], Viraj Pahuja[4*], Shreyaa Sanjay[5*], Theodora Siu[7*], Jenny Dinh Nhu Zhang[8*], Eugene Jiang[10], Brooklyn Ratel[10], Divleen Singh[10], Shi Fu[10], Huiting Luo[10], Miriam Rafailovich[10]

[1]Maclay School, Tallahassee, FL, 32312, [2]Eastlake High School, Sammamish, WA, 98074, [3]Johns Creek High School, Johns Creek, Georgia, 30022, [4]Princeton International School of Mathematics and Science, Princeton, New Jersey, 08540, [5]The Experimental High School Attached to Beijing Normal University, Beijing, China, 100032, [6]The Wheatley School, Old Westbury, New York, 11568, [7]West Windsor-Plainsboro High School North, [8]Ward Melville High School, East Setauket, New York, 11733, [9]Renaissance International School Saigon, Hồ Chí Minh, 700000, Vietnam, [10] Stony Brook University, NY, 11790

Angiogenesis, the process of forming new blood vessels[1], plays a significant role in wounds healing by replacing damaged capillaries[2] and reestablishing normal blood flow at the wound site. Studies have shown that certain concentrations of titanium dioxide (TiO_2) induce the activation of human umbilical vein endothelial cells (HUVEC) by increasing the expression of adhesion molecules involved with the inflammatory process[3].

Hence, we hypothesize that the TiO_2 nanoparticles will facilitate wound healing by promoting angiogenesis within the skin construct. This study aims to evaluate the impact of TiO_2 on angiogenesis during wound healing by using histological analysis and Digital Image Speckle Correlation (DISC), which calculates the speckle movement

Fig 1. Skin Construct Layers for Control Mice

through x and y position vectors and displays them on a heat map. The heat maps are then used to generate bilinear interpolation graphs that depict the speckle movement along a line created between the poking site and the wound site.
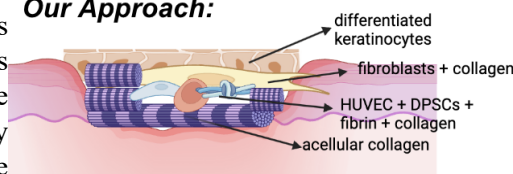
Skin grafts were prepared to be inserted on four female nude mice models. Each mice received two circular wounds, where the right wound was treated with a collagen-fibrin gel and cell suspension containing HUVEC treated with 0.1% TiO_2, Fibroblasts, and Dental Pulp Stem Cells as the experiment. The left wound was similarly treated, but with non-treated HUVEC as the control. The layers used for the skin construct on the control are displayed in **Figure 1**.

Fig 2. Standardized Procedure of Identifying Blood Vessel
Blood Vessel (Left) vs. Dispersed Red Blood Cells (Right)

After seven days of healing, the tissues were extracted from the wound site and observed under EVOS M7000 to quantify newly formed blood vessels. **Figure 2** demonstrates the standardized method used to quantify the new vasculature.

The observed correlation between TiO_2 nanoparticles and greater number of newly formed blood vessels suggests that the presence of TiO2 promoted angiogenesis. As seen in **Figure 3**, the density of blood vessels found in similar regions of tissue was higher among the experimental. To strengthen the results, DISC measured the force propagation while poking the control mice around their wound sites. **Figure 4** demonstrates peak force at the poking site and gradually decreased closer

	Blood Vessel Density (mm^-2)
TiO2 treated	64.58 mm^-2
no TiO2	24.26 mm^-2

Fig 3. Average Blood Vessel Density Comparison

Figure 4. Bilinear Interpolation: X-axis: Length along the line; Y-axis: Displacement Amplitude

to the wound site. Future steps include staining the HUVEC cells with GFP or AECA antibodies to distinguish them from mice endothelial cells.

[1]Adair, T. H., & Montani, J.-P. (2010). *Overview of Angiogenesis*. Nih.gov; Morgan & Claypool Life Sciences. https://www.ncbi.nlm.nih.gov/books/NBK53238/
[2]Schultz, G. S., Chin, G. A., Moldawer, L., & Diegelmann, R. F. (2011). Principles of Wound Healing (R. Fitridge & M. Thompson, Eds.). PubMed; University of Adelaide Press. https://www.ncbi.nlm.nih.gov/books/NBK534261/
[3]Angélica Montiel-Dávalos, José Luis Ventura-Gallegos, Alfaro-Moreno, E., Soria-Castro, E., García-Latorre, E., J.G. Cabañas-Moreno, Pilar, del, & López-Marure, R. (2012). TiO2 Nanoparticles Induce Dysfunction and Activation of Human Endothelial Cells. Chemical Research in Toxicology, 25(4), 920–930. https://doi.org/10.1021/tx200551u

Enhancing Osteogenic Differentiation of Dental Pulp Stem Cells via Iron Oxide Nanoparticles in Static Magnetic Field

Dvita Bhattacharya [1], Rohan Hablani [2], Alice He [3], Matthias Kim [4], Shi Fu [5], Huiting Luo [5], Jessica Hofflich [5], Marcia Simon [6], Miriam Rafailovich [5]
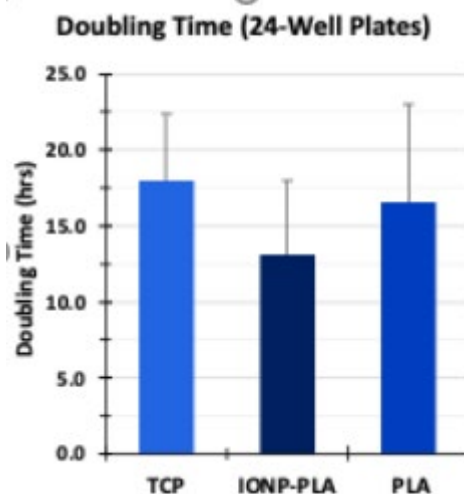
[1]Kent Place School, Summit, NJ 07902, [2]Arnold O. Beckman High School, Irvine, CA 92602, [3]Phillips Academy, Andover, MA 01810, [4]Interlake High School, Bellevue, WA 98008, [5]Department of Materials Science and Chemical Engineering, Stony Brook University, Stony Brook, NY 11794, [6]Department of Oral Biology and Pathology, Stony Brook University, Stony Brook, NY 11794

Dental pulp stem cells (DPSCs) have promising potential for stem cell-based regenerative bone therapy due to their non-invasive extraction method and high capacity for proliferation and osteogenic differentiation. Previous research indicates that culturing DPSCs within a static magnetic field (SMF) or on polylactic acid (PLA) scaffolds enhances osteogenic differentiation.[1,2] Iron oxide nanoparticles (IONPs) are known to amplify the effect of SMFs and thus osteogenic differentiation[2], but are cytotoxic when implanted within DPSCs. Culturing DPSCs in 3D aggregates (spheroids) has also been shown to result in greater multipotency compared to using 2D surfaces.[3] In this study, we combine the above techniques to investigate the viability of using IONP-infused PLA (IONP-PLA) scaffolds to enhance the effects of a SMF on osteogenic differentiation of spheroid-derived DPSCs (sd-DPSCs).

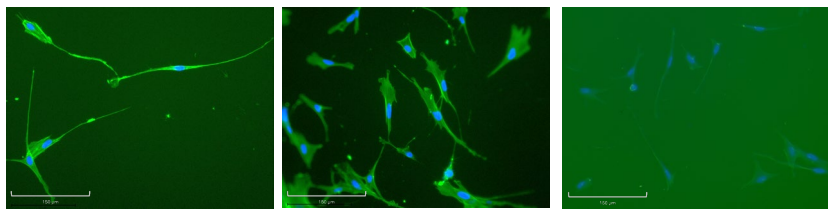*Fig 1. Doubling time of 2D-DPSCs on TCP, IONP-PLA, and PLA.*

DPSCs of strain 13, passage 7 were cultured in round bottom 96-well plates for 7 days and then resuspended to form sd-DPSCs. These cells were plated on TCP, PLA, and IONP-PLA substrates in 6-well plates, half of which were placed in a SMF. A stacked setup of alternating sd-DPSC plates and neodymium magnets held in place by aluminum structures and 3D-printed PLA supports was used to ensure uniformity of the magnetic field. Substrates were coated with 10 μg/mL of collagen solution to improve cell adhesion.

Preliminary testing demonstrated that among non-coated substrates, no statistical difference in doubling time was observed for 2D-DPSCs cultured on IONP-PLA scaffolds versus other substrates, suggesting that IONP-PLA is non-cytotoxic (Fig. 1). Further proliferation tests will be conducted to provide doubling times of sd-DPSCs for comparison. Cell elongation, an indicator of cell differentiation, was also seen on sd-DPSCs plated on all three substrates, confirming the non-cytotoxicity of PLA/IONP-PLA and viability of sd-DPSCs (Fig. 2). To compare the extent of differentiation between sd-DPSCs and 2D-DPSCs, elastic moduli will be measured using atomic force microscopy on Day 1 and 4 cells of each type.

qRT-PCR using marker genes ALP, OCN, DSPP and housekeeping gene GAPDH will be conducted on RNA extracted from Day 0, 14, 21, and 28 sd-DPSCs to determine the effect of substrate and SMFs on osteogenic differentiation. EDX, SEM, and Raman spectroscopy will also be performed on Day 28 to characterize the biomineral deposition by the differentiated DPSCs. We plan to test a modification of the PLA scaffolds sed here by coating with titania through atomic layer deposition, which has been demonstrated to further enhance osteogenic differentiation.[4]

Fig 2. EVOS images of nuclei (blue) and actin filaments (green) of sd-DPSCs plated on TCP (left), collagen-coated IONP-PLA (center), and collagen-coated PLA (right) after 7 days. Scale bar represents 150 μm.

[1] Barchiki, Fabiane, et al. "Biocompatibility of ABS and PLA Polymers with Dental Pulp Stem Cells Enhance Their Potential Biomedical Applications." *Polymers*, vol. 15, no. 24, 2023, p. 4629, https://doi.org/10.3390/polym15244629.

[2] Yang, Jiancheng, et al. "Iron Oxide Nanoparticles Combined with Static Magnetic Fields in Bone Remodeling." *Cells*, vol. 11, no. 20, Multidisciplinary Digital Publishing Institute, Oct. 2022, pp. 3298–98, https://doi.org/10.3390/cells11203298.

[3] Bu, Nam-Ung, et al. "In Vitro Characterization of Dental Pulp Stem Cells Cultured in Two Microsphere-Forming Culture Plates." *Journal of Clinical Medicine*, vol. 9, no. 1, Jan. 2020, pp. 242–42, https://doi.org/10.3390/jcm9010242.

[4] Chuang, Ya-Chen, et al. "The Role of Titania Surface Coating by Atomic Layer Deposition in Improving Osteogenic Differentiation and Hard Tissue Formation of Dental Pulp Stem Cells." *Advanced Engineering Materials,* vol. 23, no. 9, 2021, https://doi.org/10.1002/adem.202100097.

Session XI: Biopolymers
Aaron Sloutski, Yiwei Fang, Jay Gao

Chemical Characterization of *Rhizobium Tropici* Ethanol Precipitated Materials (Rt EPM) and Modeling the Rt EPM-clay interactions

Zheming Xu[1], Shede Zhang[2], Michael Cuiffo[3], Miriam Rafailovich[3]

[1]High School Affiliated to Renmin University of China, No. 37 Zhongguancun Street, Haidian District, Beijing, 100086, China, [2]Beijing National Day School, 66 Yuquan Rd, Haidian District, China, 100141, [3]Department of Materials Science and Chemical Engineering, Stony Brook University, Stony Brook, NY 11794

Rhizobium Tropici Ethanol Precipitated Materials (Rt EPM) have recently been discovered as promising polymeric materials in agriculture that facilitate the growth of plants1 due to their strong water-retaining capability2 and nutrient intaking. Rt EPS also serves an important role by automatically neutralizing the environment. This research is focused on the mechanism of this pH-adjusting attribute, hypothesizing that chemical reactions are involved in the process.

In the research, biopolymer solutions are first made with Rt EPM extracts and tap water. With the pH adjustment with sodium hydroxide solution and hydrochloric acid, two biopolymer solutions under acidic and basic environments are made to compare with another biopolymer solution without pH adjustment. The pH changes of solutions concerning days are recorded. To monitor if any electrochemical reactions occurred, cyclic voltammetry tests of solution under different pH environments are done. Beyond that, Fourier transform infrared spectroscopy (FTIR), X-ray photoelectron spectroscopy (XPS), and X-ray fluorescence spectroscopy (XRF) tests are carried out on biopolymer solutions for composition, bonding, and surface characteristics analysis. A digital microscope is also applied for observing the complexity of root systems for two groups of Bermuda grass that are planted one with tap water and another with the biopolymer solution.

As for the monitored changes in pH values, all acidic groups and basic groups are in a trend of neutralizing, while the unprocessed control group keeps a stable pH value. However, the groups with especially high or low initial pH encounter difficulties approaching 7. The cyclic voltammetry results across different pH environments reveal greater currents at the switching potential for basic and acidic groups than the unprocessed group. The XRF results of the EPM biopolymer show a high content of Chromium, Calcium, Potassium, Phosphorus, Silicon, and Chlorine. In contrast, results of clay and plants indicate high contents of Calcium, Potassium, Aluminum, Phosphorus, Sulfur, and Chlorine in biopolymer-raised plants. Through the FTIR analysis, it is identified that in the acidic group, several carbon bonds are broken. More secondary roots for the biopolymer group, which has a higher growing speed, are revealed by the digital microscopes.

Based on the pH monitoring concerning time, it is proved that Rt. EPM functions to adjust the pH level in the environments and two possible thresholds are found at around pH=3.5 and pH=11.0. In addition, the cyclic voltammetry tests give evidence that the biopolymer solutions under acidic and basic environments have a higher reactivity than those in neutral situations, which confirms the hypothesis that Rt. EPS reacts to the pH change. From the FTIR test, the acidic and basic environments change the composition of the biopolymer, which proves the hypothesis. The FTIR results for the acidic group exhibit a significant change in composition for the carbon skeleton of the biopolymer, which suggests that the extreme pH environment holds a decomposition effect on the biopolymer. Also, from the digital microscope, the enhancing effect of the biopolymer on secondary root growth helps to explain how the biopolymer maintains the soil integrity structure.

In conclusion, the hypothesis that there are chemical reactions involved has been proved. For plans, FTIR for biopolymers in the acidic environment within the threshold and composition analysis of the white substance on the control group are suggested.
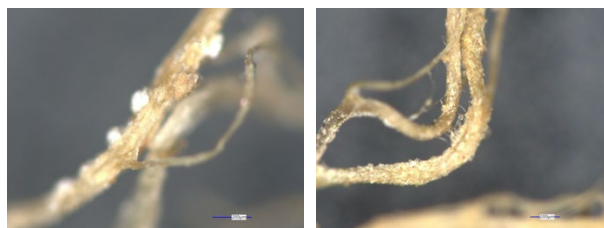
Figure 1. Digital microscope images of Bermuda grass: (left) control group (right) biopolymer group

[1] Staudt, A., et al. (2022). Effects of biopolymers produced by Rhizobium on seed germination and soil quality. *Journal of Agronomy and Crop Science*, 208(1), 34-49. https://doi.org/10.1111/jac.12345

[2] Vardharajula, S., et al. (2011). Plant-growth-promoting rhizobacteria and their effect on drought stress in plants. *Annals of Microbiology*, 61(2), 255-264. https://doi.org/10.1007/s13213-010-0117-1

Assessing the Effect of Nanofillers on Polyelectrolyte Hydrogels

Corin Wang[1*], Vinav Shah[2*], Laura Zhang[3*], Shoumik Saha[4], Dilip Gersappe[4]

1 Beijing National Day School, Beijing, China, 2 The Pingry School, Basking Ridge, NJ 07920, 3 Great Neck South High School, Great Neck, NY 11020, 4 Department of Materials Science & Chemical Engineering, Stony Brook University, Stony Brook, NY 11794

Polyelectrolyte biogels offer an environmentally-friendly alternative to invasive mainstream soil stabilizers like concrete, demonstrating promising soil-strengthening capability [1]. In polyelectrolyte gels, charged polymers form cross-linked networks, with fluid in interstitial spaces, macro-ions on chains, and counterions in surrounding networks. Additives such as nanofillers provide binding sites for polymers, which may give additional stability to gels [2]. However, there is limited theoretical literature on the molecular mechanisms behind polyelectrolyte gel formation with solvent interactions.

To understand these systems, we utilized molecular dynamics (MD) simulations and Large-scale Atomic/Molecular Massively Parallel Simulator (LAMMPS) as the software tool. We use coarse-grained simulations, treating small functional groups as single "beads" and polymer chains as "bead-and-spring", which allows for a greater time-scale for observation [3].

Our polyelectrolyte systems consist of 300 polyelectrolyte chains of 31 monomers; we tested placement of negative single-charged units on all monomers in the chain and every fifth monomer. We also tested varying numbers of nanofillers (0, 50, 100, 150, and 200) to determine their effects on gel formation. Nanofillers were modeled as rigid 19-unit hexagon sheets with positive charges; co-ions opposing these charges were modeled in the solvent.

After designing our simulation systems, we wrote and utilized Python scripts to test mechanical properties of the gel, including mean squared displacement (MSD) to determine diffusion coefficient, polymer end-to-end distance, radius of gyration (Rg), radial distribution function (RDF), and stress auto-correlation (SAC) to determine viscosity.

MSD is the Euclidean distance between the start and end positions of a "bead." A polymer's MSD is the average of MSD for all beads in the chain, accounting for center-of-mass drift. Nanofillers are expected to cross-link with polymers and reduce movement. However, we found a positive correlation between nanofiller concentration and MSD (Fig. 1). This, with decreasing end-to-end distance, shows that nanofillers made polymers travel farther.

Rg over time measures the elongation of a polymer. Our data shows that as nanofiller concentration increases, average Rg decreases linearly. RDF determines the relative distance between two kinds of particles, confirming that oppositely charged particles attract, except in the case of nanofillers and co-ions. Viscosity was calculated by integrating under the SAC function; the highest viscosity (most gel-like behavior) was found at 100 nanofillers (Fig. 2).

For future work, we intend to vary the charges of different molecules to determine optimal gel-forming conditions.
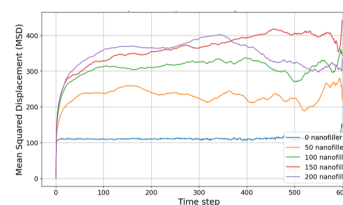
Fig. 1 Mean squared displacement (MSD) of various nanofiller
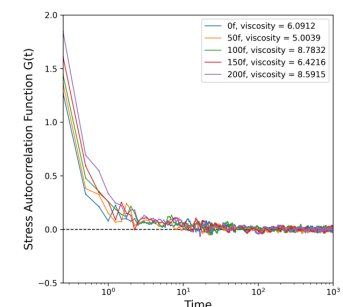
Fig. 2 Stress autocorrelation function (SAF) of varying nanofiller concentrations over time. Viscosity, time integration of SAF.

1. Huang, J., Kogbara, R. B., Hariharan, N., Masad, E. A., & Little, D. N. (2021). A state-of-the-art review of polymers used in soil stabilization. *Construction and Building Materials*, *305*, 124685. https://doi.org/10.1016/j.conbuildmat.2021.124685

2. Hoang Huy, V. P., So, S., & Hur, J. (2021). Inorganic fillers in composite gel polymer electrolytes for high-performance lithium and non-lithium polymer batteries. *Nanomaterials*, *11*(3), 614. https://doi.org/10.3390/nano11030614

3. Saha, S. (2024). Understanding the molecular mechanism behind structural and rheological properties of polymer hydrogels [Unpublished doctoral dissertation]. Stony Brook University.

Rhizobium Tropici-Produced EPS Biopolymer: Analyzing Its Influence on Gene Expression in *Arabidopsis Thaliana*

Christian Chan[1], Michelle Guo[2], Tei Kim[3], Arohi Mahajan[4], Seohee Park[5], Emily Tarrab[6], Craig Chen[7], Cosmo Perfetti[7], Aaron Sloutski[8], Marcia Simon[9], Jay Gao[10], Miriam Rafailovich[8]

[1]*South Side High School, Rockville Centre, NY, 11750, [2]Tesoro High School, Las Flores, CA, 92688, Medford, NY, 11763, [3]Stanford Online High School, Redwood City, CA, 94063, [4]Cambridge International Foundation School, India, [5]Dwight School Seoul [6]Yeshivah of Flatbush Joel Braverman High School, Brooklyn, New York, 11230, [8]Department of Materials Science and Chemical Engineering, [9]Department of Oral Biology & Pathology, Stony Brook University, Stony Brook, NY 11794, [10]Stony Brook University School of Dental Medicine, Stony Brook, NY 11794*
Authors 1–6 contributed equally to this work

Increasing soil stability is important for addressing increased stream and river turbidity, eutrophication, decreased biodiversity, and desertification of farmland. A potential solution is the use of extracellular polymeric substances (EPS) produced by the bacteria *Rhizobium Tropici,* which offers a low-cost and environmentally friendly solution to soil erosion.[1] The form of RT-EPS used in this research is Ethanol Precipitable Material (EPM). Characterized by its ability to retain water and nutrients and enhance subterranean root structure, EPM offers applications in sustainable agriculture and environmental preservation in the face of intense weather patterns. This study aims to investigate how EPM promotes root growth in Bermuda Grass, Bush Bean and *Arabidopsis Thaliana* (At) through physical observation and genomic study.

Figure 1. Comparison of *At* plants grown in control vs. 125 mg/Kg EPM conditions. EPM-treated samples had higher root mass.

EPM's adhesive properties were investigated by measuring the angle of repose. Sand was mixed with different concentrations of EPM and molded into cones. On Day 1, all EPM-treated samples had higher angle measurements than the control, indicating that the EPM strengthened its interaction with sand. By Day 10, sand castles with 50 and 125 mg/kg had the greatest angle at 57.7°, compared to the control at 51.6°, indicating that the EPM leads to higher adhesive properties.

Bermuda Grass samples were allowed to germinate and mature over a 2 month period. On average, the shoot count and root mass increased with higher EPM concentrations (25 and 125 mg/kg). For the Bush Bean Plants, samples grown with 25 mg/kg EPM in sand produced the greatest number of bean pods and had the highest overall root mass and root-shoot mass ratio. Further XRF analysis was performed to quantify the presence of important minerals in the bean pods, and there was a significant increase in the amount of potassium with higher amounts of EPM.

Figure 2. Comparison of Lateral Roots Between 0% EPM and 5% EPM.

Initial studies on *At* plants showed enhanced root density and plant growth with greater concentrations of EPM (Figure 1). As the entire genome of *At* has been sequenced, the plants were used to analyze how EPM influences their gene expression. RNA extraction and initial qPCR analyses were performed and different expression levels were noted for several genes. Further studies are to be conducted over time to confirm these differences. *At* plants were also grown in agarose to eliminate the influence of mechanical factors from the growth medium. The percentage of sprouts per dish was recorded each day. The density of lateral roots was also counted using the Keyence 3-D Microscope, and this will be continued for other concentrations (Figure 2). Future steps involve performing additional qPCR analyses to better understand how EPM influences the expression of specific genes involved in root growth in At, which can be used as a proxy for other plants.

---

[1] Larson, Steven, et al. "An Innovative Non-Petroleum Rhizobium Tropici Biopolymer Salt for Soil Stabilization." Volume 5: Energy Systems Analysis, Thermodynamics and Sustainability; NanoEngineering for Energy; Engineering to Address Climate Change, Parts A and B, Jan. 2010, doi:10.1115/imece2010-38933.

Analyzing the Rheology of a *Rhizobium tropici*-produced Entangled Exopolysaccharide and Its Effect on Soil Stability

Damien Crowley[1], Yiwei Fang[2], Miriam Rafailovich[2]
[1]*Wantagh High School, Wantagh, NY, 11793*, [2]*Stony Brook University, Stony Brook, NY, 11794*

A promising strategy to combat erosion has recently emerged from a *Rhizobium tropici*-produced exopolysaccharide, which effectively transforms the mechanical properties of soil, reducing erosion[1]. Research has also uncovered that applying *Rhizobium tropici*-produced extracellular polymeric substance (EPS) enhances root and vegetation growth, offering prospective improvements in soil stability[1]. In addition, RT-EPS's prolific yielding, improvement of soil adhesion and nutrient and water retention, and biodegradability[2] provide a sustainable and inexpensive method for curtailing erosion. However, the properties and influence of RT-biopolymer entanglement in gelled solutions remain largely uncertain, limiting the efficacy of its field utilization. Thus, this study aims to understand RT-EPS rheological characteristics and how these properties can improve basin and littoral soil stability. It was hypothesized that EPM is an entangled polymer and higher EPM concentrations in gels would result in heightened viscoelasticity.

Gels of DI water and RT-EPS concentrations (c) ranging from 2 mg/mL to 15 mg/mL were utilized to investigate the rheological properties of EPM. A three-dimensional analysis was initially conducted during which EPM shear elastic (G') and viscous (G'') moduli and damping coefficient (Tanδ) variation was compiled over an oscillation cycle ($0.63 \leq \omega \leq 63$) for samples maintained at temperatures between 25°C and 85°C; however, thermal conditions had no significant effect on viscoelasticity.

Figure 1: η_{red} (cm³·g⁻¹) vs. Concentration (mg/mL) ($P < .001$).

Dynamic mechanical analysis (DMA) was then performed at 25°C, which revealed a critical gel point of roughly 2.69 mg/mL. Samples were then tested at increasing shear rates ($0.01 \leq \gamma \leq 10^3$) at a constant temperature of 25°C and frequency of 1 Hz. RT-EPS gels typically transitioned to elastoplastic behavior between $60 \leq \gamma \leq 90$, and yield strain modeling presented dramatic increases for c ≥ 0.4% compared to $0.2\% \leq c \leq 0.4\%$ (Figure 1).

EPM gel shear viscosity (Pa-s) was then measured against shear rate (s⁻¹), and Newtonian plateaus occurred at low shear rate (≈ 0.01 s⁻¹). Reduced viscosities (η_{red}) were calculated and the Huggins equation ($\eta_{red} = \eta + k_H(\eta)^2 c$) was utilized to determine RT-EPS intrinsic viscosity (η) and the Huggins viscosity coefficient (k_H). Increases in EPM concentration, which is assumed to have augmented RT-biopolymer entanglement, reflected growing η_{red} (cm³·g⁻¹) values. A linear regression model ($\eta_{red} = 434 + .001752(434^2)(c)$) was used to determine that $\eta = 434$ and $k_H \approx .001752$, which is notably low. 200 mL samples containing 160mL sand and 40 mL of gelled DI samples concentrated with .1%, .3%, and .5% EPM were then used for soil stability analysis. Future work includes thermogravimetric analysis (TGA), further soil stability testing, and reanalysis of K_H.
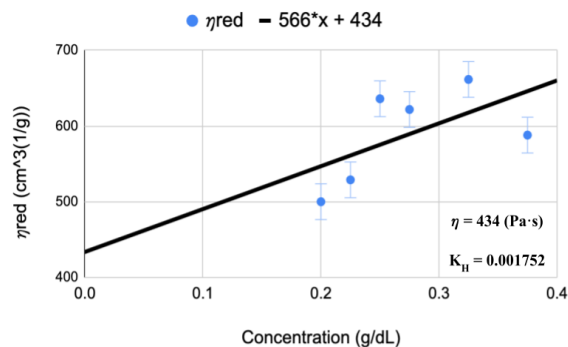
[1]Luo, H., Yu, S. X. Y., Zheng, Y., Wang, L., Fernandez, M. R., Rafailovich, M., Simon, M., Walker, S., Gao, J., & Larson, S. (2022). The influence of Rhizobium tropici produced EPM biopolymer on green bush bean root and plant growth. *Forestry Research and Engineering International Journal*, 5(1), 17–20. https://doi.org/10.15406/freij.2022.05.00102

[2]Larson, S., Nijak, G., Corcoran, M., Lord, E., & Nestler, C. (2016). Evaluation of Rhizobium tropici-derived Biopolymer for Erosion Control of Protective Berms. Field Study: Iowa Army Ammunition Plant. In *US Army Corps of Engineers Engineer Research and Development Center*. https://apps.dtic.mil/dtic/tr/fulltext/u2/1011606.pdf

GARCIA
CENTER FOR POLYMERS AT ENGINEERED INTERFACES
2024 Research Scholar Program

Maya Puterman

Ishita Banerjee

GARCIA
CENTER FOR POLYMERS OF ENGINEERED INTERFACES

GARCIA
CENTER FOR POLYMERS AT ENGINEERED INTERFACES
2024

Peter Yao

Logos!

GARCIA
SUMMER SCHOLARS
2024
Damien Crowley

GARCIA
2024
CENTER FOR POLYMERS AT ENGINEERED INTERFACES
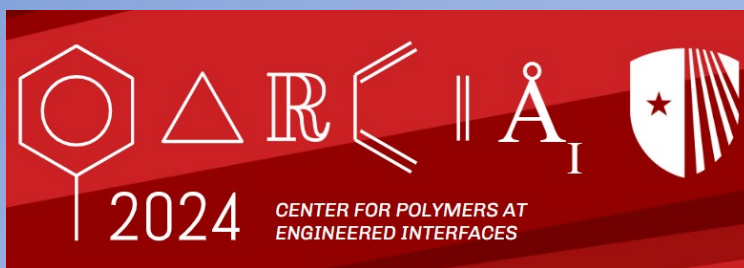
Kevin Zhang

Garcia
2024
Ava Zhou, Sichen Liu
Dennis Xu, Ruoheng Liu

We gratefully acknowledge the support of
the Louis Morin Charitable Trust

Thanks for a great summer!